Max-Planck-Institut für Kolloid- und Grenzflächenforschung

Abteilung Biomaterialien

Dynamic and Equilibrium Adsorption Behaviour of ß-lactoglobulin at the Solution/Tetradecane Interface: Effect of Solution Concentration, pH and Ionic Strength

Dissertation
zur Erlangung des akademischen Grades
"doctor rerum naturalium"
(Dr. rer. nat.)
in der Wissenschaftsdisziplin "Colloid and Interface Science"

eingereicht an der
Mathematisch-Naturwissenschaftlichen Fakultät
der Universität Potsdam

von
Jooyoung Won

Potsdam, den 15. Mai 2016

Published online at the
Institutional Repository of the University of Potsdam:
URN urn:nbn:de:kobv:517-opus4-99167
http://nbn-resolving.de/urn:nbn:de:kobv:517-opus4-99167

ABSTRACT

Proteins are amphiphilic and adsorb at liquid interfaces. Therefore, they can be efficient stabilizers of foams and emulsions. β-lactoglobulin (BLG) is one of the most widely studied proteins due to its major industrial applications, in particular in food technology.

In the present work, the influence of different bulk concentration, solution pH and ionic strength on the dynamic and equilibrium pressures of BLG adsorbed layers at the solution/tetradecane (W/TD) interface has been investigated. Dynamic interfacial pressure (Π) and interfacial dilational elastic modulus (E') of BLG solutions for various concentrations at three different pH values of 3, 5 and 7 at a fixed ionic strength of 10 mM and for a selected fixed concentration at three different ionic strengths of 1 mM, 10 mM and 100 mM are measured by Profile Analysis Tensiometer PAT-1 (SINTERFACE Technologies, Germany). A quantitative data analysis requires additional consideration of depletion due to BLG adsorption at the interface at low protein bulk concentrations. This fact makes experiments more efficient when oil drops are studied in the aqueous protein solutions rather than solution drops formed in oil. On the basis of obtained experimental data, concentration dependencies and the effect of solution pH on the protein surface activity was qualitatively analysed. In the presence of 10 mM buffer, we observed that generally the adsorbed amount is increasing with increasing BLG bulk concentration for all three pH values. The adsorption kinetics at pH 5 result in the highest Π values at any time of adsorption while it exhibits a less active behaviour at pH 3.

Since the experimental data have not been in a good agreement with the classical diffusion controlled model due to the conformational changes which occur when the protein molecules get in contact with the hydrophobic oil phase in order to adapt to the interfacial environment, a new theoretical model is proposed here. The adsorption kinetics data were analysed with the newly proposed model, which is the classical diffusion model but modified by assuming an additional change in the surface activity of BLG molecules when adsorbing at the interface. This effect can be expressed through the adsorption activity constant in the corresponding equation of state. The dilational visco-elasticity of the BLG adsorbed interfacial layers is determined from measured dynamic interfacial tensions during sinusoidal drop area variations. The interfacial tension responses to these harmonic drop oscillations are

interpreted with the same thermodynamic model which is used for the corresponding adsorption isotherm.

At a selected BLG concentration of 2×10^{-6} mol/l, the influence of the ionic strength using different buffer concentration of 1, 10 and 100 mM on the interfacial pressure was studied. It is affected weakly at pH 5, whereas it has a strong impact by increasing buffer concentration at pH 3 and 7. In conclusion, the structure formation of BLG adsorbed layer in the early stage of adsorption at the W/TD interface is similar to those of the solution/air (W/A) surface. However, the equation of state at the W/TD interface provides an adsorption activity constant which is almost two orders of magnitude higher than that for the solution/air surface.

At the end of this work, a new experimental tool called Drop and Bubble Micro Manipulator DBMM (SINTERFACE Technologies, Germany) has been introduced to study the stability of protein covered bubbles against coalescence. Among the available protocols the lifetime between the moment of contact and coalescence of two contacting bubble is determined for different BLG concentrations. The adsorbed amount of BLG is determined as a function of time and concentration and correlates with the observed coalescence behaviour of the contacting bubbles.

LIST OF ABBREVIATIONS

Latin Symbols

A	surface/interfacial area
A	cross sectional area of the dividing surface (section 3.3)
a	interaction constant
a_i	activity of the component i
a_p	protein intermolecular interaction parameter
b	radius of curvature at (0, 0) in Figure 6
b	adsorption activity coefficient
b_i	adsorption activity coefficient in the i-th state
b_p	total adsorption constant for the protein molecule in all states
b_{pi}	adsorption equilibrium constant for the protein in the i-th state
c	bulk concentration
c*	critical protein concentration
c_c	surfactant counter-ion concentration
c_i	concentration of component i
c_p	protein concentration
c_s	surfactant concentration
c_0	initial bulk protein concentration
D	diffusion coefficient
E	surface/interfacial dilational visco-elasticity modulus
E_0	surface/interfacial dilational limiting elasticity (high frequency limit)
E'	storage modulus = elasticity
E''	loss modulus = viscosity
$\|E\|$	visco-elasticity modulus
f	cyclical frequency (Hz) of oscillations
f_a	average activity coefficient of ions in the bulk solution in Eq. (3.16)
f_i	activity coefficient of component i in Eq. (3.10)
g	local gravitational constant
k	kinetic constant
K_H	Henry constant
K_L	Langmuir equilibrium constant
m	number of ionized groups in a protein molecule
n_a	aggregation number
ΔP	pressure difference
ΔP_0	pressure difference at a reference plane
R	gas law constant
R_1	radius of curvature at the point (x, z) in Figure 6
r	radius of curvature
S	entropy
s	arc length
T	absolute temperature
t	time
U	internal energy of the total system
U^α	internal energy of the bulk phase α
U^β	internal energy of the bulk phase β
U^σ	excess free energy associated with the surface
z	vertical height measured from the reference plane

Greek Symbols

β	shape factor in Eq. (4.6)
Γ	adsorption as a function of the bulk concentration
Γ^*	critical value of protein adsorption
Γ_i^σ	surface excess concentration of component i
Γ_p	total adsorption of protein in all states
Γ_{pi}	protein adsorption in the i-th state
Γ_s	surfactant adsorption
Γ_Σ	total adsorption in m layers
Γ_∞	maximum surface/interfacial coverage
γ	surface/interfacial tension
γ_0	surface/interfacial tension of pure solvent
ε	two-dimensional relative surface layer compressibility coefficient
θ	surface/interfacial coverage
θ_p	total surface/interfacial coverage by protein molecules
μ_0	chemical potential of the component i at a reference state
μ_i	chemical potential of the component i
σ	surface region of the Gibbs dividing surface
τ	dummy variable with time unit
τ_{ind}	induction time
Π	surface/interfacial pressure; is the difference between the interfacial tension γ of a solution and γ_0 as the tension for the pure W/TD interface
Π^*	critical value of surface pressure
$\Delta\rho$	density difference
Φ	normal angle
ϕ	phase angle
ω_D	characteristic frequency of diffusion relaxation
ω_i	molar area of component i
ω_{max}	maximum partial molar area
ω_{min}	minimum partial molar area
ω_p	average molecular area of an adsorbed protein molecule
ω_s	molar area of an adsorbed surfactant molecule
ω_{s0}	molar area of surfactant at zero surface pressure
ω_0	initial molar area of a surfactant or of a solvent molecule

Indicates

W/A	solution/air surface
W/TD	solution/tetradecane interface

LIST OF PUBLICATIONS

1. β-Lactoglobulin adsorption layers at the water/air surface: 2. Dilational rheology: Effect of pH and ionic strength.

Ulaganathan, V., Retzlaff, I., Won, J. Y., Gochev, G., Gehin-Delval, C., Leser, M., Gunes, D. Z., Noskov, B. A., & Miller, R. (**2016**). *Colloids Surfaces A*. http://dx.doi.org/10.1016/j.colsurfa.2016.08.064

2. Dilational viscoelasticity of BLG adsorption layers at the solution/tetradecane interface - Effect of pH and ionic strength.

Won, J. Y., Gochev, G., Ulaganathan, V., Krägel, J., Aksenenko, E. V., Fainerman, V. B., & Miller, R. (**2016**). *Colloids Surfaces A*. http://dx.doi.org/10.1016/j.colsurfa.2016.08.054

3. Mixed adsorption mechanism for the kinetics of BLG interfacial layer formation at the solution/tetradecane interface.

Won, J. Y., Gochev, G., Ulaganathan, V., Krägel, J., Aksenenko, E. V., Fainerman, V. B., & Miller, R. (**2016**). *Colloids Surfaces A*. http://dx.doi.org/10.1016/j.colsurfa.2016.08.024

4. Profile analysis tensiometry for studies of liquid interfacial dynamics.

Won, J. Y., Ulaganathan, V., Tleuova, A., Kairaliyeva, T., Sharipova, A. A., Hu, X. W., Karbaschi, M., Gochev, G., Javadi, A., Rahni, M. T., Makievski, A. V., Krägel, J., Aidarova, S. B. and Miller, R. **(2016)**, In M.L. Pascu (Ed.), *Laser Optofluidics in Fighting Multiple Drug Resistance*, BENTHAM Publ.

5. β-Lactoglobulin adsorption layers at the water/air surface: 1. Adsorption kinetics and surface pressure isotherm: Effect of pH and ionic strength.

Ulaganathan, V., Retzlaff, I., Won, J. Y., Gochev, G., Gehin-Delval, C., Leser, M., Gunes, D. Z., Noskov, B. A., & Miller, R. (**2016**). *Colloids Surfaces A*. http://dx.doi.org/doi:10.1016/j.colsurfa.2016.03.008

6. Completely engulfed olive/silicone oil Janus emulsions with gelatin and chitosan.

Kovach, I., Won, J. Y., Friberg, S. E., & Koetz, J. (**2016**). *Colloid and Polymer Science,* 294(4), 705-713.

7. Effect of solution pH on the adsorption of BLG at the solution/tetradecane interface.

Won, J. Y., Gochev, G., Ulaganathan, V., Krägel, J., Aksenenko, E. V., Fainerman, V. B., & Miller, R. (**2016**). *Colloids Surfaces A*. http://dx.doi.org/doi:10.1016/j.colsurfa.2016.05.042

8. Adsorption of equimolar aqueous sodium dodecyl sulphate/dodecyl trimethylammonium bromide mixtures at solution/air and solution/oil interfaces.

Mucic, N., Gochev, G., Won, J., Ulaganathan, V., Fauser, H., Javadi, A., Aksenenko, E. V., Krägel, J., & Miller, R. (**2015**). *Colloid and Polymer Science*, 293(11), 3099-3106.

9. Dynamics of drops—Formation, growth, oscillation, detachment, and coalescence.

Karbaschi, M., Rahni, M. T., Javadi, A., Cronan, C. L., Schano, K. H., Faraji, S., Won, J. Y., Ferri, J. K., Krägel, J., & Miller, R. (**2015**). *Advances in colloid and interface science*, 222, 413-424.

10. Bubble–bubble interaction in aqueous β-Lactoglobulin solutions.

Won, J. Y., Krägel, J., Gochev, G., Ulaganathan, V., Javadi, A., Makievski, A. V., & Miller, R. (**2014**). *Food Hydrocolloids*, 34, 15-21.

11. Drop and bubble micro manipulator (DBMM)—A unique tool for mimicking processes in foams and emulsions.

Won, J. Y., Krägel, J., Makievski, A. V., Javadi, A., Gochev, G., Loglio, G., Pandolfini, P., Leser, M. E., Gehin-Delval, C., & Miller, R. (**2014**). *Colloids and Surfaces A.*, 441, 807-814.

12. Characterization methods for liquid interfacial layers.

Javadi, A., Mucic, N., Karbaschi, M., Won, J. Y., Lotfi, M., Dan, A., Ulaganathan, V., Gochev, G., Makievski, A. V., Kovalchuk, V. I., Kovalchuk, N. M., Krägel, J., & Miller, R. (**2013**). *European Physical Journal-Special Topics*, 222(1), 7-29.

13. Capillary pressure experiments with single drops.

Javadi, A., Krägel, J., Karbaschi, M., Won, J. Y., Dan, A., Makievski, A. V., Loglio, G., Liggieri, L., Ravera, F., Kovalchuk, N. M., Kovalchuk, V. I., & Miller, R. (**2013**). In P. Kralchevsky, R. Miller, & F. Ravera (Eds.), *Colloid and Interface Chemistry for Nanotechnology* (pp. 271-312). Boca Raton: CRC Press.

14. Inferfacial dynamics methods.

Javadi, A., Mucic, N., Karbaschi, M., Won, J., Fainerman, V. B., Sharipova, A., Aksenenko, E. V., Kovalchuk, V. I., Kovalchuk, N. M., Krägel, J., & Miller, R. (**2013**). In T. Tadros (Ed.), *Encyclopedia of Colloid and Interface Science* (pp. 637-676). Weinheim: Wiley-VCH.

15. Charakterisierung von Grenzflächen zwischen zwei Flüssigkeiten.

Miller, R. and Won J. Y. (**2012**). In K. Köhler (Ed.), *Emulgiertechnik*, Hamburg: B. Behr's Verlag, pp. 37-53.

1. INTRODUCTION

Proteins are widely studied due to its various applications in food technology, biochemistry, cosmetics, pharmacology etc. [1, 2]. In particular, comprehending colloidal systems stabilized by proteins and the dynamic behaviour of proteins at interfaces are very important in food systems [2, 3, 4, 5, 6, 7, 8, 9, 10]. Proteins are important stabilizers in various food products such as milk, ice cream or salad dressings. For this purpose various types of proteins were investigated, as an example, vegetable proteins from wheat and soy, and milk proteins like caseins and β-lactoglobulin (BLG) [4, 11, 12, 13, 14, 15, 16, 17, 18, 19]. The stabilization of foams [20] and emulsions [15] depend to a great extent on the interfacial properties, adsorption dynamics, surface activity, and surface rheology. Such fundamental studies concerning food protein adsorption at the water/oil interface can draw corresponding information to understand complex phenomena such as the digestion processes [21, 22].

Proteins are large biomacromolecules consisting of a number of amino acid residues. Proteins have zwitterionic nature since they contain both acidic and basic functional groups, therefore, the solution pH plays a crucial role. Amino acids design proteins which may be positive, negative, or neutral, and as a result, proteins have an overall electrical net charge. The isoelectric point p*I* is the pH value at which the net charge is zero. Proteins carry a positive net charge at a pH below their p*I*, whereas they carry a negative net charge above their p*I*. The value of p*I* is specific for every protein because of its unique primary structure. The molecular net charge is affected by the solution pH and can become positive or negative due to the gain or loss, respectively, of protons (H^+). The p*I* value can affect the solubility of molecules at a given pH. Protein molecules have the minimum solubility at the pH that corresponds to their p*I*. The effect of the protein net charge on the interfacial pressure and the adsorption kinetics can be attributed to changes of the surface activity of the protein molecules and the existence of an electrostatic barrier of adsorption [23]. The higher the net charge the lower the chance for hydrophobic segments (usually buried in the aqueous environment) to be exposed to the interface with a hydrophobic phase (solid or fluid). In summary, reduction of protein net charge causes increasing the affinity of the protein to the interface, thus adsorption will be enhanced [24, 25].

In literature, various theoretical models have been introduced to qualitatively characterize the dynamic and equilibrium adsorption behaviour of proteins and surfactant. Joos and Serrien [26] were the first who suggested the theory of protein adsorption layers. The properties of such layers differ from those of regular surfactants in many respects. As compared with the adsorption of surfactants, proteins have been transported to the interface, as well as their conformation may be changed. Protein molecules tend to be in a folded conformation at interfaces at the beginning of the adsorption process. Depending on the species of protein, surface concentration and the fluid which forms the interface with the protein solution, the degree of the unfolding process is determined. It was reported that changes in orientation of globular protein molecules could influence the adsorption kinetics in case of short adsorption times [27]. It elucidates why the value of the partial molar area for proteins is large and variable, as compared with usual surfactants.

The present thesis discusses the behaviour of protein adsorbed layers based on a number of experimental data. The experiments presented here, have been performed with various concentration of aqueous BLG solution at the interface with tetradecane (TD). The globular protein BLG is one of the main components of the bovine milk. It is a relatively small protein of 162 residues, with 18.4 kDa molecular weight [28, 29, 30]. Since the properties of BLG can be considered beneficial or harmful in dairy products, BLG has major interest in food industry [31]. To the best of our knowledge, there are no extensive studies in the literature, which comprise results on the adsorption behaviour of BLG in a wide protein concentration and pH ranges (including pH-values below, at and above the isoelectric point), neither for the case of water/oil interface nor for water/air surface. In the latter case, recently Ulaganathan et al. [25, 32] attempted to systematically investigate the effects of pH and ionic strength on BLG surface layers. In the proposed thesis, we investigate the effect of BLG bulk concentration, solution pH and the dilational rheology of BLG adsorbed layers at the (W/TD) interface by measuring the dynamic interfacial pressure as a function of BLG concentration, pH and ionic strength of the solutions to obtain information about the mechanism of adsorption of BLG. The dynamic interfacial pressure, interfacial pressure isotherm and dilational visco-elastic rheology were obtained at pH 3, 5 and 7 ($pI_{BLG} \approx 5.1$) on the basis of the $\Pi(t)$ data measured during the adsorption process for about 23.5 hours.

To describe the behaviour of protein adsorbed layers at the W/TD interface, the classical diffusion controlled model has been modified by assuming an additional change in the surface activity of BLG molecules when adsorbing at the interface. This new theoretical model which is used here, assumes a physically reasonable diffusion coefficient for the protein molecules and an adsorption activity constant as a function of the adsorbed amount. A smaller adsorption coefficient is required at the beginning of the adsorption process while a larger one is required for the longer lasting adsorption process. This is due to conformational change of the protein when BLG molecules contact with the hydrophobic TD phase at the interface. This conformational change is considered in terms of changes in the surface activity. We show the agreement of this mixed theoretical model with experimental data for BLG solutions at three pH value of 3, 5 and 7 in the presence of 10 mM buffer solution.

2. TARGET OF THIS THESIS

This thesis aims at better understanding of the mechanism of the BLG adsorption at solution/tetradecane (W/TD) interfaces. As the adsorption of proteins at liquid/liquid interfaces is a time process, the Profile Analysis Tensiometer PAT-1 (SINTERFACE Technologies, Germany) is used to quantitatively study the formation of adsorption layer of BLG at liquid/liquid interface via measuring the dynamic interfacial tension. Using PAT-1, we studied the effect of BLG bulk concentration, solution pH and solution ionic strength on the interfacial pressure and the dilational rheology. While the tensiometer provides information on the formation of adsorption layers over a certain time interval, dilational elasticity and viscosity can be obtained from relaxation experiments via the responses of the interfacial layer to harmonic perturbations (oscillations) in a certain frequency range.

The adsorption behaviour of proteins at liquid/fluid interfaces can be attributed to several factors which influence the conformational changes of protein molecules in the adsorption layer. The interaction between adsorbed protein molecules and the oil molecules at the interface can be considered with changing concentration and pH of the BLG solution or the ionic strength of the BLG solution [24, 33, 34, 35, 36, 37, 38, 39, 40, 41].

Generally, the rate of interfacial pressure change and the equilibrium values of interfacial pressure are increasing with the BLG bulk concentration while in parallel the induction time is decreasing. Furthermore, increasing the ionic strength increases the adsorption and leads typically to increasing Π values. The mechanism of BLG adsorption layers will be investigated via dynamic interfacial tension measurements. It will be shown that the classical diffusion controlled adsorption cannot quantitatively describe the gained data. A modification of this diffusion model will be presented that considers also the change in conformation of protein molecules upon adsorption at the W/TD interface [42].

The effect of BLG concentration and solution pH on the surface pressure, the dilational rheology and the structure of BLG adsorbed layers at the solution/air (W/A) surface were recently reported by Ulaganathan et al. [25, 32] and Gochev et al. [43]. In the present work, we are going to treat the obtained experimental data at the W/TD interface in the same manner. This includes the equilibrium interfacial pressure isotherms, and the dilational visco-elasticity in the range of low frequencies, most relevant for protein adsorption layers. The set of experimental data is presented and analysed by the most advanced thermodynamic model

recently proposed in [44]. It will be shown how the presence of TD molecules changes the absolute molar parameters of adsorbed BLG while the regularities with regard to the effects of pH and ionic strength are similar to adsorption layer of BLG at the W/A surface [45]. The same is true for the viscoelasticity of BLG layers at the W/TD interfacial layers [46].

The Drop Bubble Micro Manipulator DBMM (SINTERFACE Technologies, Germany) is used to describe the characterization of the stabilizing effect of BLG for air bubbles in aqueous protein solutions. Using DBMM the time of rupture of the liquid film between two bubbles (could be fresh bubbles or aged bubbles) in a BLG solution for a given time in a certain concentration of BLG solution can be determined. Since the presented study aims at stabilizing emulsions, DBMM is a suitable measuring technique for the elementary processes in foams and emulsions, in particular coalescence studies. This deserves large systematic studies, which is the reason why it is not part of this work.

3. FUNDAMENTALS OF ADSORPTION LAYERS

3.1. Foams and Emulsions

Foams are systems in which a gas phase is dispersed in a liquid or solid medium and it is easy to find from beer, cappuccino and whipped cream. Emulsions are the general term for systems in which one liquid phase is dispersed in another liquid phase which is immiscible. It is called O/W (oil in water) emulsion when the dispersed phase is an organic liquid and the continuous phase is water or an aqueous solution and is called W/O (water in oil) emulsion for the opposite situation. Emulsions are common in our life such as food, for example, milk, ice cream, mayonnaise, butter, and margarine, pharmaceutics, personal care and cosmetic products. To be an O/W emulsion or a W/O emulsion can generally be determined by the Bancroft rule that the phase in which the emulsifier is better soluble is the continuous phase [47]. Emulsifiers can be classified as water-soluble and oil-soluble by their HLB (Hydrophilic-Lipophilic Balance) value. It can be used in order to choose good emulsifiers for the desired emulsion. In O/W emulsions, use high HLB surfactants that are more soluble in water than in oil while in W/O emulsions use low HLB surfactants that are more soluble in oil than in water.

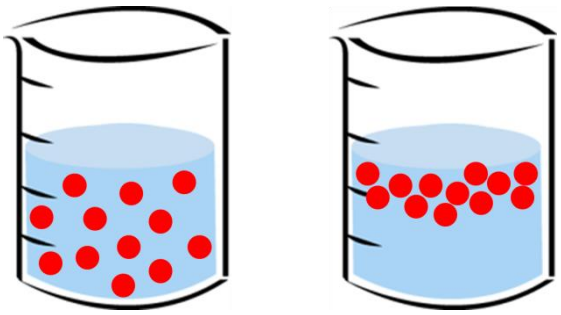

(a) (b)

Figure 1 (a) stable emulsion **(b)** unstable emulsion – it progressively separates

It is essentially impossible to create everlastingly stable foams or emulsions, it is necessary to add a surface-active substance as a third component to prevent phase separations. In this case, the surface active substance is called emulsifier. One class of emulsifiers are surface active

agents known as surfactants. When it is added to foams or emulsions as stabilizer, they facilitate lower interfacial free energy by adsorbing and orienting at the water/oil interface, and at the same time it suppress the rate of phase separation between water and oil to keep the foams or emulsion state [48]. Another class of emulsifiers are macromolecular substances such as polymers and proteins. They reduce the interfacial tension not as much as surfactants, but they can stabilize foams and emulsions via steric forces [49, 50, 51]. In food technology, often proteins and their mixtures with low molecular weight surfactants are used together as emulsifiers [52, 53, 54, 55, 56, 57] due to the efficiency of both compounds – surfactants for their low interfacial tension and proteins for their steric stabilization.

3.2. Surface and Interfacial Tension

Surface tension is an important property of surfactant systems [58, 59]. When a fresh interface of a surfactant or protein solutions is formed, the corresponding surface tension is the same as that of the solvent, because there is no surfactant or protein yet adsorbed. And then the surface tension will be decreased with time until the equilibrium state of adsorption is reached. This relaxation can be in a time range from a few seconds (or even less) up to hours and even days depending on the surfactant type and solution conditions such as concentration, pH, temperature and ionic strength. The equilibrium surface tension guides the way to better understand of dynamic behaviour of adsorption layers.

Believe it or not, we are living under the influence of surface tension. The phenomena, for example, water dripping from a tap which is stretched to a certain point and then separates as a spherical drop, or being round as a rain drop on a leaf, or raised liquid along the wall of a container in a vertical tube, are all due to the tension acting on the liquid surface. As shown in Figure 2, between the molecules constituting a liquid there are various interaction forces. In the bulk, as shown in Figure 2 (b), the forces of attraction and repulsion between the fluid molecules are symmetric and in equilibrium, so that the net force is zero. However, at the surface, as shown in Figure 2 (a), the interaction with molecules in the second fluid phase is different, i.e. asymmetric. Therefore, there is a net force directed towards the inside of the fluid. The resulting excess force is called surface tension or surface energy. Itsaction is directed towards minimization of the liquid surface area. The surface tension is a commonly occurring phenomenon and it can be also defined as the work required to create a certain area

of a new surface. As the water/oil interface is the subject of the thesis, the terminology "interfacial tension" instead of "surface tension" is used for liquid/liquid interfaces here.

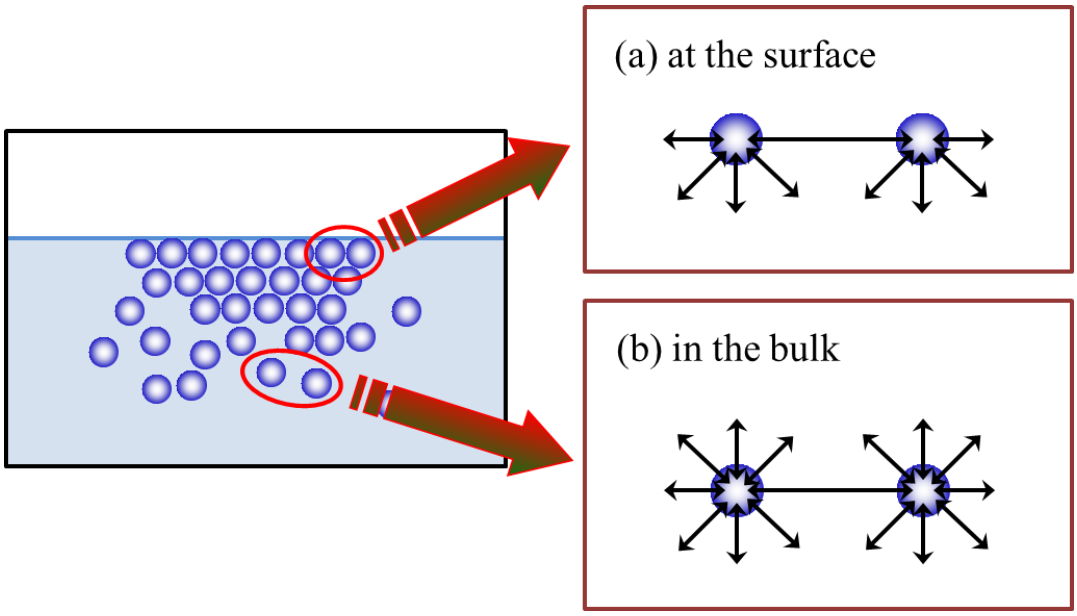

Figure 2 Diagram of the forces acting on molecules of a liquid

3.3. Adsorption and Gibbs Dividing Surface

The adsorption of molecules at the interface of a liquid phase occurs when this liquid phase is in contact with another immiscible phase. This phase can be a gas, a solid, or another liquid. Surface tension is affected by adsorption. Adsorbed layers may affect the interactions of the dispersed phase and as a result, these layers may play for example a key role in emulsion stabilization.

In the presence of two phases, the surface phase is located in between them. Josiah Willard Gibbs proposed an idealized model which is based on the concept of a "dividing surface" with zero thickness. In this model, the chemical components of the bulk phases α and β are not changed except in the vicinity of the dividing surface and even the total moles of any component is constant in the bulk phases but not in the dividing surface. However, in reality, the total moles of component vary depending on the position of the dividing surface. This is described schematically in Figure 3.

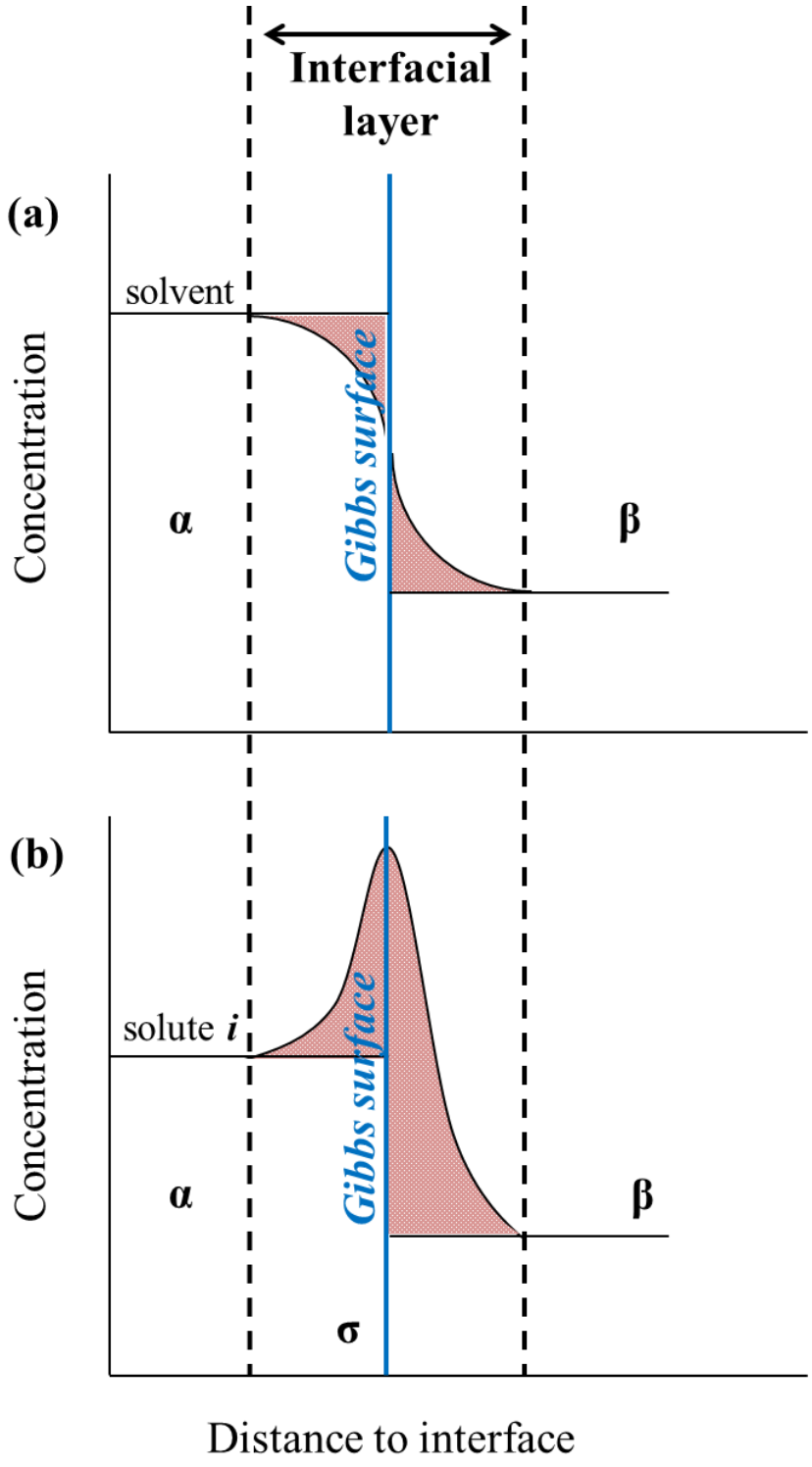

Figure 3 Schematic illustration of the concept of Gibbs' dividing plane; **(a)** solvent excess concentration is zero (the coloured area is equal on both sides of the Gibbs dividing surface), **(b)** the surface excess of component *i* is the difference (coloured area) in the concentrations of that component on either side of the Gibbs dividing surface.

The surface excess concentration of component *i* is given by

$$\Gamma_i^\sigma = \frac{n_i^\sigma}{A} \tag{3.1}$$

where A is the interfacial area. Γ_i^σ can be positive, negative or zero.

The internal energy U of the system consisting of the bulk phases α and β, and the interfacial region σ can be written as:

$$U = U^\alpha + U^\beta + U^\sigma \tag{3.2}$$

The corresponding expression for the thermodynamic energy of the interfacial region σ is as follows:

$$U^\sigma = \mathrm{T}S^\sigma + \gamma A + \sum_i \mu_i n_i^\sigma \tag{3.3}$$

where T is the temperature, S is the entropy, γ is the surface tension, A is the cross sectional area of the dividing surface, and μ_i is the chemical potential of the component i. For any infinitesimal change in $T, S, A, \mu, n,$ the differentiation of Equation (3.3) gives:

$$\mathrm{d}U^\sigma = TdS^\sigma + S^\sigma dT + \gamma dA + Ad\gamma + \sum_i \mu_i dn_i^\sigma + \sum_i n_i^\sigma d\mu_i \tag{3.4}$$

from Equation (3.2), the differential total internal energy in any bulk phase which is isobaric and isothermal leads to:

$$dU = TdS - PdV + \sum_i \mu_i dn_i \tag{3.5}$$

Similarly for the differential internal energy in the interfacial region σ from Equation (3.3) we get:

$$dU^\sigma = TdS^\sigma + \gamma dA + \sum_i \mu_i dn_i^\sigma \tag{3.6}$$

By subtracting Equation (3.6) from Equation (3.4), it is obtained:

$$S^\sigma \mathrm{dT} + \mathrm{A}\mathrm{d}\gamma + \sum_i n_i^\sigma d\mu_i = 0 \tag{3.7}$$

Then at constant temperature, by introducing in this equation the surface excess Γ_i^σ of component *i,* which is defined in Equation (3.1), finally the general form of the Gibbs fundamental equation can be represented by:

$$d\gamma = -\sum_i \Gamma_i^{\sigma} d\mu_i \tag{3.8}$$

Using this Gibbs adsorption equation it is feasible to connect the concentration of the solute with the surface tension of a solution, which results in a corresponding change in surface energy.

The chemical potential μ_i of the component *i* is given by

$$\mu_i = \mu_i^0 + RT\ln a_i \tag{3.9}$$

where μ_0 is the standard chemical potential of the component *i* at a reference state, *R* is the gas constant, *T* is the absolute temperature, and a_i is the activity of component *i*. Differentiation of the chemical potential equation leads to:

$$\mathrm{d}\mu_i = RT\frac{da_i}{a_i} = RTdlnf_i c_i \tag{3.10}$$

where *f* is the activity coefficient of component *i*, and c_i is the concentration of species *i* in the bulk phase. If the solutions in the phases α and β are dilute, the activity coefficient *f* of the component *i* approaches unity and the Gibbs isotherms:

$$\Gamma_i = -\frac{1}{RT}\left(\frac{\partial\gamma}{\partial lnc_i}\right)_{T,p} \tag{3.11}$$

3.4. Thermodynamic Adsorption Models

3.4.1. The Henry Adsorption Model

The simplest adsorption isotherm is the linear Henry isotherm [60].

$$\Gamma = K_H c \tag{3.12}$$

where Γ is the adsorbed amount at the bulk concentration *c* and K_H is the equilibrium adsorption constant so-called Henry constant. This isotherm has a relatively limited range of application and applies only for very low surface concentrations and conforms to non-interacting gaseous monolayers (ideal gas). Note, this adsorption model was originally derived by Henry for the gas adsorption and was applied to surfactant adsorption layers much later, using analogue quantities characteristic for surfactant interfacial layers.

3.4.2. The Langmuir Adsorption Model

The most frequently used non-linear adsorption isotherm is the Langmuir model [61].

$$\Gamma = \Gamma_\infty \frac{K_L c}{1+K_L c} \tag{3.13}$$

where Γ is the adsorbed amount at the bulk concentration c of the surfactant, Γ_∞ is the maximum surface coverage and K_L is the so-called Langmuir equilibrium constant. The Langmuir model assumes that adsorption in a single molecular layer takes place, all adsorption sites are equivalent and the surface is uniform, and there are no interactions between neighbouring adsorbed molecules. The corresponding Szyszkowski-Langmuir equation of state has the form [62]:

$$\Pi = \gamma_0 - \gamma = RT\Gamma_\infty \, ln(1 + K_L c) \tag{3.14}$$

here Π is the surface pressure, γ and γ_0 are the interfacial tensions of the solution and the pure solvent, respectively. B. von Szyszkowski derived his equation as an empirical relationship combining the measured quantity of surface tension with the surfactant bulk concentration. Only later it was shown that the Langmuir adsorption model can be transferred into the von Szyszkowski equation via the Gibbs fundamental equation (3.11). The physical meaning behind this adsorption model is a localized adsorption layer where each molecule requires a certain area at the interface.

3.4.3. The Frumkin Adsorption Model

In the following, the general form of the Frumkin adsorption model is given by the adsorption isotherm and the equations of state.

$$\Pi = -\frac{2RT}{\omega_{s0}}[\ln(1-\theta) + a\theta^2] \tag{3.15}$$

$$b[c_s(c_s + c_c)]^{1/2} f_a = \frac{\theta}{1-\theta} exp(-2a\theta) \tag{3.16}$$

where $\theta = \omega\Gamma$ is the surface coverage, a is the interaction constant, b is the adsorption equilibrium constant, c_s is the surfactant concentration. ω_{s0} is the molar area required by one surfactant molecule at zero surface pressure, c_c is the counter-ion concentration, and f is the

average activity coefficient of ions in the bulk solution. The molar area of a surfactant ω_s can be dependent on Π [48, 63].

$$\omega_s = \omega_{s0}(1 - \varepsilon\Pi\theta) \tag{3.17}$$

here ε is the two-dimensional relative surface layer compressibility coefficient, which characterizes the intrinsic compressibility of the molecules in the surface layer [64]. At high concentrations of inorganic electrolyte, which is higher than that of the surfactant, it is possible to describe the usual Frumkin equation for non-ionic surfactants as [63]:

$$\Pi = -\frac{RT}{\omega_{s0}}[ln(1-\theta) + a\theta^2] \tag{3.18}$$

$$bc_s = \frac{\theta}{1-\theta} exp(-2a\theta) \tag{3.19}$$

In surfactant science this equation as a generalization of the Langmuir adsorption model is also often applied to surfactant adsorption layers. Often, both equations are also applied to adsorption layers of globular proteins due to their simplicity as compared to models derived specifically for proteins.

3.4.4. Model for the Adsorption of Proteins in Different Adsorption States

Various theoretical models exist to describe the adsorption of polymer molecules at liquid interfaces. However, for a long time no specific adsorption models for proteins existed yet in the literature and the authors used the equation proposed by Singer [65] for analysing the measured surface pressure isotherms. The work by Graham and Phillips [66, 67, 68] is widely referred to in the field of protein adsorption, however, such rather general model for polymers cannot take any specific properties of proteins into account. Hence, Joos and Serrien [26] proposed the theory of protein adsorption based on the principle of Braun-Le Châtelier for describing liquid interfacial layers, in which proteins adsorb onto the interface in two states characterized by different partial molar areas [69]. Due to the folding properties of protein, adsorbed protein molecules at an interface can show more than two different adsorption states and cause different molar areas [70, 71]. The model derived in [41] is based on this principle and is suitable to describe the adsorption of protein molecules over a broad concentration range. The model assumes that the partial molar area of the adsorbed protein molecules can

vary from a maximum value (ω_{max}) at low concentration and low surface coverage to a minimum value (ω_{min}) at higher concentrations when the protein layer is closely packed at the interface. The value of the molar area ω_i is the molar area of the component *i*, given by $\omega_i = \omega_1 + (i-1)\omega_0$ $(1 \leq \mathrm{i} \leq \mathrm{n})$ with $\omega_1 = \omega_{min}$ and $\omega_{max} = \omega_1 + (n-1)\omega_0$, in order to describe the different unfolded states of the protein. Another assumption is that ω_0 is much smaller than the minimum molar area of the protein. When ω_p is the average molecular area of an adsorbed protein molecule and Γ_{pi} is the "partial" protein adsorption in the *i*-th state, $\Gamma_p = \sum_{i=1}^{n} \Gamma_{pi}$ is the total adsorption of protein in all *n* states, so that $\theta_p = \omega_p \Gamma_p = \sum_{i=1}^{n} \omega_i \Gamma_{pi}$ is the total surface coverage by protein molecules. The equation of state for protein adsorption is as follows [69]:

$$-\frac{\Pi\omega_0}{RT} = \ln(1-\theta_p) + \theta_p\left(1-\frac{\omega_0}{\omega_p}\right) + a_p\theta_p^2 \tag{3.20}$$

where ω_p is the average molar area of protein, ω_0 is the molar area increment between two "neighbouring" states, which is approximately equal to the molar area of an adsorbed protein segment or a water molecule, and a_p is the protein intermolecular interaction parameter. The equation of the adsorption isotherm for each state (*j*) of the adsorbed protein is defined by:

$$b_{pj}c_p = \frac{\omega_p\Gamma_{pj}}{(1-\theta_p)^{\omega_j/\omega_p}}\exp[-2a_p\left(\frac{\omega_j}{\omega_p}\right)\theta_p] \tag{3.21}$$

where b_{pj} is the adsorption equilibrium constant of the protein in the *j*-th state, c_p is the bulk concentration of the protein solution and ω_j is the "partial" molar area of protein in the *j*-th state. When we assume that b_{pj} are constant for any state of the protein adsorption ($b_{pj} = b_p$, for any *j*), the adsorption constant for the protein molecule as a whole is $\sum b_p = nb_p$. By this assumption the distribution function of various adsorption states can be calculated from Equation (3.21):

$$\Gamma_{pj} = \Gamma_p \frac{(1-\theta_p)^{\frac{\omega_j-\omega_1}{\omega_p}}\exp[2a_p\theta_p\frac{\omega_j-\omega_1}{\omega_p}]}{\sum_{i=1}^{n}(1-\theta_p)^{\frac{\omega_i-\omega_1}{\omega_p}}\exp[2a_p\theta_p\frac{\omega_i-\omega_1}{\omega_p}]} \tag{3.22}$$

Note that the adsorption activity coefficient of the *j*-th state is related to that of the *1*-st state via the parameter α: $b_j = (\frac{\omega_j}{\omega})^{\alpha} \times b_1$, which reflects the fact that the conformational changes

lead to the changes in the surface activity of the adsorbed protein molecules. The isotherm adsorption equations for each adsorbed state (j) of the protein are [69]:

$$b_{Pj}c = \frac{\omega_P \Gamma_{Pj}}{(\omega_j/\omega_1)^{\alpha}(1-\theta_P)^{\omega_j/\omega}} \exp\left[-2a_P(\omega_j/\omega)\theta_P\right] \tag{3.23}$$

From Equation (3.22), one can define the relationship between the interfacial coverage and the molar area of the protein by introducing the total surface coverage by protein molecules $\theta_p = \omega_p \Gamma_p = \sum_{i=1}^{n} \omega_i \Gamma_{pi}$:

$$\omega = \frac{\sum_{i=1}^{n} \omega_i (1-\theta)^{\frac{\omega_j-\omega_1}{\omega}} \exp[2a\theta\frac{\omega_j-\omega_1}{\omega}]}{\sum_{i=1}^{n} (1-\theta)^{\frac{\omega_i-\omega_1}{\omega}} \exp[2a\theta\frac{\omega_i-\omega_1}{\omega}]} \tag{3.24}$$

When all $b_j = (\frac{\omega_j}{\omega})^{\alpha} \cdot b_1$ are identical for any j, the adsorption constant for the protein molecule as a whole is $\Sigma b_j = n b_j = b$ [69]. This leads to the distribution function of adsorptions over all states of the protein molecules:

$$\Gamma_{Pj} = \Gamma \frac{\left(\frac{\omega_j}{\omega_1}\right)^{\alpha} (1-\theta_P)^{\frac{\omega_j-\omega_1}{\omega}} \exp\left[2a_P\theta_P\frac{\omega_j-\omega_1}{\omega}\right]}{\sum_{i=1}^{n}\left(\frac{\omega_j}{\omega_1}\right)^{\alpha} (1-\theta_P)^{\frac{\omega_i-\omega_1}{\omega}} \exp\left[2a_P\theta_P\frac{\omega_i-\omega_1}{\omega}\right]} \tag{3.25}$$

From this model we can conclude that with increasing total adsorption, the adsorbed protein molecules occupying larger areas are progressively displaced by those requiring smaller areas at the interface. This fact, $b_j = (\frac{\omega_j}{\omega})^{\alpha} \times b_1$, results in the equation which expresses the average molar area via the partial areas of protein molecule in different states:

$$\omega = \frac{\sum_{j=1}^{n} \omega_j (\frac{\omega_j}{\omega_1})^{\alpha} \exp[\frac{\omega_j-\omega_1}{\omega}\ln(1-\theta)]}{\sum_{j=1}^{n} (\frac{\omega_j}{\omega_1})^{\alpha} \exp[\frac{\omega_j-\omega_1}{\omega}\ln(1-\theta)]} \tag{3.26}$$

With the increase of protein concentration in the solution, surface pressure increased but it is found that Equation (3.20)-(3.23) are valid only for relatively low protein concentration due to the fact that proteins can be aggregated or became a bilayer at higher protein concentrations [69, 72]. However, the theory is extended to explain also data for higher concentrations by taking into account a two-dimensional condensation within the protein

layer [73]. Assume that there is a critical bulk concentration c^* above which the adsorption appears pressure independent [41].

The adsorption isotherm in this post critical concentration range is the same as in the pre-critical regime, while the equation of state becomes dependent on the aggregation number n_a:

$$\Pi = \Pi^*(1 + \frac{1}{n_a}\frac{\Gamma-\Gamma^*}{\Gamma^*}) \tag{3.27}$$

Also, to account for a multilayer adsorption, an additional adsorption activity coefficient b_i is introduced, which can be referred to as the secondary layer constant. The value of this parameter is much lower than b_1. This assumption was successfully applied for the theoretical description of BLG adsorption layers at the W/A surface [74]. For the total adsorption in m layers Γ_Σ is calculated as:

$$\Gamma_\Sigma = \Gamma \sum_{j=1}^{m} \left(\frac{b_i c}{1+b_i c}\right)^{j-1} \tag{3.28}$$

where $\Gamma = \frac{\theta}{\omega}$ is the adsorption of protein in the first layer.

3.5. Dynamic Adsorption Models

3.5.1. Diffusion Controlled Model to Describe the Adsorption Kinetics

The typical adsorption mechanism of surfactants is based on the diffusional transport of molecules to and from the interface. The diffusion equation was first proposed by Ward and Tordai [75], leading to an integral equation of the form

$$c(0,t) = c_o - \frac{2}{\sqrt{D\pi}}\int_0^{\sqrt{t}} \frac{d\Gamma(t-\tau)}{dt} d\sqrt{\tau} \tag{3.29}$$

or alternatively

$$\Gamma(t) = 2\sqrt{\frac{D}{\pi}}\left[c_0\sqrt{t} - \int_0^{\sqrt{t}} c(\tau)d(\sqrt{t-\tau}\right] \tag{3.30}$$

Here D is the diffusion coefficient in the bulk, c_0 is the initial bulk protein concentration, t is the time and τ is a dummy integration variable with time unit. It shows the relationship

between the adsorbed amount *Γ(t)* and the subsurface concentration *c(0, t)* for freshly formed surfaces.

The equation proposed by Ward and Tordai (3.30) is only suitable for planar interfaces. Liu et al. [76] derived a modification of the Ward-Tordai equation for a spherical interface.

$$\Gamma(t) = 2\sqrt{\frac{D}{\pi}}\left[c_0\sqrt{t} - \int_0^{\sqrt{t}} c(\tau)d(\sqrt{t-\tau})\right] \pm \frac{D}{r}\left[c_0 t - \int_0^t c(\tau)d(t-\tau)\right] \qquad (3.31)$$

where *r* is the radius of curvature. The plus and minus sign in the additional second term of the Ward-Tordai equation means the diffusion from outside and inside to the droplet surface, respectively. In [68] Graham and Phillips used a simplified approach based on the account for the first term only in the right hand side of Ward-Tordai equation. This so-called "square-root-of-time-approach" works well for surfactants at low concentrations and short adsorption times, however, not for proteins.

When protein molecules come into contact with the interface, they are subject to conformational changes. In particular at the water/oil interface the hydrophobic parts of the protein molecules have the tendency to penetrate into the hydrophobic oil phase, by this changing the molecular conformation. At low bulk concentrations the process of self-assembly at the interface is rather slow, hence, the protein molecules have enough space and time for molecular modifications. There is a period of time in which the progress of protein adsorption does not yet lead to an increase in the interfacial pressure. This time interval is called induction time which is best observed experimentally at low concentrations.

A possibility to describe experimental data for proteins properly is to consider, besides the transport of the molecules in the solution bulk by diffusion, a mechanism that takes somehow the conformational changes of the adsorbed protein molecules into account. It appears realistic to assume that conformational changes lead to an increase in the surface activity. Accordingly, a combined model of diffusional transport and an additional time process is proposed in [42, 45]. Instead of the integral equation proposed by Ward and Tordai [75] for a plane interface, the Fick's law for diffusional transport in form of a partial differential equation was used in a geometry assuming that a spherical TD oil drop was surrounded by the aqueous protein solution. Fick's law in spherical coordinates reads:

$$\frac{\partial c}{\partial t} = D\left(\frac{\partial^2 c}{\partial r^2} + \frac{2}{r}\frac{\partial c}{\partial r}\right) \qquad (3.32)$$

where $c=c(r, t)$ is the protein concentration at distance r from the centre of the drop and at time t, and D is the diffusion coefficient. The main parameters of this adsorption model are the surfactant bulk concentration c_0 and the diffusion coefficient D. The boundary conditions at the interface include two time functions, the sub-surface concentration $c(0,t)$ and the amount of adsorbed surfactants $\Gamma(t)$. Hence, Eq. (3.32) can be solved only in combination with an additional relationship between $\Gamma(t)$ and the measurable dynamic interfacial tensions $\gamma(t)$, typically in form of the equation of state $\Pi(\Gamma(t))$. This assumes that the equation of state is also applicable under dynamic conditions, i.e. a local equilibrium exists between the adsorption layer and the sub-surface layer (bulk phase layer adjacent to the surface).

As an additional time-dependent process for the protein adsorption, it is proposed that the adsorption activity of the protein increases with the adsorbed amount. Typically, the adsorption activity coefficients in each state b_j are assumed to be independent of the bulk concentration c, which is also true under dynamic conditions. However, it is assumed that at short adsorption times the adsorption activity coefficient is equal to a certain value b_0 and then increases with the adsorption time. This process should allow to reflect the structure formation by the protein and TD molecules at the interface, supposing that some time is required for protein molecules to adapt to the optimum conformation at the interface. The following relation for the change of the adsorption activity coefficient b with time t was proposed in [42]:

$$b(t) = b_0(1 + k \times t), \quad \text{for } t < t_{max} \tag{3.33a}$$

$$b_m = b_0(1 + k \times t_{max}), \quad \text{for } t \geq t_{max} \tag{3.33b}$$

The increase of b is limited by a maximum time t_{max}, beyond which it remains constant and equal to b_m. Hence, at the moment the adsorption equilibrium has been reached, the adsorption activity coefficient should have the value obtained from fitting the entire experimental adsorption isotherm. The coefficient k can be called the kinetic constant. With this temporal dependence of the adsorption activity coefficient, Eq. (3.21) becomes:

$$b(t)c_p = \frac{\omega_p \Gamma_{pj}}{(1-\theta_p)^{\omega_j/\omega_p}} \exp[-2a_p \left(\frac{\omega_j}{\omega_p}\right) \theta_p] \tag{3.34}$$

It is demonstrated that the value of b_0 is remarkably lower than b_1 obtained from the fitting of the surface pressure isotherm given by Eqs. (3.20) and (3.21) (cf. Chapter 5.1.1.). This value

of b_0 appears actually to be rather close to the corresponding parameter obtained for BLG adsorbed at the W/A surface [43, 77]. This fact allows speculating that in the beginning of the BLG adsorption layer formation process, i.e. at short adsorption times, the structure of the interfacial layers at the W/TD interface is similar to that at the W/A surface. On the contrary, the b_m value is shown to be approximately equal to b_1.

3.5.2. Lucassen and van den Temple Model to Describe Surface Relaxations

The surface dilational viscoelasticity modulus has been defined by Gibbs as the increase in surface tension γ for a small relative increase of surface area d$A/A = d\ ln\ A$ [78]:

$$E = \frac{d\gamma}{dlnA} \tag{3.35}$$

The frequency ($f = \omega/2\pi$) dependent dilational modulus have been derived by Lucassen and van den Tempel assuming a diffusion controlled exchange of matter mechanism [79, 80]. The surface dilational modulus can be expressed as a complex number: $E = E' + iE''$ which can be split into the visco-elasticity modulus |E| and the phase angle ϕ:

$$|E| = \sqrt{(E')^2 + (E'')^2} \quad \text{and} \quad \phi = arctan(E''/E') \tag{3.36}$$

where the real part E' is the storage modulus equal to the dilational elasticity contribution and the imaginary part E'' is the loss modulus equal to the viscosity contribution [81].

$$E(i\omega) = E' + iE'' = E_0 \frac{\sqrt{i\omega}}{\sqrt{i\omega}+\sqrt{2\omega_D}} \tag{3.37}$$

$$E'(\omega) = E_0 \frac{\sqrt{\omega_D/\omega}}{1+2\sqrt{\omega_D/\omega}+2\omega_D/\omega} \tag{3.38}$$

$$E''(\omega) = E_0 \frac{\sqrt{\omega_D/\omega}}{1+2\sqrt{\omega_D/\omega}+2\omega_D/\omega} \tag{3.39}$$

which contain the limiting elasticity $E_0 = \mathrm{d}\Pi/\mathrm{dln}\Gamma$ and characteristic frequency of diffusion relaxation $\omega_D = \frac{D}{2}(\frac{dc}{d\Gamma})^2$.

4. MATERIALS AND EXPERIMENTAL METHODS

4.1. Materials

4.1.1. Protein (β-lactoglobulin, BLG)

The protein β-Lactoglobulin (BLG) used in the present studies has a molecular weight of 18,300 Da and was isolated from whey protein isolate WPI 895 (Fonterra, New Zealand, Lot No. CT08) containing 96.3% (w/w) native whey protein (20.2% α-la, 45.5% BLG A, 33.5% BLG B), 1.4% caseinomacropeptide (CMP), 6.4% moisture and 1.8% ash and supplied by José Toro-Sierra from Technische Universität München [82]. The supplied BLG was dissolved in buffer solution and purified with activated charcoal (BLG/charcoal mass ratio 1/3) [83] to prepare BLG stock solutions of 10^{-4} mol/l. The solution was stirred for 30 min and then filtered with Millipore filter (GE infrastructure, USA) which has a pore size of 0.45 µm. The prepared stock solutions were kept in the refrigerator no longer than 5 days and required solutions were prepared from these stock solutions by dilution with buffer. A buffer mixture of Na_2HPO_4/citric acid (purchased from Fluka, Germany, assay > 99%) with various buffer concentrations of C_{buff} = 1, 10 and 100 mM were used to prepare protein aqueous solutions at pH 3, 5 and 7. All buffer solutions in this work have been prepared with ultrapure Milli-Q water (resistivity = 18.2 MΩ cm).

4.1.2. Oil Phase (n-tetradecane, TD)

The oil phase chosen in this work is n-tetradecane (TD) (≥ 99%) purchased from Alfa Aesar, purified first by distillation and then by washing several times with chromatography resins Florisil 60-100 mesh. The interfacial tension of the TD against buffer solution without BLG was 52.5 mN/m at room temperature of T = 22 ± 1 ° C.

4.2. Experimental Methods

4.2.1. Profile Analysis Tensiometer (PAT-1)

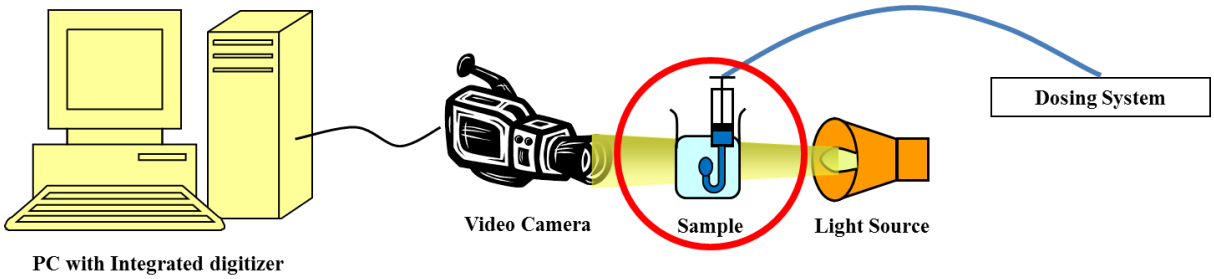

Figure 4 Scheme of the Profile Analysis Tensiometer, PAT-1 (SINTERFACE Technologies, Germany).

In the field of surface tension measurement, drop shape techniques are widely used for several decades. Since the correct value of surface tension of nearly spherical drops or bubbles can be difficult to find, axisymmetric drop shape analysis (ADSA) is successfully used for surface tension measurement [84]. The coordinates of the drop profile extracted from the image taken by an electronic camera are compared with those from the theoretical Laplacian curve calculated for a known surface tension using a nonlinear optimization process [85, 86, 87]. With the development of electronic computers, ADSA technique became accurate due to the pioneering work of Neumann and his group [88].

In this study, dynamic interfacial tension experiments have been performed with the drop and bubble Profile Analysis Tensiometer PAT-1 (SINTERFACE Technologies, Germany) [89]. The scheme of this instrument is shown in Figure 4. It is composed of a cell where a drop or a bubble is formed at the tip of a vertical or U-shape capillary, a dosing system, a light source and a video camera which is connected to a computer with an integrated digitizer. The main principle of this method is to determine the surface tension of liquid or the interfacial tension between two immiscible liquids based on the shape of a drop or bubble. The coordinates of drop taken from a video image by the camera, for instance, is fitted with the Gauss-Laplace equation, as schematically shown in Figure 5.

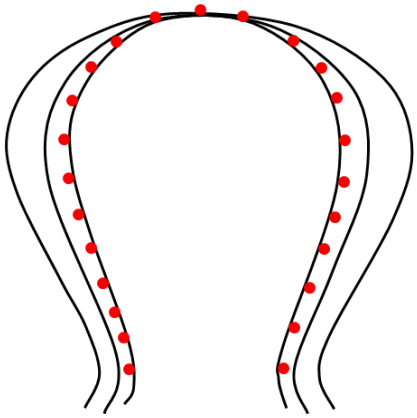

Figure 5 Coordinates of a buoyant drop profile (red dots) and calculated profiles.

$$\gamma\left(\frac{1}{R_1}+\frac{1}{R_2}\right)=\Delta P \tag{4.1}$$

here γ is the interfacial tension, R_1 and R_2 are the two principal radii of interface curvature, and ΔP is the pressure difference across the interface. This equation describes the mechanical equilibrium status of two homogeneous fluids separated by an interface. It shows the relationship between the interfacial tension and the curvature of a liquid meniscus which is given by Gauss-Laplace equation.

$$\Delta P=\Delta P_0+\Delta\rho g z \tag{4.2}$$

where ΔP_0 is the pressure difference at a reference plane, $\Delta\rho$ is the density difference, g is the local gravitational constant, and z is the vertical height measured from the reference plane. Surface force tends to make the drop spherical while gravity tends to elongate the drop. The shape of the drop is determined by a combination of these two forces: the surface tension and the gravity effects. Therefore, the interfacial tension can be determined from the shape of the drop.

The model profile can be numerically calculated using the Gauss-Laplace equation [90]. This equation can be represented as a set of three first-order differential equations by the geometric parameters of the drop profile as shown in Figure 6. Using a fourth-order Runge-Kutta integration algorithm a time efficient solution can be performed [91].

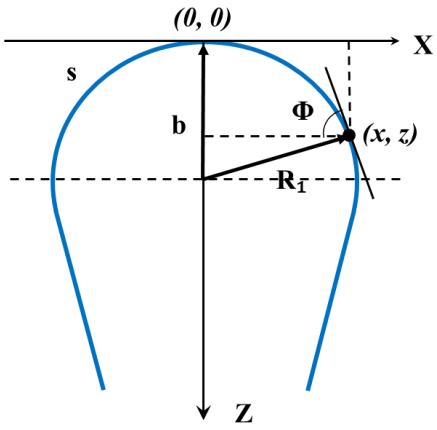

Figure 6 Definition of geometric parameters of the drop profile.

$$\frac{dx}{ds} = \cos \Phi \tag{4.3}$$

$$\frac{dz}{ds} = \sin \Phi \tag{4.4}$$

$$\frac{d\Phi}{ds} = \frac{1}{R_1} = \pm \frac{\Delta \beta z}{b^2} + \frac{2}{b} - \frac{\sin \Phi}{x} \tag{4.5}$$

$$\beta = \frac{\Delta \rho g b^2}{\gamma} \tag{4.6}$$

Here s is the arc length, Φ is the normal angle, x and z are the coordinates of the profile points, R_1 is the radius of curvature at the point (x, z), b is the radius of curvature at $(0, 0)$, and β is the shape factor.

The Profile Analysis Tensiometer PAT-1 allows measurements of dynamic surface and interfacial tension in a time range from a few seconds up to hours and even days with a constant interfacial area or volume of the drop or bubble. It requires very small amounts of sample and it is suitable for numerous experiments such as at liquid/vapour [92], liquid/gas and liquid/liquid interfaces [63]. With a pre-set frequency and amplitude an external perturbation in form of a harmonic oscillation can be generated in the frequency range between 10^{-5} and 10^{-1} Hz. The embedded software provides not only the interfacial tension and the contact angle, but also the drop or bubble surface area and volume.

All measurements reported in this work were performed with PAT-1 for time intervals of 84,500 s (about 23.5 hours) by using the buoyant drop configuration using a TD drop formed

in the aqueous BLG solution of 25ml to minimize the depletion of BLG molecules from the bulk due to BLG adsorption at the interface [71]. In addition, harmonic oscillations are performed to gain information about the interfacial dilational rheology of the BLG solution/TD layers.

4.2.2. Drop Bubble Micro Manipulator (DBMM)

The Drop Bubble Micro Manipulator DBMM (SINTERFACE Technologies, Germany) is an instrument to analyse the interaction between two droplets or two bubbles or a single droplet and a bubble in an immiscible liquid medium [93, 94, 95]. It is an extention module of the Oscillating Drop and Bubble pressure Analyser ODBA (SINTERFACE Technologies, Germany) which is using the capillary pressure technique [96]. As shown in Figure 7 DBMM consists of two identical cells which are each equipped with a syringe dosing system, pressure sensor, piezo-excitation actuator for exact drop size and drop oscillations and a capillary. The capillaries are mounted such that they face to each other. One cell is fixed to the instrument while the second cell can be moved in xyz-directions relative to the first cell. The capillaries can be designed in various size and materials [95] but the one used here are stainless steel capillaries which had inner and outer diameter of 0.67 mm and 0.90 mm, respectively.

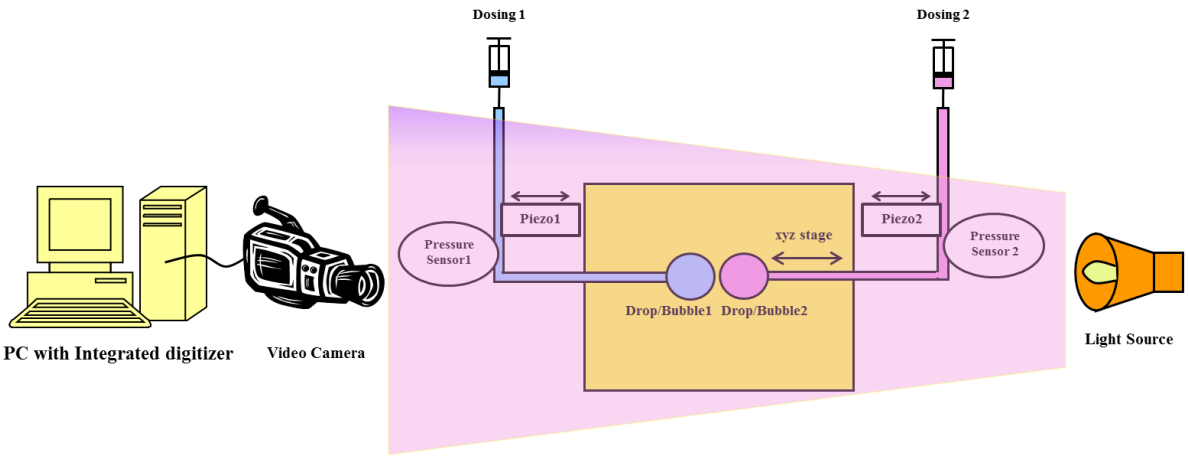

Figure 7 Scheme of the Drop Bubble Micro Manipulator, DBMM (SINTERFACE Technologies, Germany) with its main elements.

The standard CCD camera allows video recording with a sampling rate of 20 fps. Simultaneously a dedicated software enables us to determine the radii of the two objectives on both sides and the corresponding capillary pressure in real time. These values are recorded in a file with a selected data acquisition rate. The instruments allow several experimental protocols such as shown in Figure 8, but the easiest experiment is just approaching two droplets against each other. In this case the two droplets are prepared one by one and brought into contact by moving the mobile one towards the fixed one. Note, it is needed to bring the two menisci right opposite to each other in one symmetry axis or into any other planned position. After contacting of the drops the time until coalescence, i.e. life time of the thin film created between the drops, can be determined. The coalescence is detected by a very steep and sudden change in capillary pressure registered in both cells [94, 95]. Depending on the amount of adsorbed layer of stabilising agent such as protein or surfactant, this measured life time can be seconds, minutes or hours.

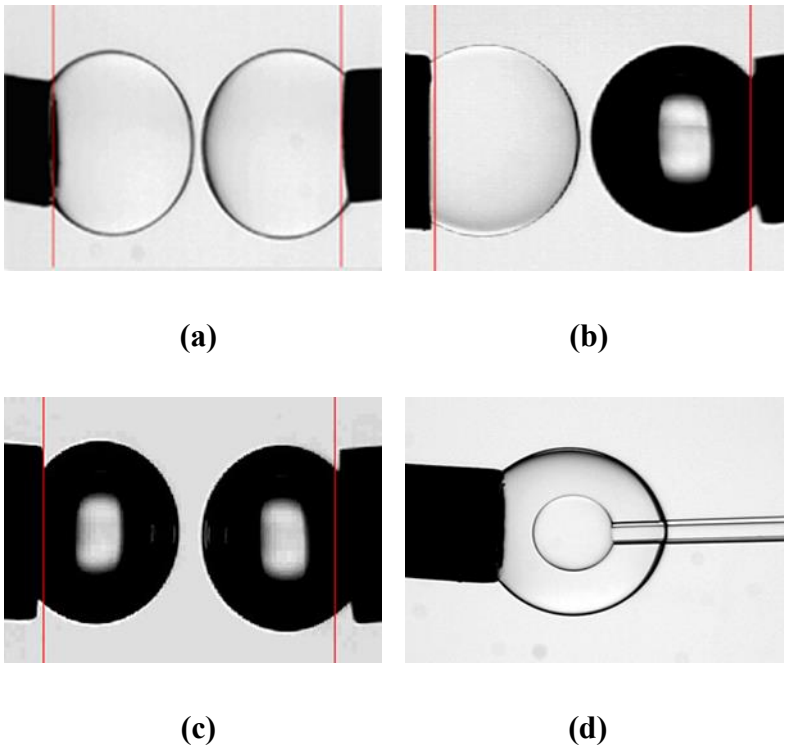

Figure 8 Experimental examples of DBMM: **(a)** two hexane droplets in water, **(b)** hexane droplet (left) and air bubble (right) in water, **(c)** two air bubbles in water, **(d)** water droplet in hexane droplet immersed in water.

5. RESULTS AND DISCUSSION

The process of adsorption can be defined by dynamic interfacial tensions, while the equilibrium values correspond to the adsorption isotherm. The measurement of dynamic interfacial tension is relatively easy but efficient for analyzing the kinetics and rheology of adsorbed molecules. In a large series of experiments we measured the interfacial tension of a TD drop ageing in BLG solutions at various BLG concentrations in the range of 10^{-10} – 2×10^{-6} mol/l in the presence of 10 mM buffer at pH 3, 5 and 7. To study the effect of ionic strength, C_{buff} = 1 mM and C_{buff} = 100 mM were also used, however, only for 10^{-6} mol/l BLG solutions. The interfacial pressure $\Pi = \gamma_0 - \gamma$ was calculated with γ_0 = 52.5 mN/m for the pure aqueous buffer/TD interface. In order to obtain information about the interfacial dilational rheology of the studied BLG adsorbed layers, sinusoidal oscillations of the drop surface area (generated by simusoidal changes of the drop volume) were applied and the interfacial tension responses were recorded [89, 97]. In Figure 9 the timeline of the experimental protocol is shown. It contains periods of area oscillations at a fixed frequency of 0.1 Hz in the course of adsorption and at a set of different frequencies of 0.01, 0.02, 0.05, 0.1 and 0.2 Hz performed after the adsorption equilibrium was reached, i.e. after 80,000 s.

(a)

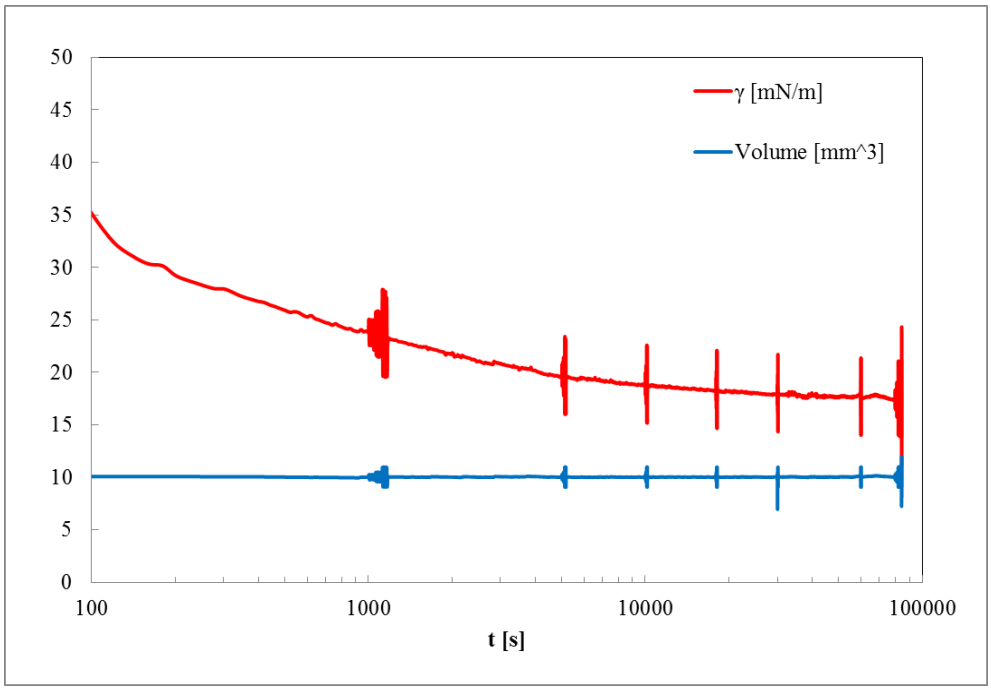

(b)

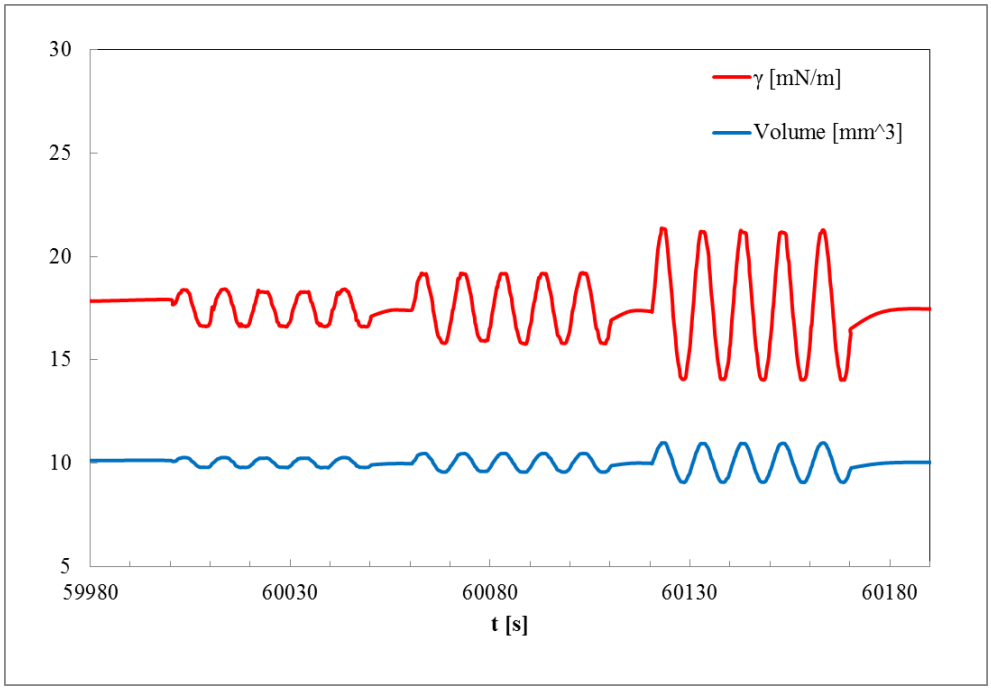

(c)

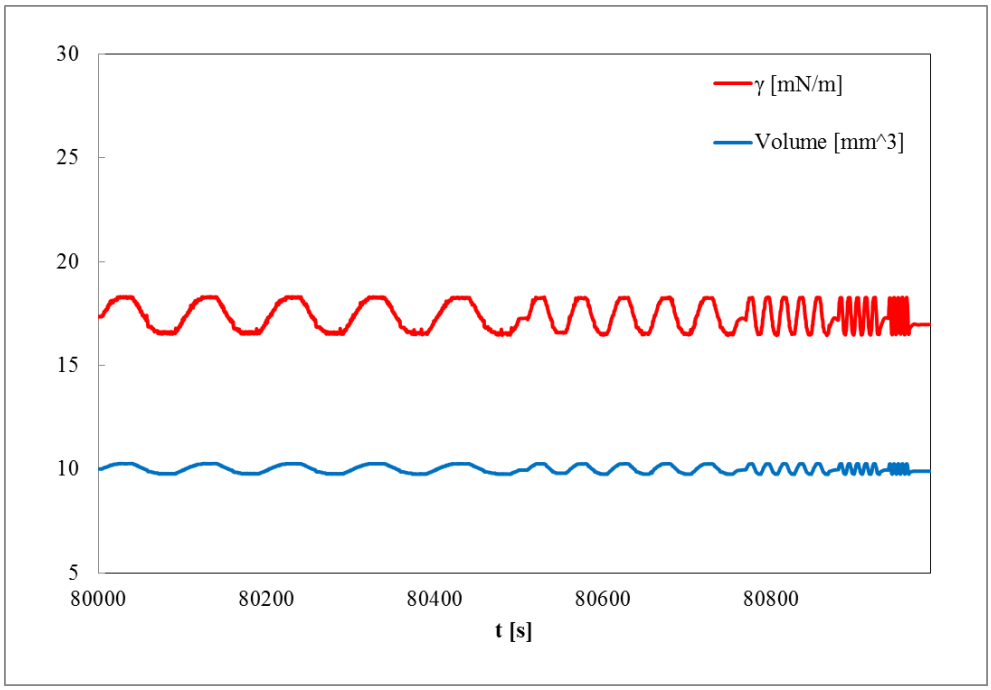

Figure 9 Timeline of the experimental protocol; γ – interfacial tension, Volume – volume of a TD drop in BLG solutions (a) general view, (b) a set of oscillations at frequency 0.1 Hz which is used at 1000, 5000, 10 000, 18 000, 30 000, 60 000 s, (c) oscillations at frequency 0.01, 0.02, 0.05, 0.1, 0.2 Hz after 80 000 s.

5.1. Dynamic Interfacial Pressures of BLG Solutions

The dynamic interfacial tension of protein solutions is different from that of usual surfactants in many aspects. It is mainly because of the conformational changes of protein molecules at the adsorption layer. At low bulk concentrations, the protein molecules start to adsorb at the interface in a folded conformation and they find quite a large free space at the interface. When these molecules become unfolded, the molecules occupy a larger interfacial area. Once there are sufficiently many molecules adsorbed, i.e. once a sufficient amount of protein adsorption is reached, the interfacial tension starts to decrease. The interfacial tension decreases immediately, however, when the protein bulk concentration is sufficiently high. Often a further weak decrease of interfacial tension can be observed beyond the state of a complete surface coverage has been reached. This can be explained by molecular aggregation at the interface or by the formation of multilayers [67]. The rate of adsorption is related with conformational changes, molecular rearrangement, and diffusional processes of molecules into the adsorption layer.

Most proteins reveal a higher affinity to adsorb at the water/oil interface than at the W/A surface. This is also valid for BLG solutions. It can be explained by the data in this thesis and via a direct comparison with the experiments performed by Ulaganathan et al. in [25, 32]. The interfacial tension of freshly formed TD drop in an aqueous BLG solution at the interface is about 52.5 mN/m, while the surface tension of a freshly formed air bubble in an aqueous BLG solution at the surface is about 72.5 mN/m at room temperature 22 ± 1 ℃.

5.1.1. Effect of BLG Bulk Concentration

Figure 10 illustrates the dynamic interfacial pressure data for different BLG concentrations at pH 3 at the W/TD interface as measured by profile analysis tensiometry (PAT-1) [98, 99]. As expected, the interfacial pressure values increase and the initial adsorption rate is faster with increasing BLG concentration [27, 100]. At higher BLG concentrations (above 10^{-6} mol/l, see Fig. 10) a noticeable plateau is reached during the measurements while the interfacial pressures at lower concentration continuously increase in the studied time region. At the same time the rate of adsorption is slower at low concentrations, as it is expected. Therefore, it can

be assumed that at the maximum measurement time of 80,000 s the surface layers are close to the equilibrium state of adsorption only for the higher BLG bulk concentrations.

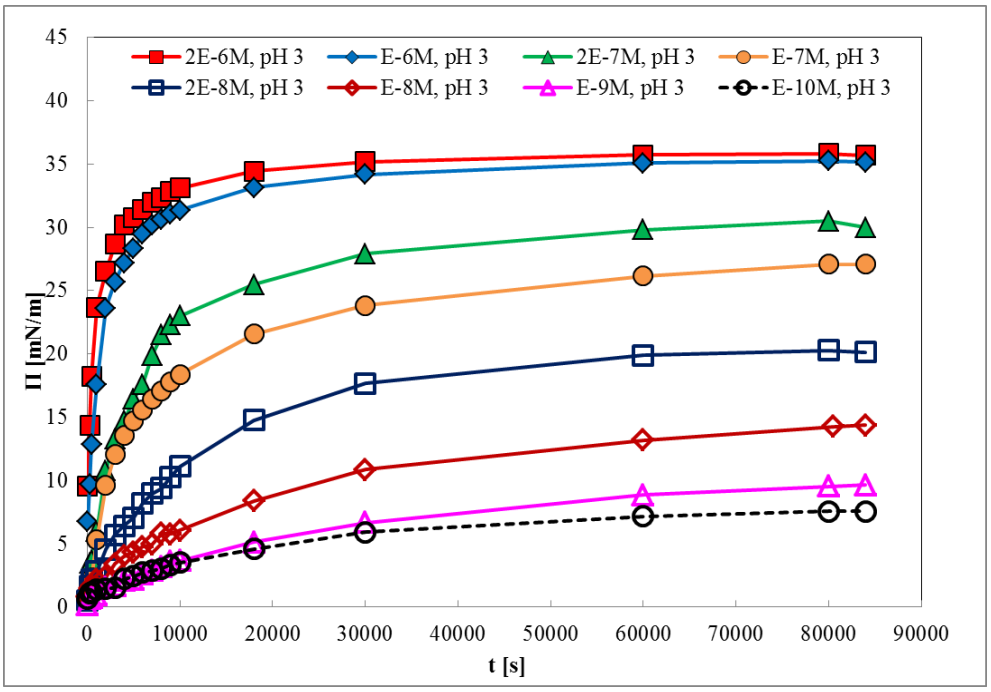

Figure 10 Dynamic interfacial pressure Π(t) for different BLG concentrations at pH 3 at the W/TD interface (lines are guides for the eye).

In the same way, the dynamic interfacial pressure measured for a series of aqueous BLG solutions at the W/TD interface in the concentration range between 10^{-10} mol/l and 2×10^{-6} mol/l at pH 5 and 7 are studied and summarised in Figure 11 and 12, respectively. Similarly, as discussed for the case of pH 3, the adsorption rate is increasing with increasing BLG concentration. The difference is that the final interfacial pressure value of the highest studied BLG concentration at pH 7 is about 5mN/m lower than that of pH 3 and 5. The dependence of solution pH on the interfacial tension isotherms will be discussed in more detail in the next section.

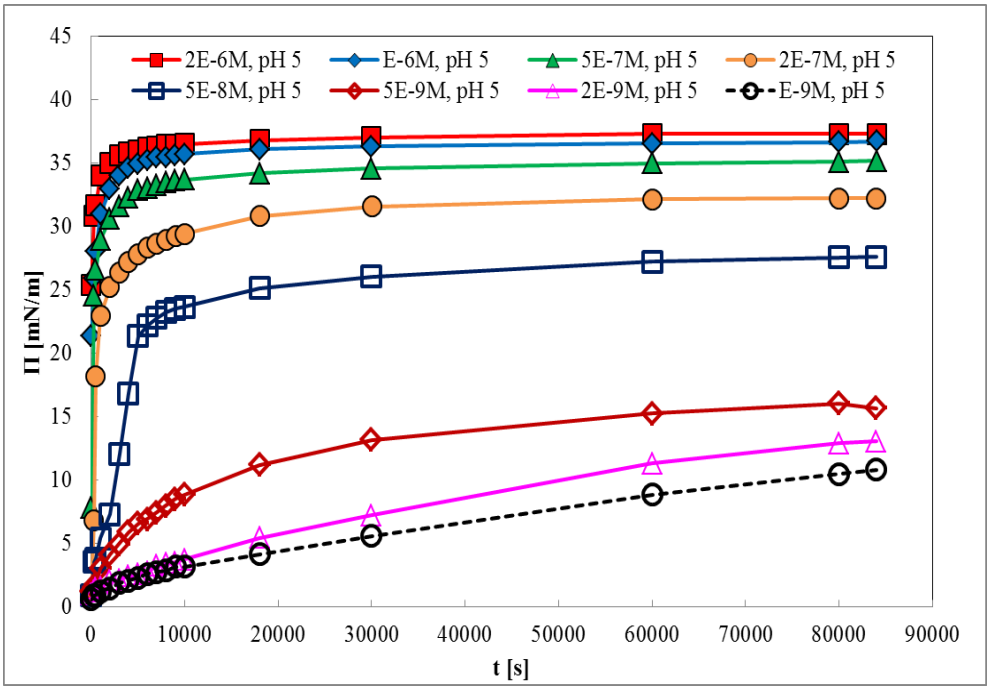

Figure 11 Dynamic interfacial pressure Π(t) for different BLG concentrations at pH 5 at the W/TD interface (lines are guides for the eye).

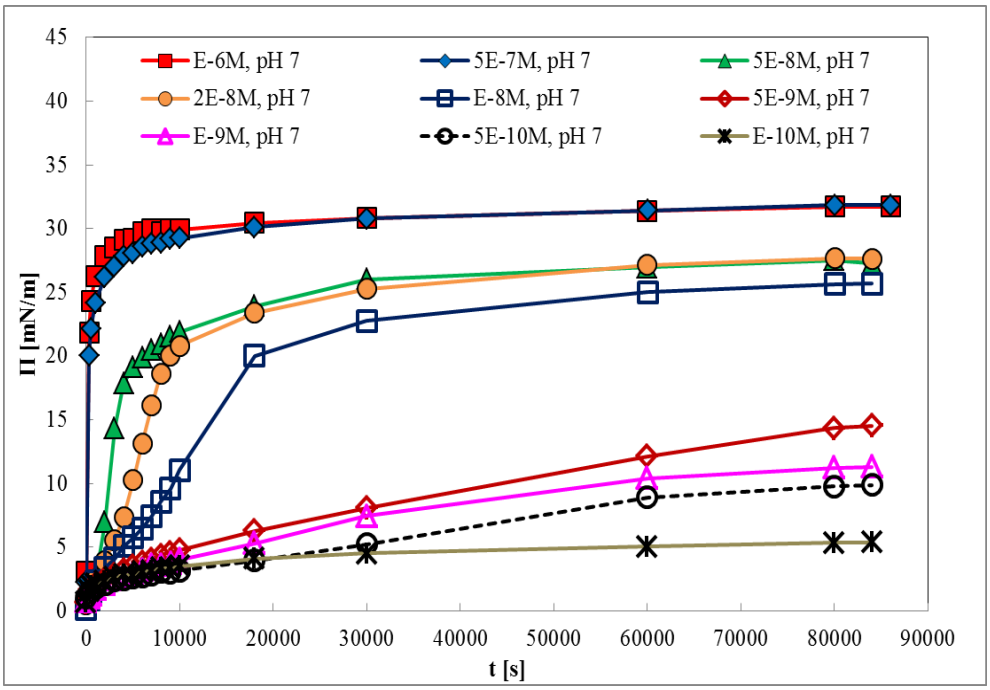

Figure 12 Dynamic interfacial pressure Π(t) for different BLG concentrations at pH 7 at the W/TD interface (lines are guides for the eye).

In the previous chapter 3.5.1, a diffusion controlled model to describe the adsorption kinetics was derived. To describe experimental data of protein adsorption, a mechanism which takes the conformational changes of the adsorbed protein molecules into account is considered. Hence, a combined model of diffusional transport and an additional time process is proposed. The TDC model ("the model with time-dependent adsorption activity coefficient") is given by a diffusional transport and the Eqs. (3.20), (3.24), (3.28), (3.29), (3.33), (3.34), while the model which implements Eqs. (3.20), (3.21), (3.24), (3.28), (3.29) together with a diffusional transport is referred to as the TIC model ("the model with time-independent adsorption activity coefficient"). Hence, the TIC model corresponds to the classical diffusion controlled adsorption kinetics while the TDC model is based on a mixed mechanism of diffusional transport of protein molecules in the solution bulk and a conformational change at the interface characterised by a change in the adsorption activity coefficient.

In Figure 13 the experimental dynamic interfacial tensions (blue curves) for a bulk concentration of 10^{-7} mol/l BLG at pH 3 at the W/TD interface are shown together with three calculated curves for diffusion coefficient D; black curves – 7×10^{-11} m^2/s, green curve – 1.3×10^{-11} m^2/s, and red curve – 2×10^{-10} m^2/s. The black curve has been calculated with the TIC model for a diffusion controlled adsorption kinetics taking the spherical shape of the TD drop (surrounded by the aqueous BLG solution) into consideration. The parameters used for the model calculations are those in Table 1, and the radius of the drop is assumed to be 1.2 mm. The optimum diffusion coefficient for these data is 7×10^{-11} m^2/s. As one can see, however, the description of the experimental data is not very good.

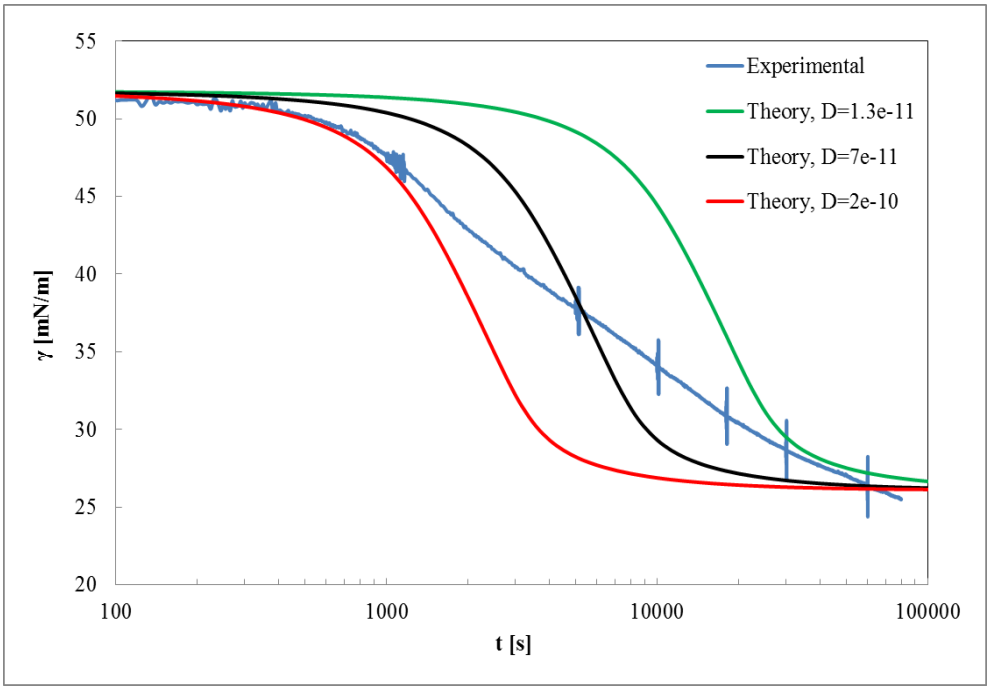

Figure 13 Dynamic interfacial tensions at a bulk concentration of 10^{-7} mol/l BLG at pH 3 at the W/TD interface; blue curves- experimental data, black curves – calculated with the optimum diffusion coefficient using diffusion controlled adsorption model $D=7\times10^{-11}$ m^2/s, green curve $D=1.3\times10^{-11}$ m^2/s, red curve $D=2\times10^{-10}$ m^2/s; data are taken from [42].

To get a reasonable description of the experimental data a large diffusion coefficient is required at the beginning of the adsorption process for some initially adsorbed BLG molecules at the interface or some possible convection around the drop. The longer the adsorption process lasts, the smaller is the diffusion coefficient required for a good agreement between theory and experiment. However, to improve the agreement between the experimental data and their theoretical description, a mechanism which describes the conformational changes of BLG molecules in the adsorption layer can be considered, as it was discussed further above. It is realistic to assume that conformational changes in the interfacial layer can lead to an increase in the surface activity of the protein molecules. Thus, let us propose that the adsorption activity of the protein increases during the process of adsorption. At short adsorption times we assume an adsorption constant b equal to b_0. This coefficient increases with increasing adsorption time t due to the structure formation of the protein and TD molecules at the interface. Hence, at the moment the adsorption equilibrium has been reached the coefficient b_m should have the value obtained from fitting the experimental adsorption isotherm [42].

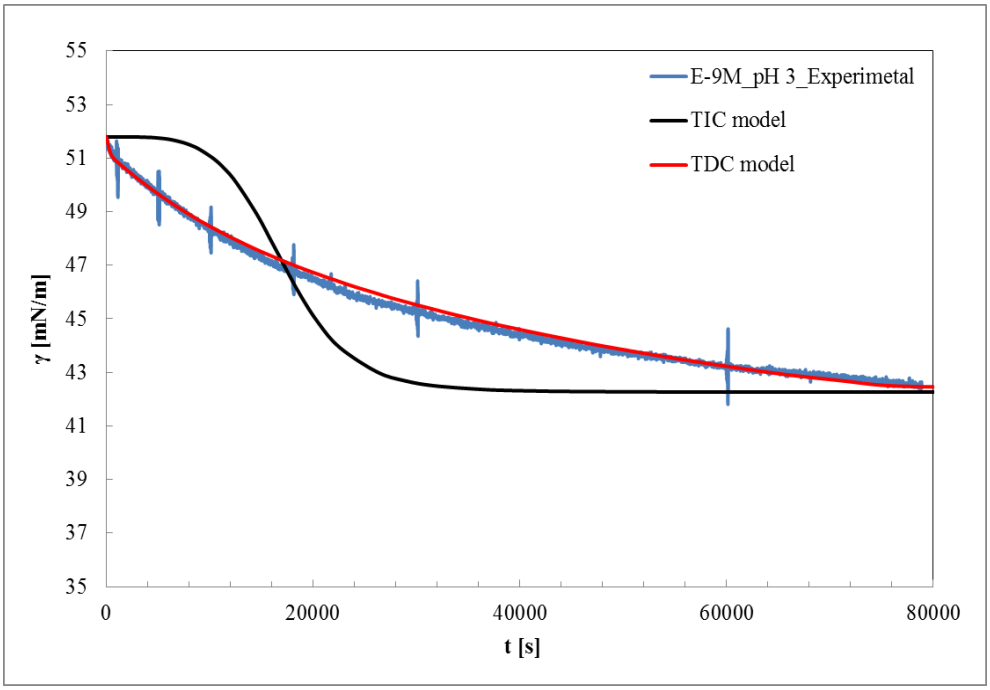

Figure 14 Dynamic interfacial tensions at pH 3 for BLG at the W/TD interface at a bulk concentration of 10^{-9} mol/l; blue curve – experimental data, black curve – calculated with the TIC model, red curve – calculated with the TDC model. For all other studied concentrations the data are plotted in Appendix 1; data are taken from [42].

In Figure 14 and Appendix 1 the experimental data for different bulk concentrations of BLG are shown together with model calculations. The black curves correspond to a best fitting with the TIC model for a diffusion controlled adsorption kinetics (using the parameters given in Table 1), and the red curves were obtained using the TDC model. Using the new TDC model proposed here, which is based on the assumption of an additional change in the surface activity of the adsorbing BLG molecules, it is possible to describe the measured dynamic interfacial tensions in a much better way. The used diffusion coefficients for the two models are summarised in Figure 15. The values of the constant k in the given equation $b_1=b_0(1+k\times t_{max})$ (see Eq. (3.33)) for an optimum fitting of the experimental data are summarised in Table 1. Note, the value of b_m is close to the one used to describe the isotherm, i.e. the equilibrium state of the adsorption layer, which is an important fact for the applicability of the proposed kinetics model.

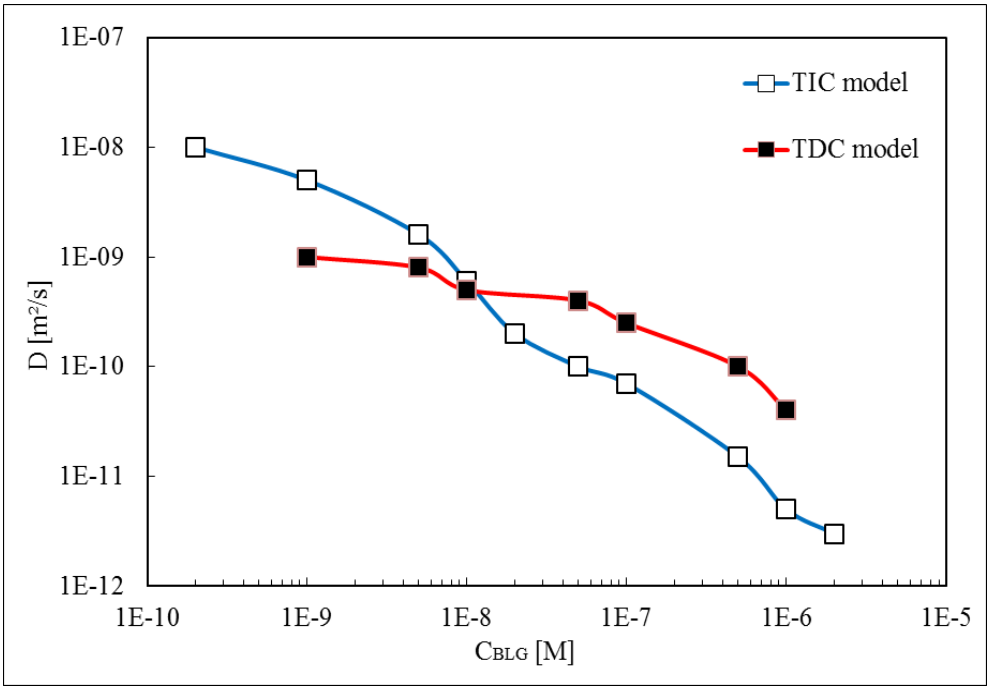

Figure 15 Diffusion coefficients obtained from a best fitting of experimental data as a function of BLG bulk concentration; open symbols and blue curve - the TIC model, black symbols and red curve - the TDC model; data are taken from [42].

Dynamic interfacial tensions at pH 5 and 7 for different concentration of BLG at the W/TD interface using the TDC model are studied in the same manner as the solutions with pH 3. In Figures 16 and 17 the experimental data for different bulk concentrations of BLG are shown together with model calculations at pH 5 and 7, respectively. While the black curves refer again to the TIC model, the red curves are obtained with the TDC model taking a diffusional transport and additionally conformational changes into account. The values of the diffusion coefficients were in the range between 10^{-9} and 10^{-11} m^2/s at pH 5 and between 10^{-9} and 10^{-10} m^2/s at pH 7. In Table 2 and 3 the values of the respective model parameters for pH 5 and 7 are summarized, respectively. Note, at pH 5 the values of b_m are almost identical to the value 6.0×10^5 m^3/mol obtained for the isotherm and at pH 7 the values of b_m agree quite well with the one 4.8×10^5 m^3/mol obtained for fitting the isotherm as shown in Figure 22 (a) and Table 4. For all other studied concentrations besides those displayed here the corresponding results are plotted in Appendices 2 and 3.

Table 1 Values for the parameters in the adsorption activity equation $b_m=b_0\,(1+k\times t_{max})$ valid at pH 3; data are taken from [42].

BLG concentration 10^{-7} M	b_0 10^3 m^3/mol	k 10^{-4} s^{-1}	t_{max} 10^4 s	b_m 10^4 m^3/mol
10	2.5	8.0	4.5	9.3
5	3.0	7.0	3.5	7.7
1	2.0	7.4	6.7	10.1
0.5	1.0	10	6.0	6.1
0.1	2.5	3.5	8.0	7.25
0.05	2.5	6.0	7.0	10.8
0.01	3.5	5.0	6.0	10.9

Table 2 Values for the parameters in the adsorption activity equation $b_m=b_0\,(1+k\times t_{max})$ valid at pH 5; data are taken from [42].

BLG concentration 10^{-7} M	b_0 10^3 m^3/mol	k 10^{-4} s^{-1}	t_{max} 10^4 s	b_m 10^5 m^3/mol
0.5	150	0.32	5.5	4.1
0.2	2.0	30	4.0	2.4
0.1	1.0	28	8.0	2.24
0.05	60.0	65.0	5.5	215.1
0.02	3.0	8.0	9.0	2.16

Table 3 Values for the parameters in the adsorption activity equation $b_m=b_0\,(1+k\times t_{max})$ valid at pH 7; data are taken from [42].

BLG concentration 10^{-8} M	b_0 10^3 m^3/mol	k 10^{-4} s^{-1}	t_{max} 10^4 s	b_m 10^5 m^3/mol
5	3.0	45	3.5	4.7
2	2.5	80	4.5	7.2
1	2.5	40	7.0	7.0
0.5	60	0.65	5.5	2.7
0.05	1.0	10	6.0	6.1

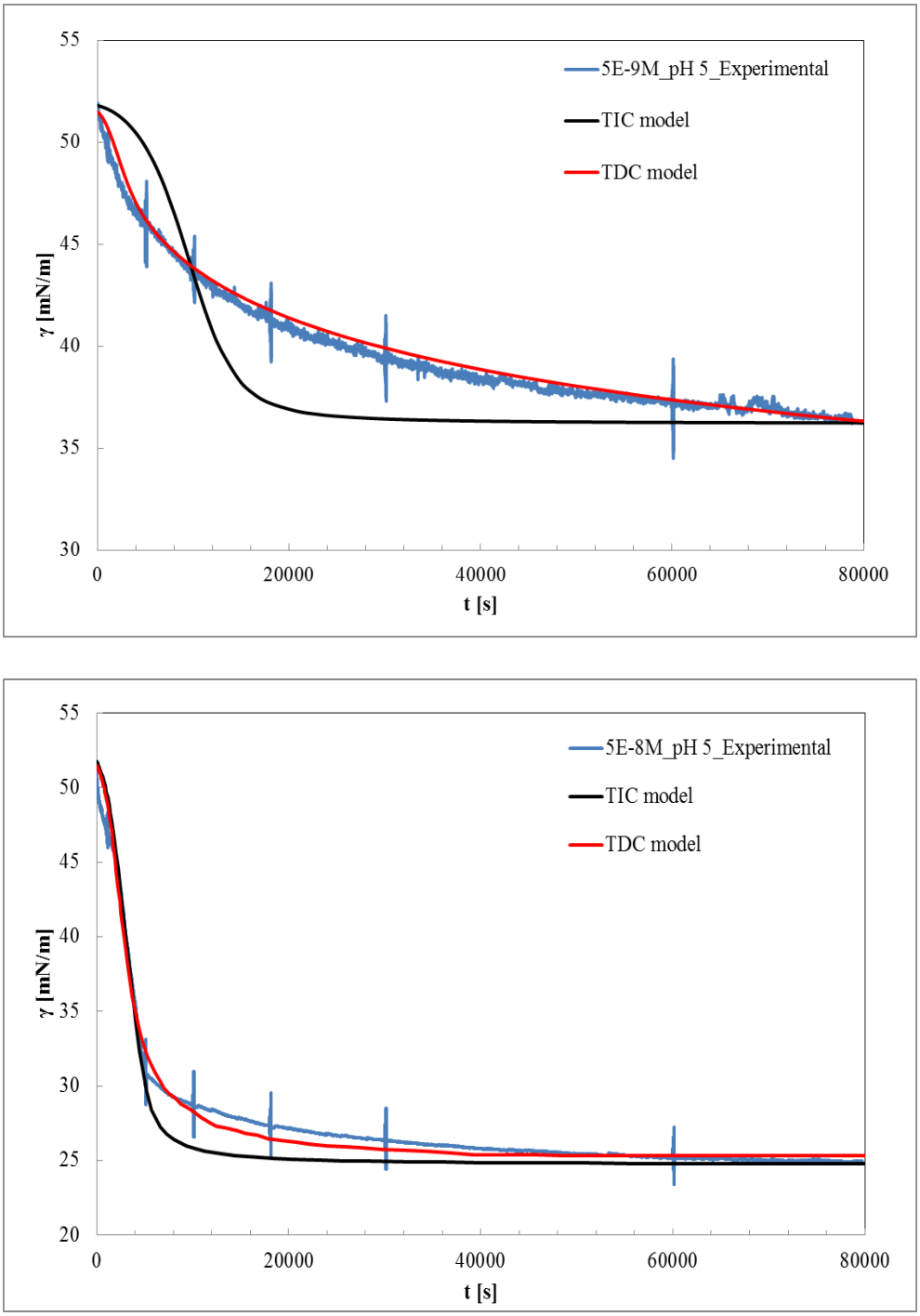

Figure 16 Dynamic interfacial tensions at pH 5 for BLG at the W/TD interface at a bulk concentration of **(top)** 5×10^{-9} mol/l, **(bottom)** 5×10^{-8} mol/l; blue curves – experimental data, black curves – calculated with the TIC model, red curves – calculated with the TDC model. For all other studied concentrations the data are plotted in Appendix 2; data are taken from [42].

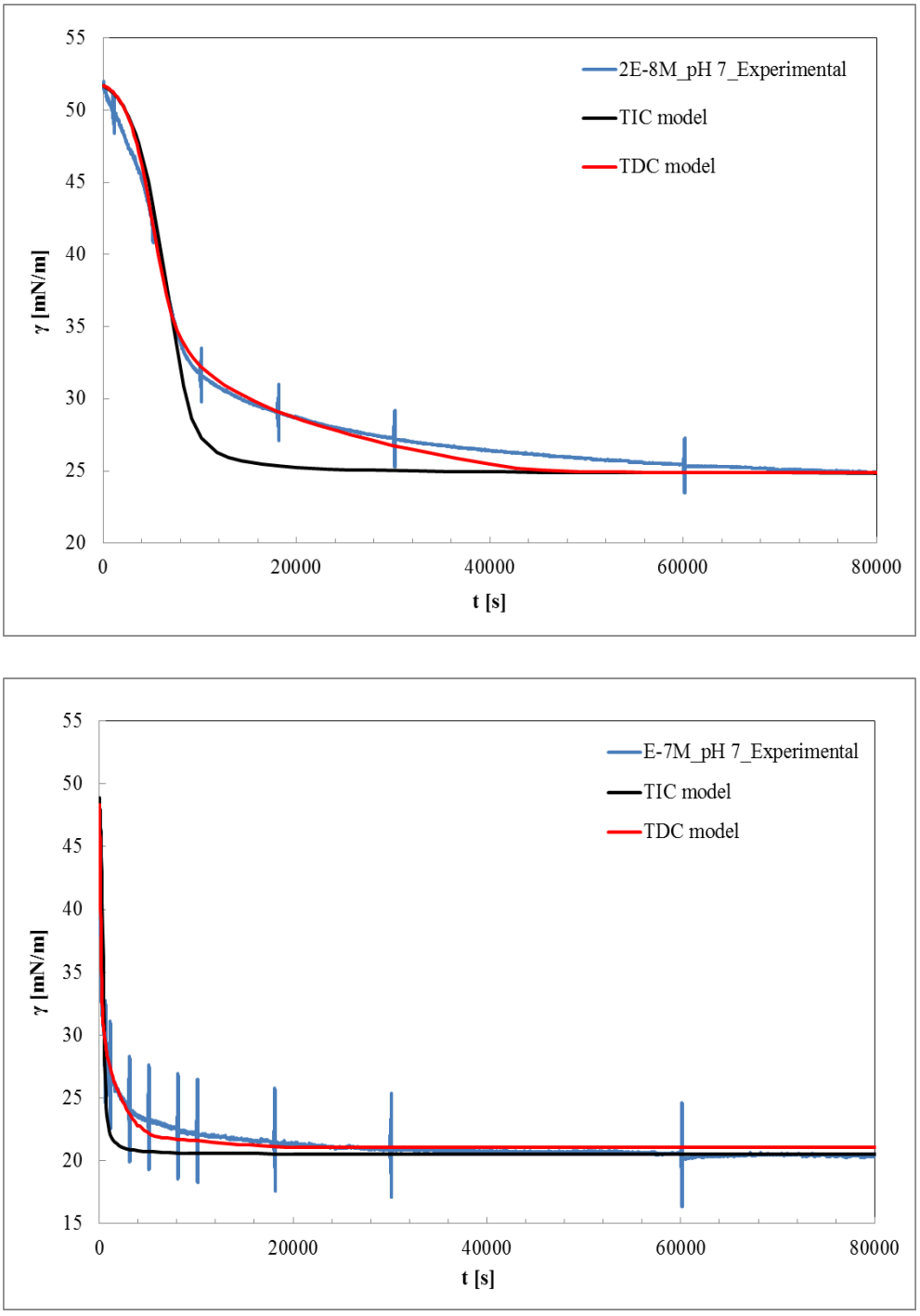

Figure 17 Dynamic interfacial tensions at pH 7 for BLG at the W/TD interface at a bulk concentration of **(top)** 2×10^{-8} mol/l, **(bottom)** 10^{-7} mol/l; blue curves – experimental data, black curves – calculated with the TIC model, red curves – calculated with the TDC model. For all other studied concentrations the data are plotted in Appendix 3; data are taken from [42].

5.1.2. Effect of Solution pH

The evolution of dynamic interfacial pressure with time for different BLG concentrations in the range of 10^{-9} – 10^{-6} mol/l at three pH values pH 3, 5 and 7 at the W/TD interface are shown in Figure 18 and Appendix 4. To illustrate the effect of pH on the interfacial pressure, corresponding data for three pH values are discussed at different concentrations. At a relatively low BLG concentration of 10^{-9} mol/l (Figure 18 (a)), the Π(t) data for all three pH values pH 3, 5 and 7 are quite similar. At a BLG concentration 10^{-8} mol/l (Figure 18 (b)), we observed that the adsorption kinetics at pH 3 results in the lowest Π values at any time of adsorption and this trend continues until a BLG concentration of 5×10^{-7} mol/l (Figure 18 (d)). Beyond this BLG concentration the lowest Π values were measured at pH 3, however, it crosses the data for pH 7 at 5,000 s for $C_{BLG}=10^{-6}$ mol/l (Figure 18 (e)) and 3,000 s for $C_{BLG}=2\times10^{-6}$ mol/l (Figure 19). In addition, at a BLG concentration 5×10^{-8} mol/l (Figure 18 (c)), we observed that generally the adsorption kinetics at pH 5 result in the highest Π values at any time of adsorption and this trend continues for all other higher protein concentrations in the range studied in this work. On the contrary, dynamic interfacial pressure data shown in Figure 18 (b) indicate an unfamiliar behaviour. This is due to its low concentration. We assumed that the maximum measurement time of 80,000 s is close to equilibrium in which the protein adsorption layer is regarded to as a steady regime although it is far from its equilibrium state. At the relatively high protein concentrations, the final interfacial pressure data which is measured after 80,000 s of adsorption reaches values of about 35 mN/m for pH 3 and 5, whereas it reaches only a value of around 30 mN/m for pH 7 (cf. also the summary of isotherms in Figure 23 (a)).

(a)

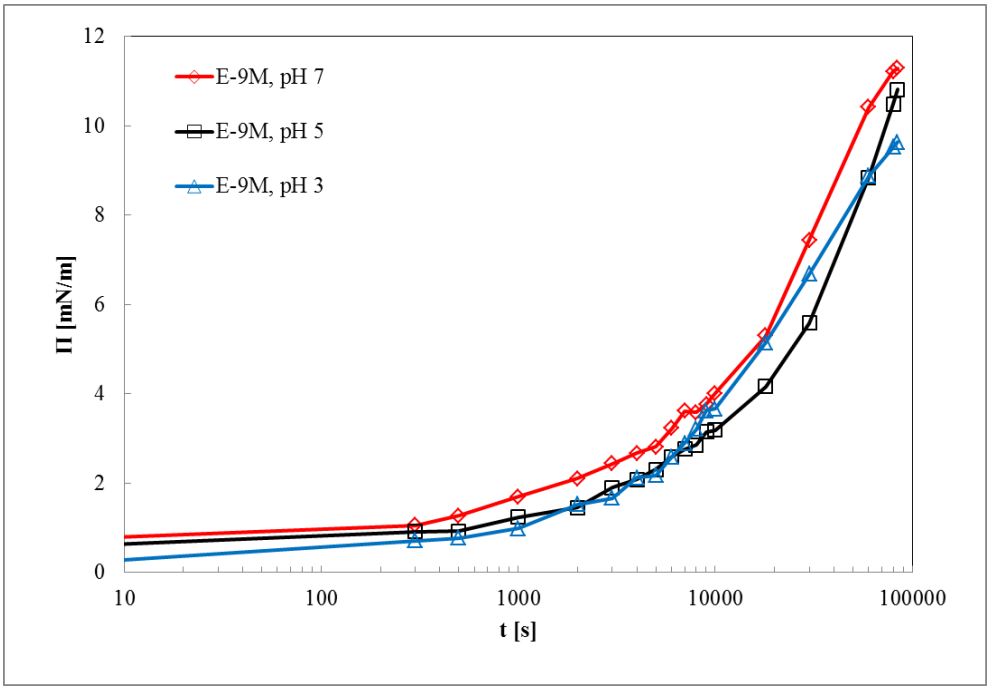
E-9M, pH 7
E-9M, pH 5
E-9M, pH 3
Π [mN/m]
t [s]
0
2
4
6
8
10
12
10
100
1000
10000
100000

(b)

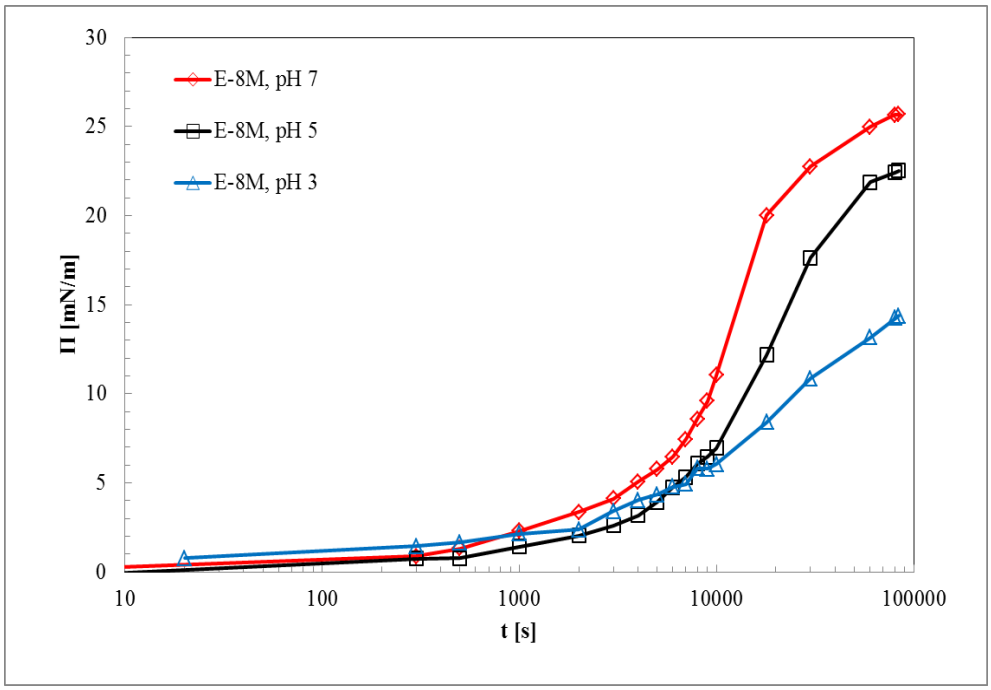
E-8M, pH 7
E-8M, pH 5
E-8M, pH 3
Π [mN/m]
t [s]
0
5
10
15
20
25
30
10
100
1000
10000
100000

(c)

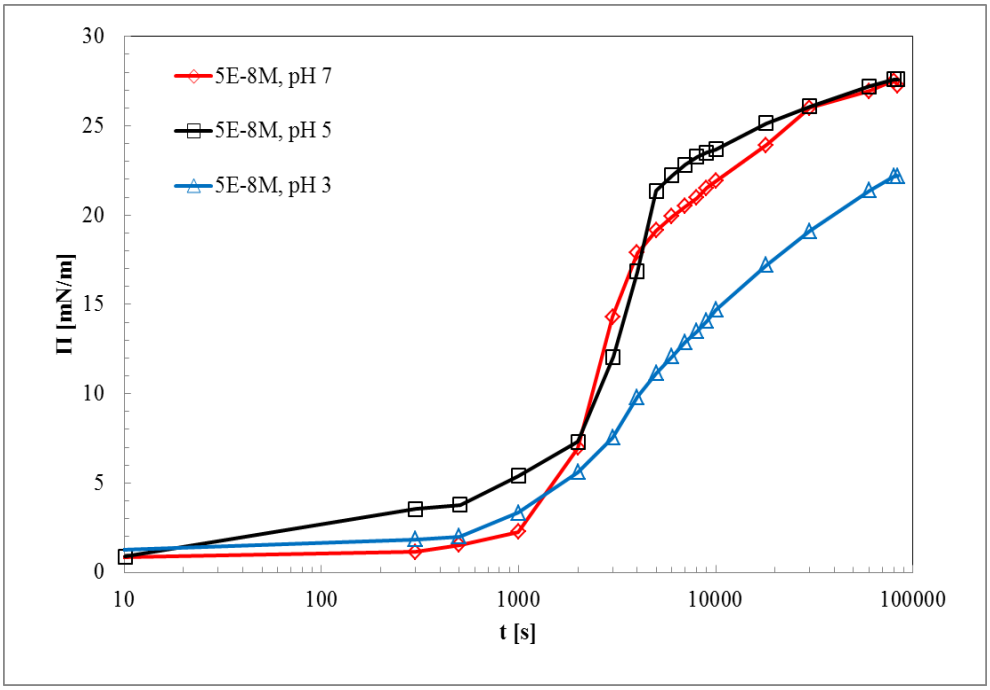
5E-8M, pH 7
5E-8M, pH 5
5E-8M, pH 3
Π [mN/m]
t [s]
0
5
10
15
20
25
30
10
100
1000
10000
100000

(d)

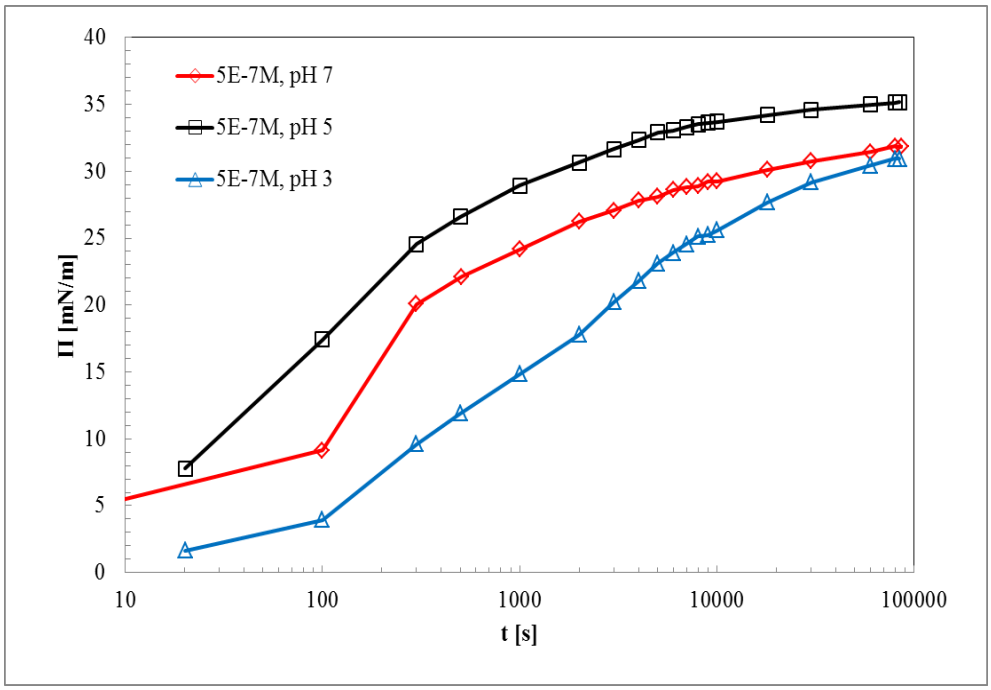
5E-7M, pH 7
5E-7M, pH 5
5E-7M, pH 3
Π [mN/m]
t [s]
0
5
10
15
20
25
30
35
40
10
100
1000
10000
100000

(e)

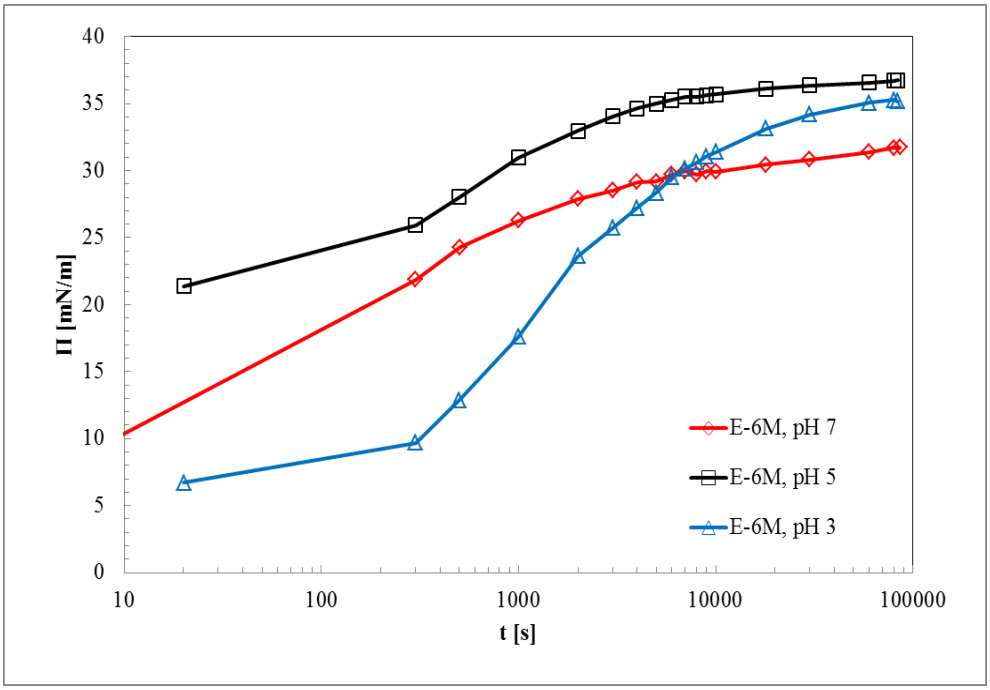

Figure 18 Evolution of the interfacial pressure Π(t) for different BLG concentrations at three pH value of pH 3, 5 and 7 at the W/TD interface; **(a)** 10^{-9} mol/l, **(b)** 10^{-8} mol/l, **(c)** 5×10^{-8} mol/l, **(d)** 5×10^{-7} mol/l, **(e)** 10^{-6} mol/l; for concentrations between (a) - (b) and (c) – (d) additional data are plotted in Appendix 4; (lines are guides for the eye).

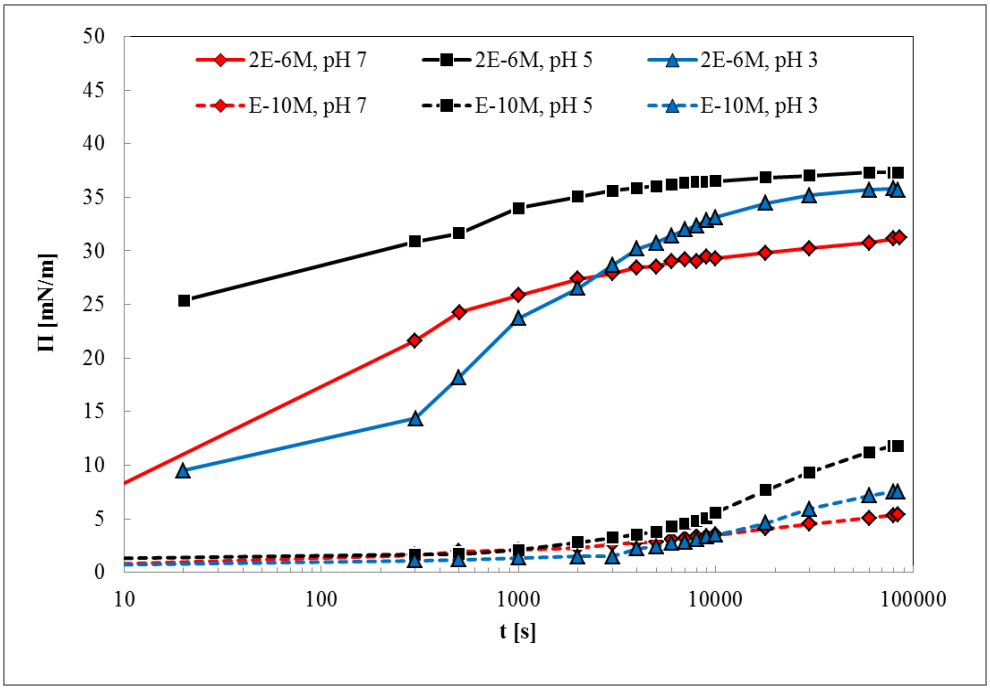

Figure 19 Evolution of the interfacial pressure Π(t) at the lowest and highest protein concentrations (C_{BLG} = 10^{-10} mol/l and 2×10^{-6} mol/l) measured in this study at pH 3, 5 and 7 at the W/TD interface; (lines are guides for the eye).

Figure 19 shows the evolution of the interfacial pressure with time at pH 3, 5 and 7 for the lowest (10^{-10} mol/l) and highest (2×10^{-6} mol/l) BLG concentrations measured in this study. The trend of the Π(t) curves for pH 3, 5 and 7 is similar for both concentrations. The adsorption kinetics at pH 5 is the fastest and results in the highest Π values at any time of adsorption while it is crossed for those at pH 3 and 7. At the beginning of adsorption, pH 3 is slower than pH 7, but it is reversed after ca. 5,000 s for 10^{-10} mol/l and 9,000 s for 2×10^{-6} mol/l. The induction time for the low concentrations was detected to be few minutes only, whereas it is hard to distinguish for the higher concentrations due to the fast adsorption process.

Surface activity and molecular net charge of the protein are well known factors for the effect of pH on the adsorption behaviour of BLG [24]. In general, proteins carry a certain net charge with an absolute value $|Z|$; Z = 0 at the isoelectric point p*I*, negative Z (–Z) at pH > p*I* and positive Z (+Z) at pH < p*I*. H^+ titration experiments of BLG solutions revealed that $|Z|_{pH7}$ is about 2.5-3 times lower than $|Z|_{pH3}$ [25, 101, 102]. This is corresponding to the data shown

here except the crossing adsorption behaviour of pH 3 and 7 at the highest concentration of BLG.

The results shown here demonstrate that the adsorption kinetic at pH 5 is the strongest in comparison to pH 3 and 7, beyond a certain protein concentration (ca. $C_{BLG} \geq 5\times10^{-8}$ mol/l), which was reported for the W/A surface as well [35, 37]. The reason can be found in strong intermolecular interactions at pH values close to the isoelectric point (≈ 5.1) of BLG while the interactions between adsorbed BLG molecules at pH 3 and 7 are mainly electrostatic and thereby long ranged and relatively weak. By reduction of $|Z|$, the affinity of the BLG to the interface can be increased and finally adsorption can be enhanced [24].

In Figure 20 interfacial pressures of BLG adsorbed layer for constant $C_{BLG} = 10^{-6}$ mol/l at different adsorption times at the W/TD interface for three studied pH values of pH 3, 5 and 7 are shown. Apparently it is demonstrated that the value of interfacial pressure is the lowest at pH 3 and the highest at pH 5 at any adsorption time.

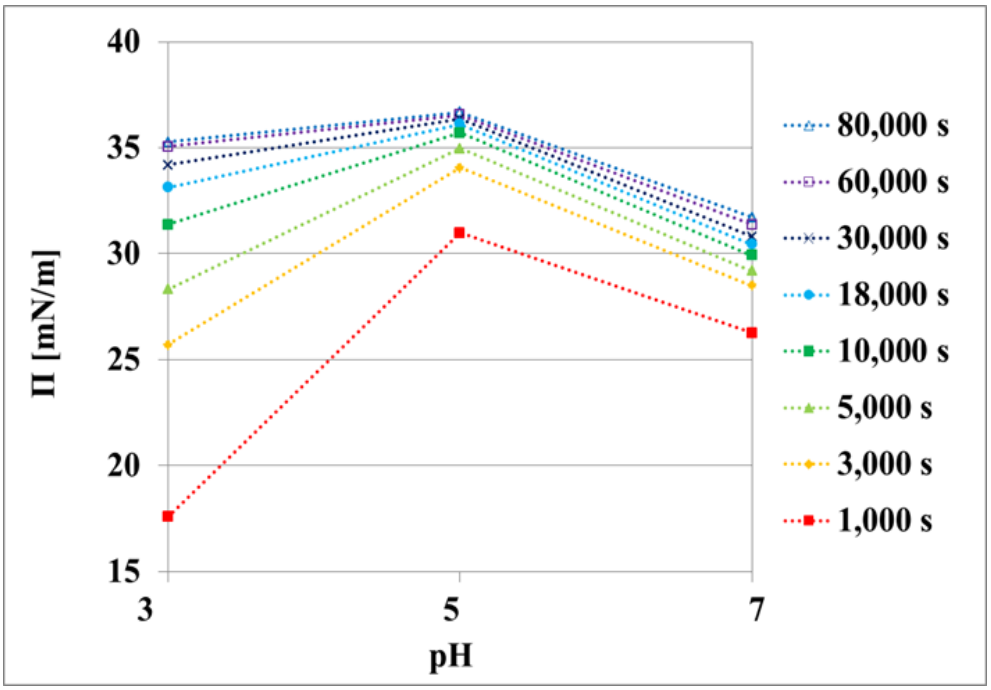

Figure 20 Interfacial pressure Π(pH) at pH 3, 5 and 7 for constant $C_{BLG} = 10^{-6}$ mol/l at different adsorption times at the W/TD interface (lines are guides for the eye).

5.1.3. Effect of Solution Ionic Strength

In order to investigate the role of different ionic strength on the adsorption kinetics of BLG, we measured the dynamic interfacial pressure of BLG layers at pH 3, 5 and 7 for a constant concentration of C_{BLG} =10^{-6} mol/l at the W/TD interface for three different buffer concentrations of 1, 10 and 100 mM. Generally, increasing the electrolyte concentration increases the BLG adsorption [24, 34, 35]. This fact can be ascribed to the screening of the protein net charge by counter-ions, thus increasing the protein surface activity [25]. This is confirmed in our experiments for pH 3 and 7 as shown in Figures 21 (a) and (c). Increasing buffer concentration from 1 to 100 mM does not appreciably reduce the induction time, but all data-sets reach similar final interfacial pressure after 80,000 s of adsorption at pH 3, whereas it is not the case at pH 7. The interfacial pressures at pH 5 for the same three different buffer concentrations, however, are almost equal as shown in Figure 21 (b). Similar results were presented by Ulaganathan et al. for the W/A surface [25]. Likewise, one can assume that the changed ionic strength of the solutions do not influence considerably the surface activity of the protein molecules at negligible molecular net charge [35]. In the solutions at pH ≠ p*I*, on the contrary, the influence of electrolytes on the BLG adsorption is very remarkable [24, 34, 35].

In Figure 22 the dynamic interfacial pressures at pH 3, 5 and 7 for constant $C_{BLG} = 10^{-6}$ mol/l at different buffer concentrations are shown. For a qualitative comparison of the electrolyte effects at different pH values, the interfacial pressure for buffer concentrations of 1, 10 and 100mM at two different pH values are shown on each graph. In general, BLG is less surface active at pH 3 and it is getting more surface active by increasing the buffer concentration at pH 3 and 7. The adsorption at pH 7 which is higher than at the isoelectric point of BLG is enhanced with increasing buffer concentration until the adsorption for C_{buff} = 100 mM reaches interfacial pressures similar to those at pH 5, as shown in Figure 22 (a). It follows a comparable scenario at pH 3 as shown in Figure 22 (b). Note, however, the final interfacial pressure after 80,000 s of adsorption is almost the same for all solutions at pH 3 but it is slightly lower than those at pH 5. As one can see in Figure 22 (c), the adsorption of BLG at pH 3 is slower than at pH 7 for the first few minutes but it is reversed en route and it leads the higher final interfacial pressure at pH 3 as compared to those at pH 7. The results in Figure 21 and 22 indicate that the protein net charge $|Z|$ is negligible for pH 5 and it can be also neglected at sufficiently high buffer concentration such as 10 mM and 100 mM.

(a)

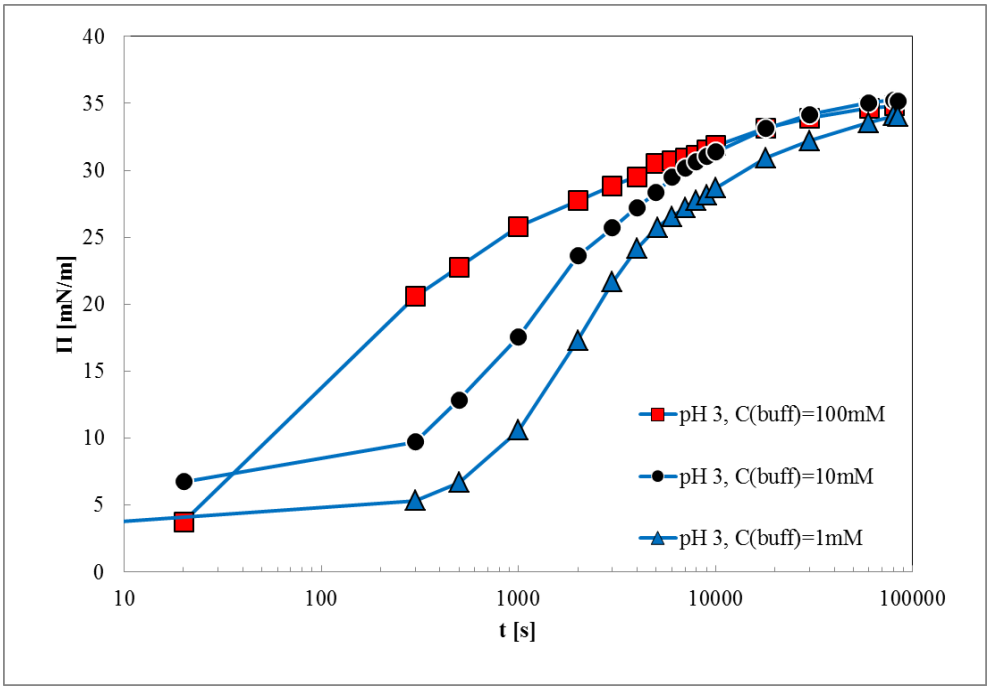
Π [mN/m]
t [s]
pH 3, C(buff)=100mM
pH 3, C(buff)=10mM
pH 3, C(buff)=1mM

(b)

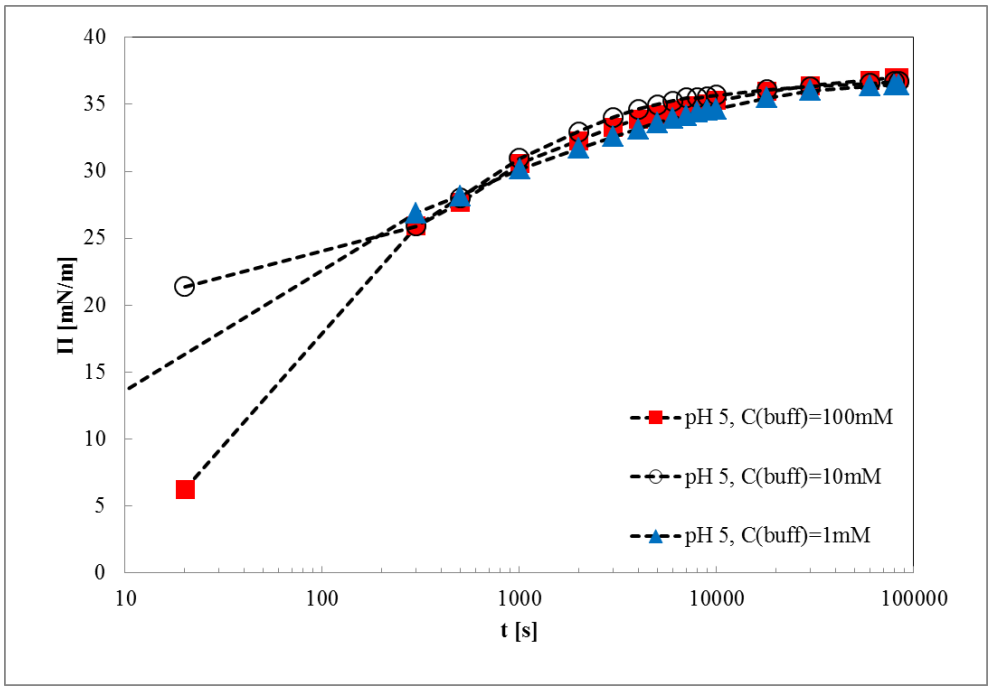
Π [mN/m]
t [s]
pH 5, C(buff)=100mM
pH 5, C(buff)=10mM
pH 5, C(buff)=1mM

(c)

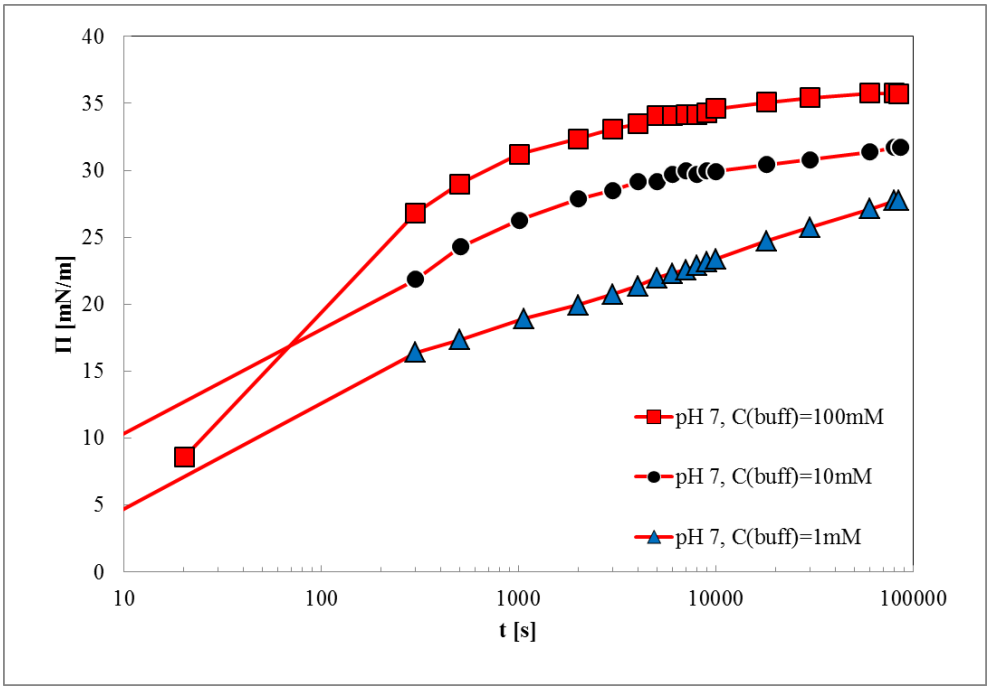

Figure 21 Buffer concentration (ionic strength) dependence of the measured interfacial pressure Π(t) at the W/TD interface for solutions with $C_{BLG} = 10^{-6}$ M at **(a)** pH 3, **(b)** pH 5, **(c)** pH 7; (lines are guides for the eye).

(a)

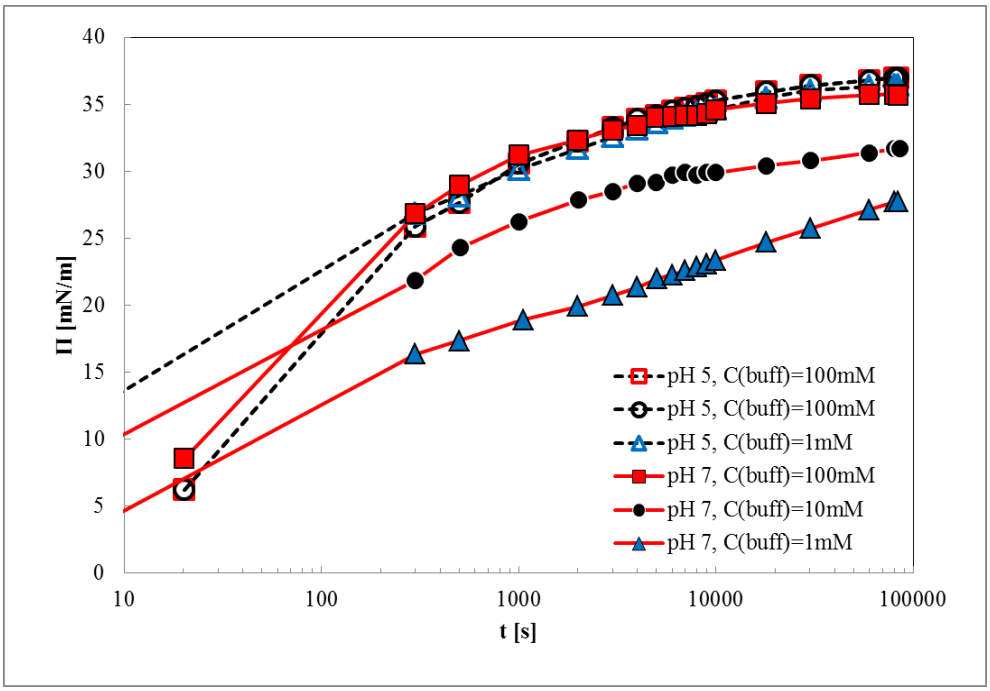

(b)

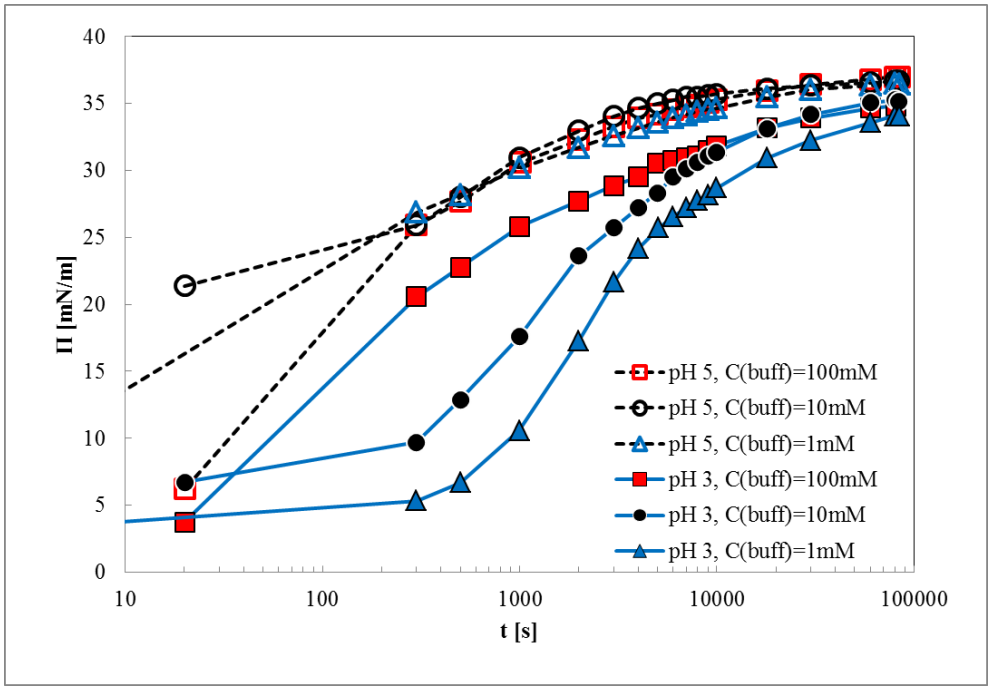

(c)

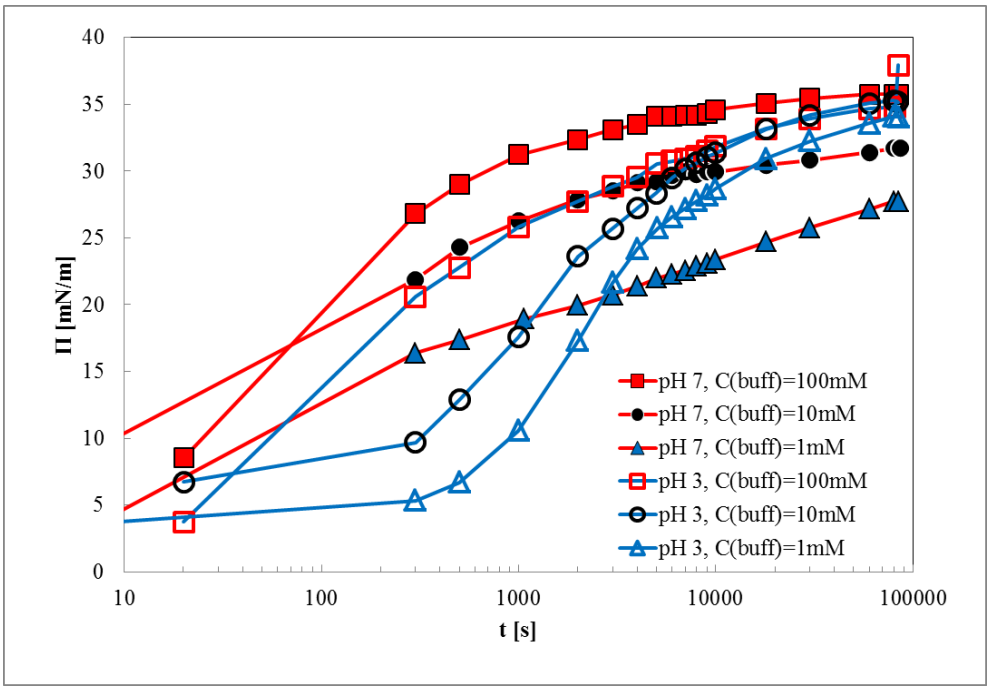

Figure 22 Evolution of the interfacial pressure Π(t) at the W/TD interface for solutions of $C_{BLG} = 10^{-6}$ M; **(a)** pH ≥ p*I*, **(b)** pH ≤ p*I*, **(c)** pH ≠ p*I* with values of p*I* ≈ 5.1 at different buffer concentrations; (lines are guides for the eye).

5.2. Interfacial Pressure Isotherms of BLG Solutions: Effect of Solution pH

The interfacial pressure isotherm plays a key role to better understand the behaviour of BLG adsorbed layers depending on BLG solution pH. In [22] BLG was studied at water/oil interfaces at pH 2.5 and 7, and in [103] the adsorption isotherms of several proteins at the water/air and different water/oil interfaces are presented. To the best of our knowledge, however, there are so far no systematic investigations about the adsorption behaviour of BLG at a water/oil interface at different pH values of the aqueous phase. Only recently, Ulaganathan et al. [25] reported on the effect of solution pH on the adsorption kinetics and the surface pressure isotherm for BLG adsorbed layers at the W/A surface.

The experimental data for BLG adsorbed layers at the W/TD interface for the three studied pH values of 3, 5 and 7 are shown in Figure 23 (a). The three obtained isotherms $\Pi(C_{BLG})$ show significant interfacial pressure values of about 5 mN/m already at bulk concentrations of $C_{BLG} = 10^{-10}$ mol/l, i.e. the isotherms start at much lower bulk concentrations as compared to the W/A surface (cf. [25]). Also the maximum interfacial pressure values of about 31 mN/m for pH 7 and 36 mN/m for pH 3 and pH 5, are significantly higher as compared to about 20 to 25 mN/m measured at the W/A surface. Apparently the W/TD interface exhibits a higher affinity for the protein molecules to adsorb than the W/A surface. Note, there are only small differences between pH values among the interfacial pressure data in the BLG concentration region below 5×10^{-9} mol/l. Generally, at any BLG concentration in the studied range, the interfacial pressure at pH 3 is always the lowest one, which means that BLG molecules are less surface active at pH 3. This trend was also shown in other recent studies [25, 41]. The specific kinks in the isotherms are discussed in literature as a signal for the transition from a monolayer adsorption to the formation of multilayers. However, these kinks appear at concentrations of around 10^{-7} mol/l for pH 7 and at almost 10^{-6} mol/l for pH 3 and pH 5, which seem to be rather high concentrations. The possibility of the BLG molecules to protrude with their hydrophobic parts into the oil phase leads obviously to quite different structures of the interfacial layers, expressed by the shape and location of the isotherms. The model proposed in [41, 42, 74] were applied for the isotherm fitting. The values of the model parameters (cf. Equations (3.20) to (3.29) discussed above) used to obtain the best fit of the experimental data are listed in Table 4. The same parameters were not only used for the model calculations of the dynamic interfacial tensions (see section 5.1.) but also for the visco-elasticities discussed in detail further below in section 5.3.

(a)

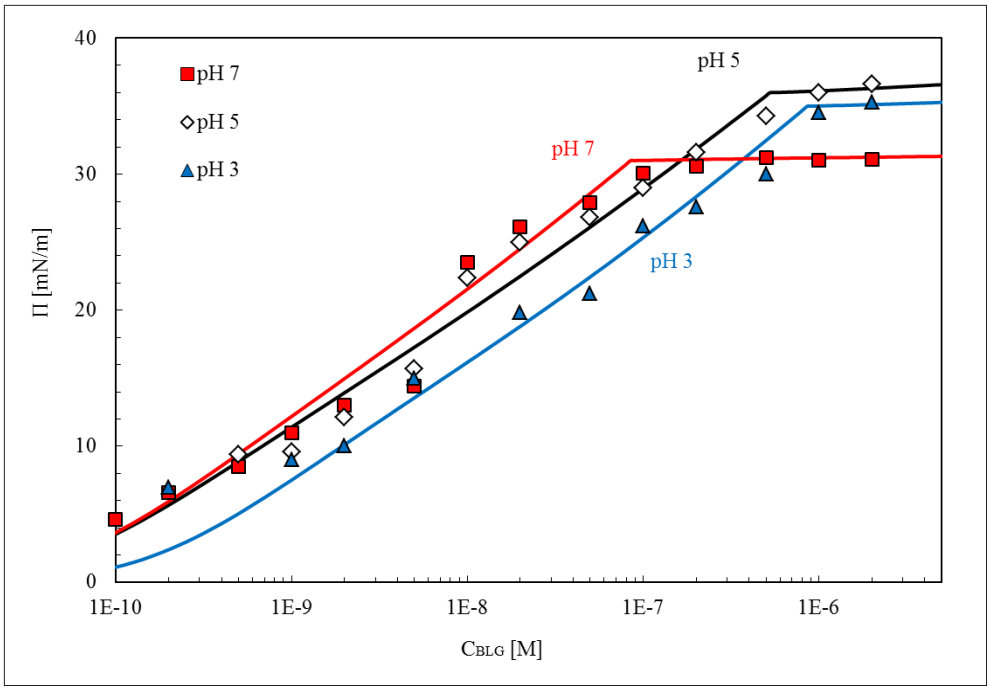

(b)

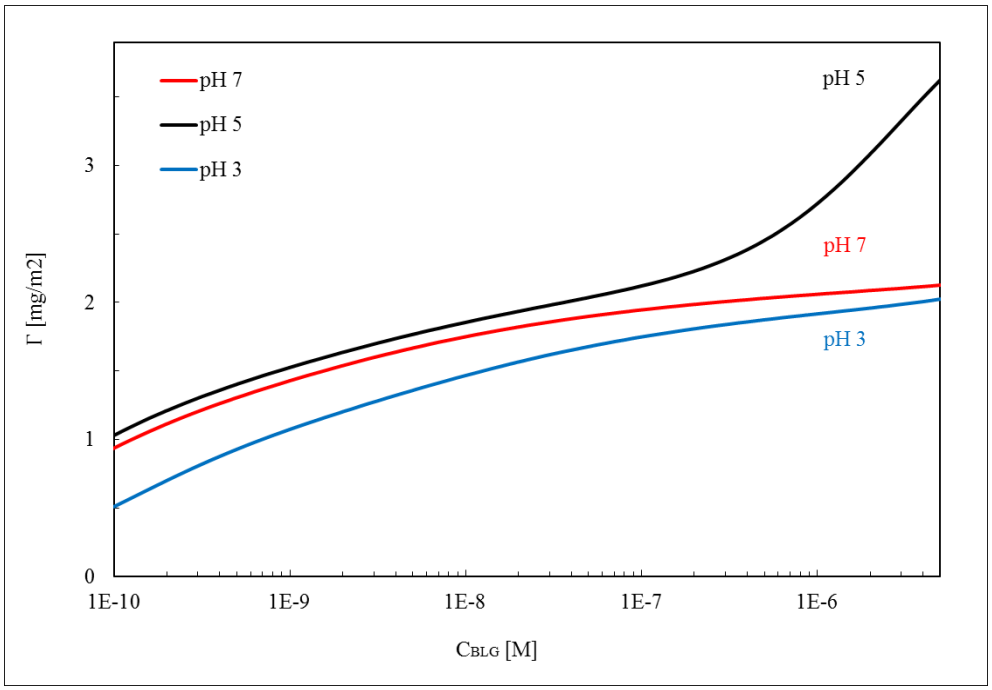

Figure 23 (a) Experimental Π–c isotherms, **(b)** Calculated adsorbed amounts for BLG at three selected pH values at the W/TD interfaces; Symbols - experimental points, Lines - best fit of the results calculated using the adsorption model described in section 3.4.4; pH 7 - red line and square symbol ■, pH 5 - black line and opened diamond symbol ◇, pH 3 - blue line and triangle symbol ▲; data are taken from [45].

While all model parameters for the three pH values are quite similar, the values for the surface activity parameter b_1 differ remarkably. A similar situation was also observed in [43] for BLG adsorption layers at the W/A surface. In Figure 23 (b) the adsorbed amounts of BLG at three different pH values at the W/TD interface are shown as calculated with the given model and the parameters listed in Table 4. The total adsorbed amounts of BLG at the W/TD interface are qualitatively comparable for pH 5 and 7, while smaller adsorbed amounts were obtained for layers formed from solutions at pH 3. The adsorbed amount of BLG at pH 5 becomes considerably high at very high bulk concentrations above $C_{BLG} > 10^{-6}$ mol/l at the W/TD interface.

Table 4 Equilibrium adsorption parameters for BLG at the W/TD interface obtained by fitting the model of Eqs. (3.20) to (3.29); data are taken from [45].

Parameters	Unit	Value		
		pH 3	pH 5	pH 7
a	-	0	0	0
α	-	1.2	1.2	1.0
ω_0	10^5 m^2/mol	4.2	4.7	4.2
ω_1	10^6 m^2/mol	8.2	7.5	7.0
ω_m	10^7 m^2/mol	2.5	2.0	2.0
n_a	-	25	28.5	38
Π*	mN/m	35	36	31
b_1	10^5 m^3/mol	1.0	6.0	5.5
b_m	10^1 m^3/mol	5.0	340	2.0
m	-	2	2	2

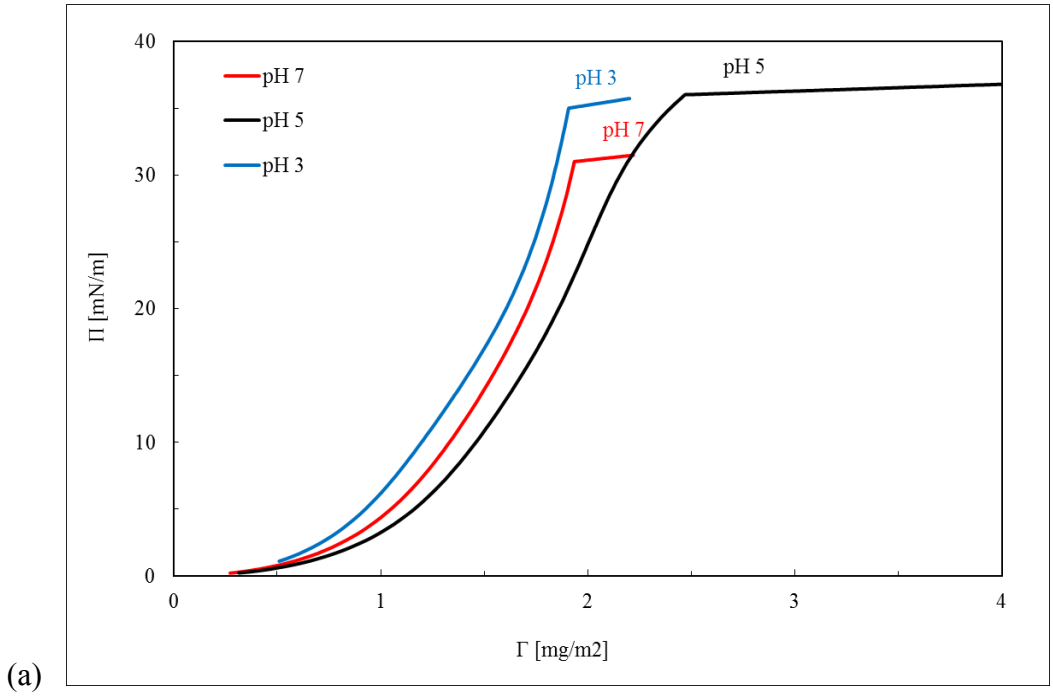

(a)

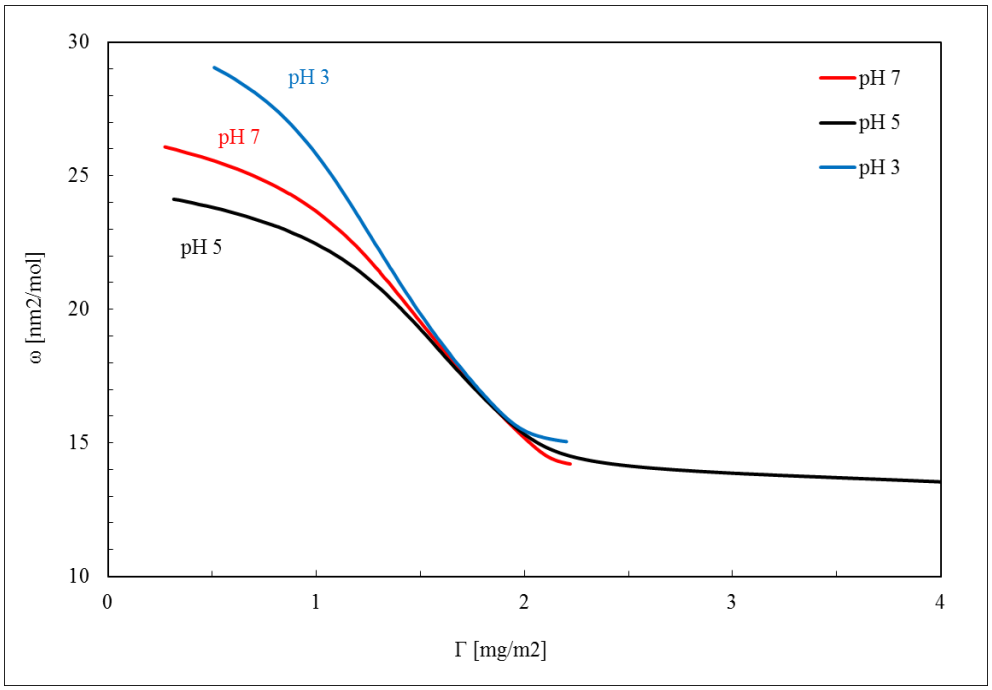

(b)

Figure 24 Calculated dependences **(a)** of the interfacial pressure Π and **(b)** of the molecular area ω on the adsorbed amount Γ of BLG at three selected pH values of 3, 5 and 7 at the W/TD interface using the parameter values listed in Table 4; pH 7 - red line, pH 5 - black line, pH 3 - blue line; data are taken from [45].

The dependencies shown in Figure 24 were also calculated using the optimum model parameters listed in Table 4. The major difference is that the critical point in the Π dependence on Γ, after which the interfacial pressure changes only very slightly with the increasing adsorbed amount, appears at a rather large adsorbed amount ($\Gamma \approx 2.2$ mg/m^2) for pH 5, whereas for pH 3 and 7 the critical points are comparable to each other, and appear at a lower adsorption value ($\Gamma \approx 1.9$ mg/m^2). Apparently, the stronger adsorption at pH 5 cannot be explained by a smaller molar area as the data of ω dependence on Γ in Figure 24 show that the molar areas in the range around the critical points Π* are very close to each other for any studied pH. Obviously, the average shape and orientation of the adsorbed BLG molecules control these dependencies. For the case of pH 5, we conclude that a secondary adsorption layer is formed onto the primary monolayer. This is also in correlation with the adsorption dependence on concentration in Figure 23, which show a strong increase of the adsorbed amount at BLG concentrations higher than the critical point of ca. 4×10^{-7} mol/l on the concentration dependency of interfacial pressure.

The induction time (τ_{ind}) is also used as a parameter to describe the effect of BLG bulk concentration and solution pH on the adsorption dynamics [25, 27, 74, 100, 104]. The induction time of BLG adsorption was also studied for different solution pH at the W/A surface and it was shown that it depends almost linearly on the BLG bulk concentration. The longest induction time of $\tau_{ind} > 50{,}000$ s were found at bulk concentrations up to 5×10^{-8} mol/l for pH 3 whereas the τ_{ind} values were lower at pH 5 and 7. In particular at pH 7 the induction times were almost one order of magnitude shorter. However, even at a bulk concentration of 10−6 mol/l an induction time of about 10 s was still determined.

In contrast to the results of the W/A surface, we cannot provide a satisfactory explanation about the effect of solution pH via induction time data due to its too short values. Thus, we only can state that the induction time has the trend to decrease with increasing BLG bulk concentration. It can be supported as well by Figure 25. As shown here, the induction time for BLG adsorbed layer at the W/TD interface in the studied pH range are very short. Even at a bulk concentration of 5×10^{-8} mol/l the induction times are of the order of 100 s at all three pH values studied here. For higher BLG concentrations the induction times are of the same order and only at very high concentrations ($> 10^{-6}$ mol/l) they get shorter. As it was discussed above, the adsorption of BLG at water/oil interfaces starts at much lower concentrations than

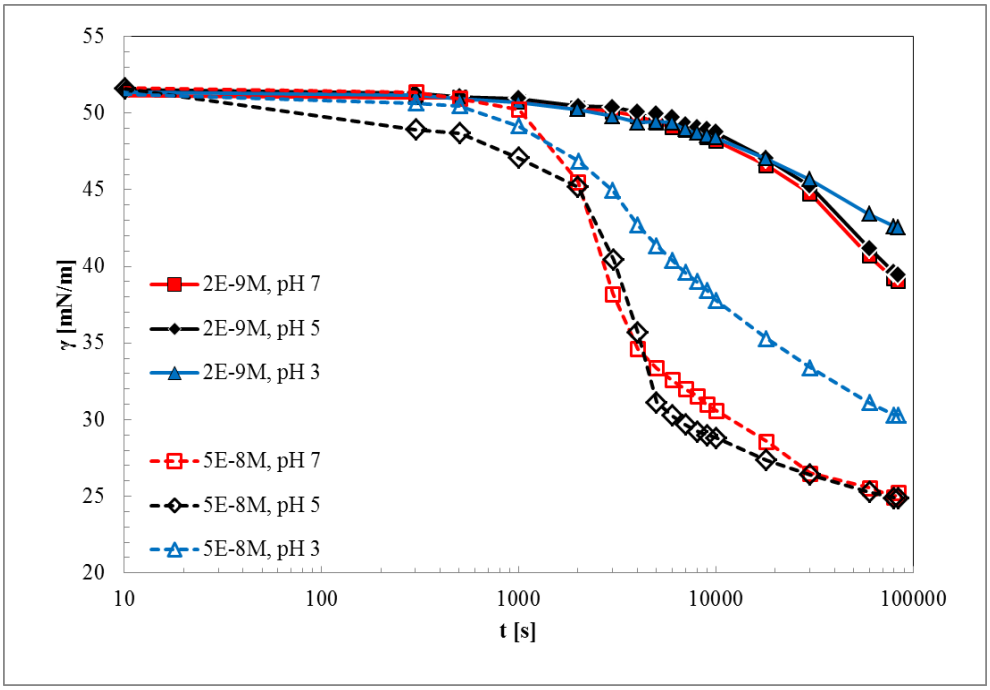

Figure 25 Dynamic interfacial tension of BLG solution at the W/TD interface with concentration 2×10^{-9} mol/l (filled symbols) and 5×10^{-8} mol/l (open symbols) at three different pH values; pH 7 (□,■), pH 5 (◊, ♦) and pH 3 (Δ, ▲); (lines are guides for the eye); data are taken from [42].

those required for the W/A surface to change the surface pressure. This goes along with the induction times observed here. Even rather small amounts of adsorbed BLG molecules start to increase the interfacial pressure. The number of molecules adsorbed at the very low BLG concentration of 10^{-10} mol/l is already quite high and obviously sufficient to change the interfacial tension (cf. Figures 23 and 24).

5.3. Dilational Rheology of BLG Adsorption Layers

Dilational rheology of protein interfaces is very useful to obtain additional information of the dynamics of adsorbed protein layers. In Figures 26 – 28 we show the analysis of interfacial tension response data to harmonic drop surface area in terms of the visco-elasticity modulus and phase angle as a function of interfacial pressure at pH 3, 5 and 7, respectively. The experiments were performed after the adsorption equilibrium status was reached, i.e. after 80,000 s. Additional data are gained during the establishment of the adsorption layer, i.e. after 1000, 5000, 10 000, 18 000, 30 000, 60 000 s adsorption times. Each oscillation was made with three full periods and the analysis provides an averaged value. Note, in some cases the adsorption layer is not in a quasi-equilibrium state during the oscillation, however, this is neglected in this work since we look mainly after the general trend of the visco-elasticity curves.

The results of the visco-elasticity in Figure 26 (a) were obtained at the adsorption equilibrium as the highest surface age studied, i.e. at about 80,000 s. The phase angle for $\Pi < 25$ mN/m is only few degrees and increases up to about 10 degrees for $\Pi > 25$ mN/m. The theoretical curves in Figure 26 (a) for the two frequencies 0.01 and 0.2 Hz were calculated with the model proposed in [41] using the parameters obtained for the isotherm shown in Figure 23 (a). The corresponding value of the diffusion coefficient was 5×10^{-12} m^2 /s. In Figure 26 (b) the adsorption times at which the oscillations at 0.1 Hz have been performed for getting the modulus data were 1000, 5000, 10 000, 18 000, 30 000 and 60 000 s. The red symbols are the data corresponding to those in Figure 26 (a) at a frequency of 0.1 Hz. The theoretical red curve was calculated with the same parameter values as for the curves in Figures 23 (a) and 26 (a). As one can see, the equilibrium data are in good agreement with those obtained under dynamic conditions with a mean difference of ± 8 mN/m.

In Figure 27 (a) we see the visco-elasticity modulus as a function of interfacial pressure at two different frequencies. The presented data have been measured after an adsorption time of more than 80,000 s. The phase angle is only few degrees for $\Pi < 25$ mN/m and it is about 10-15 degrees for $\Pi > 25$ mN/m. The black theoretical curve in Figure 27 (a) has been calculated with the same model used for Figure 23 (a) using the same parameter values and a diffusion coefficient of 10^{-10} m^2 /s. The red curve was calculated for the parameters given in Table 5. In Figure 27 (b) shows the same dependence as in Figure 27 (a), but for a frequency of 0.1 Hz.

(a)

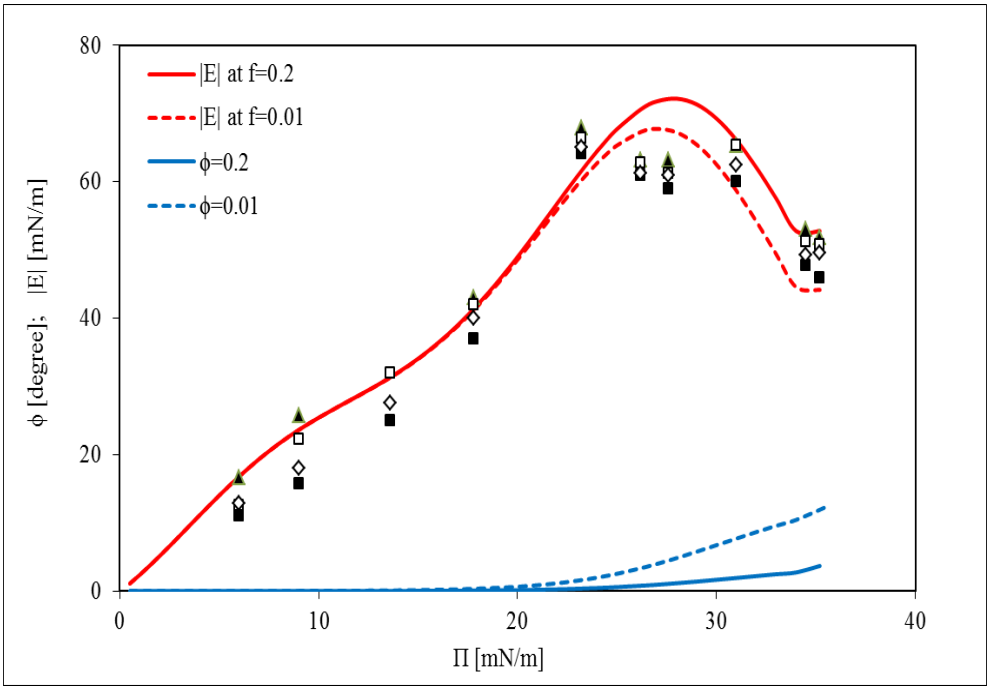

(b)

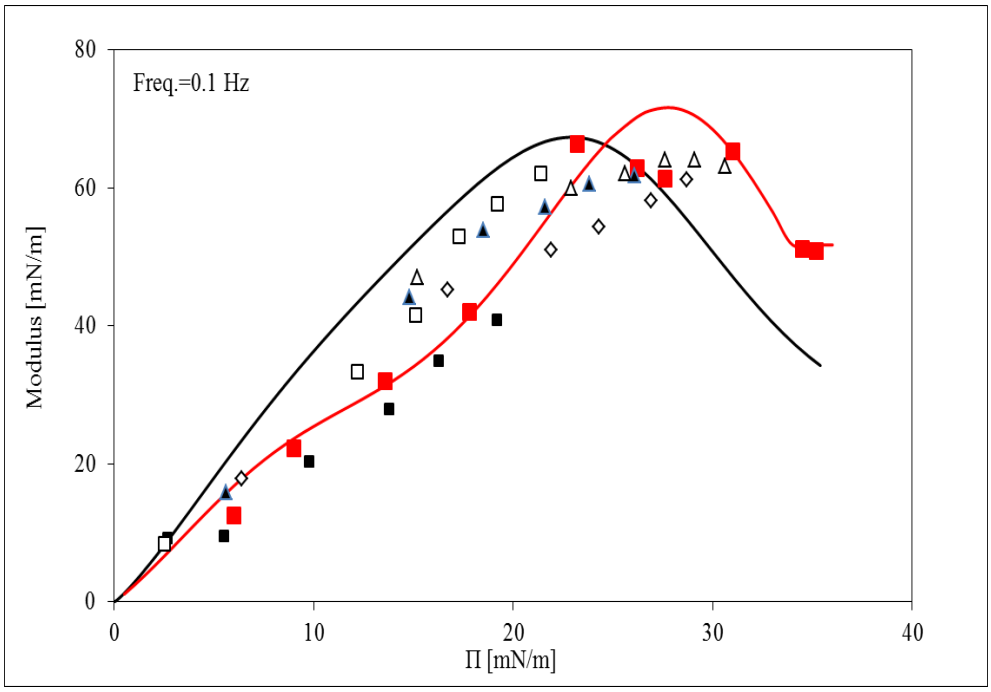

Figure 26 BLG at pH 3 at the W/TD interface **(a)** Viscoelasticity modulus |E| as a function of the interfacial pressure at different oscillation frequencies and phase angle ϕ as a function of the interfacial pressure Π at two frequencies 0.01 and 0.2 Hz; f=0.01 (■), f=0.05(◇), f=0.1 (□) and f=0.2 (▲) Hz; measured after 80,000 s; **(b)** Viscoelasticity modulus |E| as a function of the interfacial pressure at the frequency of 0.1 Hz, obtained from dynamic experiments for 5 different BLG concentrations; 2×10^{-8} (■), 5×10^{-8} (□), 10^{-7} (▲), 2×10^{-7} (△) and 5×10^{-7} (◇) mol/l; red curves – calculated with the given theoretical model, black curves – taken from [105] for comparison; measured at 1000, 5000, 10 000, 18 000, 30 000 and 60 000 s; data are taken from [46].

(a)

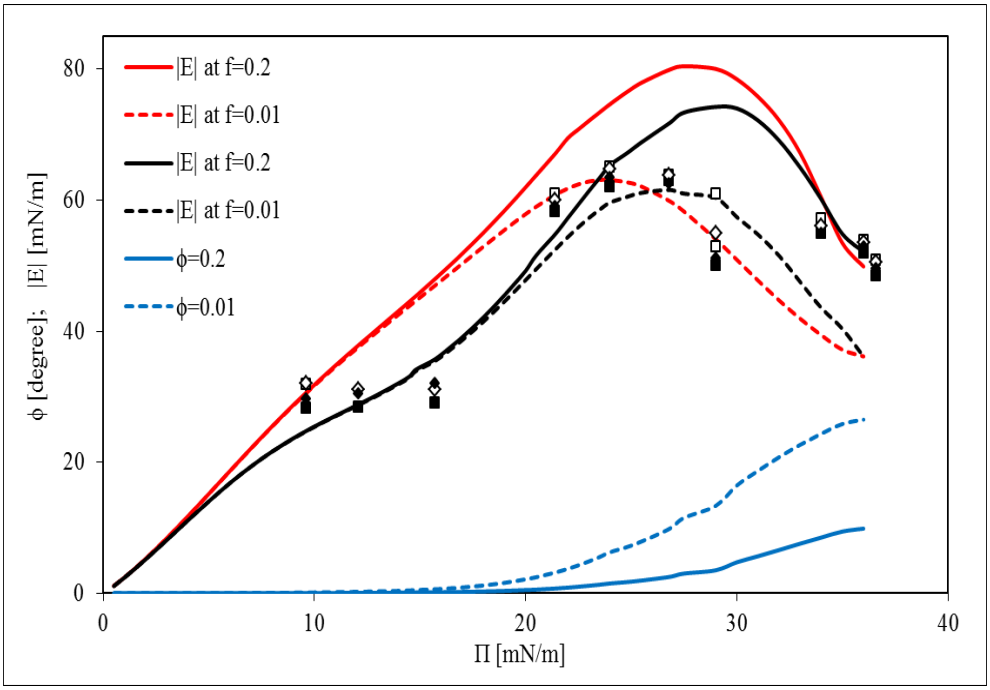

(b)

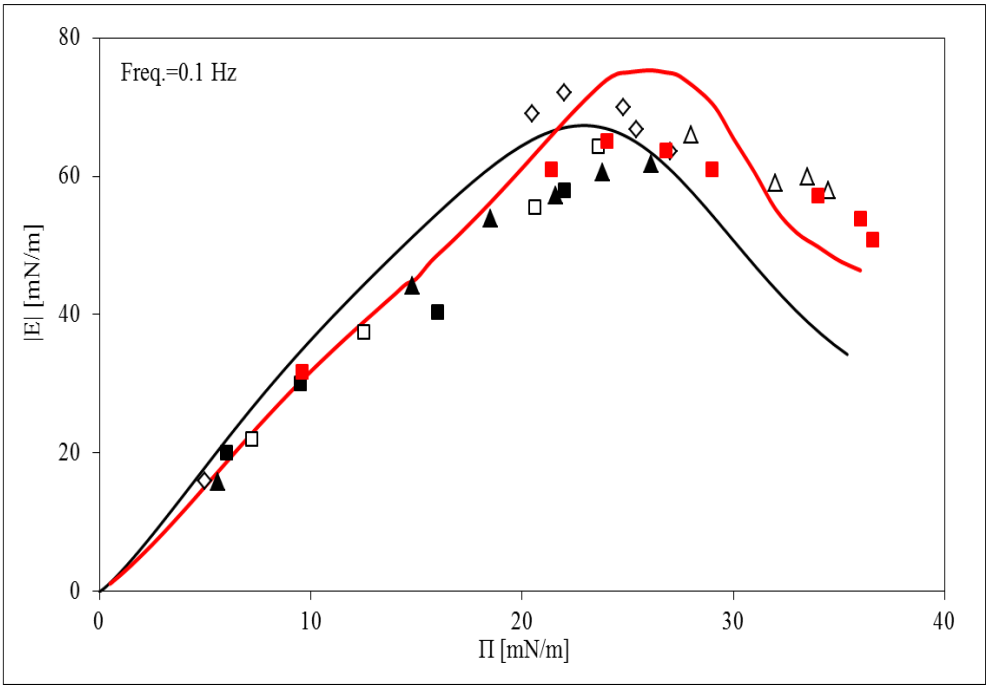

Figure 27 BLG at pH 5 at the W/TD interface **(a)** Viscoelasticity modulus |E| as a function of the interfacial pressure at different oscillation frequencies and phase angle ϕ as a function of the interfacial pressure Π at two frequencies 0.01 and 0.2 Hz; f=0.01 (■), f=0.05(◇), f=0.1 (□) and f=0.2 (▲) Hz; black curves – calculated with the parameters given in Table 4, red curves – calculated with the parameters given in Table 5; measured after 80,000 s; **(b)** Viscoelasticity modulus |E| as a function of the interfacial pressure Π at the frequency of 0.1 Hz, obtained from dynamic experiments for six different BLG concentrations; red curves – calculated with the given theoretical model, black curves – taken from [105] for comparison; measured at 1000, 5000, 10 000, 18 000, 30 000 and 60 000 s; data are taken from [46].

The results, however, were obtained from dynamic experiments, performed during the process of adsorption layer formation from BLG solutions at six different bulk concentrations. The adsorption times at which the oscillation experiments were performed during the adsorption process are again 1000, 5000, 10 000, 18 000, 30 000 and 60 000 s, respectively. The theoretical red curve was calculated with the parameters summarized in Table 5. The parameter values deviate slightly from those used for the calculation of the isotherm in Figure 23 (a). For example, the value for ω_1 is about 10% larger as that used for the red curve, calculated for the two frequencies in Figure 27 (a). In Figure 27 (b) the experimental data from [105] are shown, and also the black theoretical curve has been taken from this paper, which perfectly agrees with the data given here. All experimental conditions in [105] were identical to those used in the presented work, except for the pH which was probably 4.6 (given in [106]).

Table 5 Equilibrium adsorption parameters for BLG at the W/TD interface at pH 5, used for calculations shown in Figure 27.

a	α	ω_0 (m^2/mol)	ω_1 (m^2/mol)	ω_m (m^2/mol)	n_A	Π_c (mN/m)	b_j (m^3/mol)	b_2 (m^3/mol)	m
0.0	1.0	4.1 e+5	8.8 e+6	2.3 e+7	8.5	36.0	2.0e+5	1.0	2

In Figure 28 (a) we present the viscoelasticity value at two frequencies 0.01 and 0.2 Hz, measured after an adsorption time of 80,000 s. The phase angle is only few degrees for $\Pi < 25$ mN/m and of the order of 10 to 15 degrees for $\Pi > 25$ mN/m. The theoretical curves were calculated with the parameters given in the Table 1, using a diffusion coefficient of 10^{-10} m^2/s. In Figure 28 (b) the dependence of the viscoelasticity as a function of the interfacial pressure is shown with values obtained from oscillations performed during the adsorption process. The theoretical curve was obtained for the oscillation frequency of 0.1 Hz.

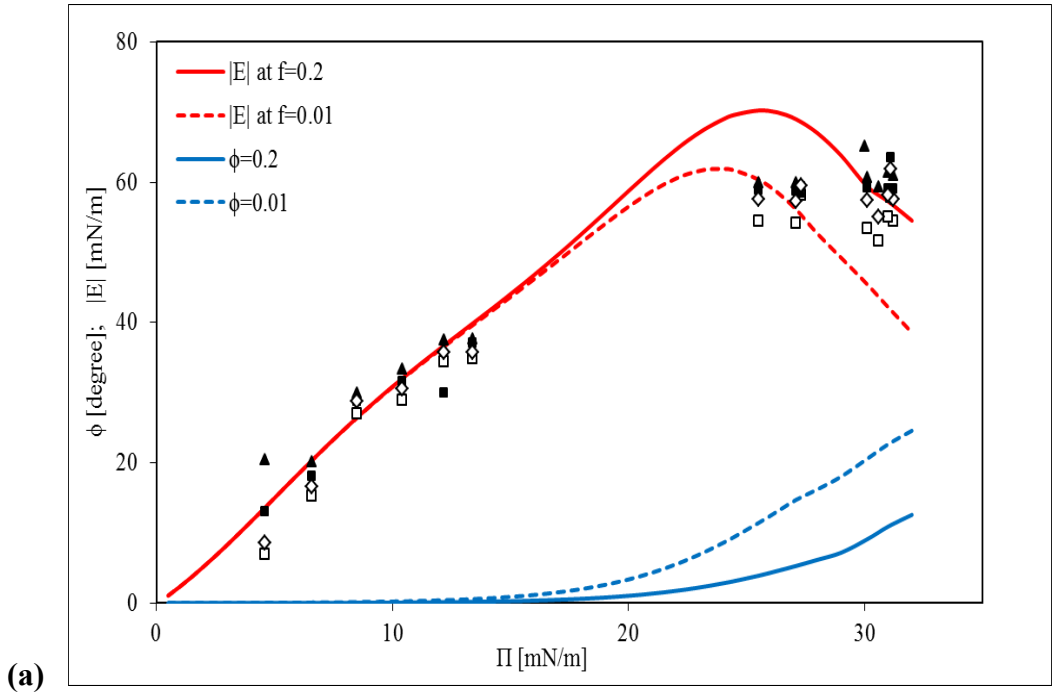

(a)

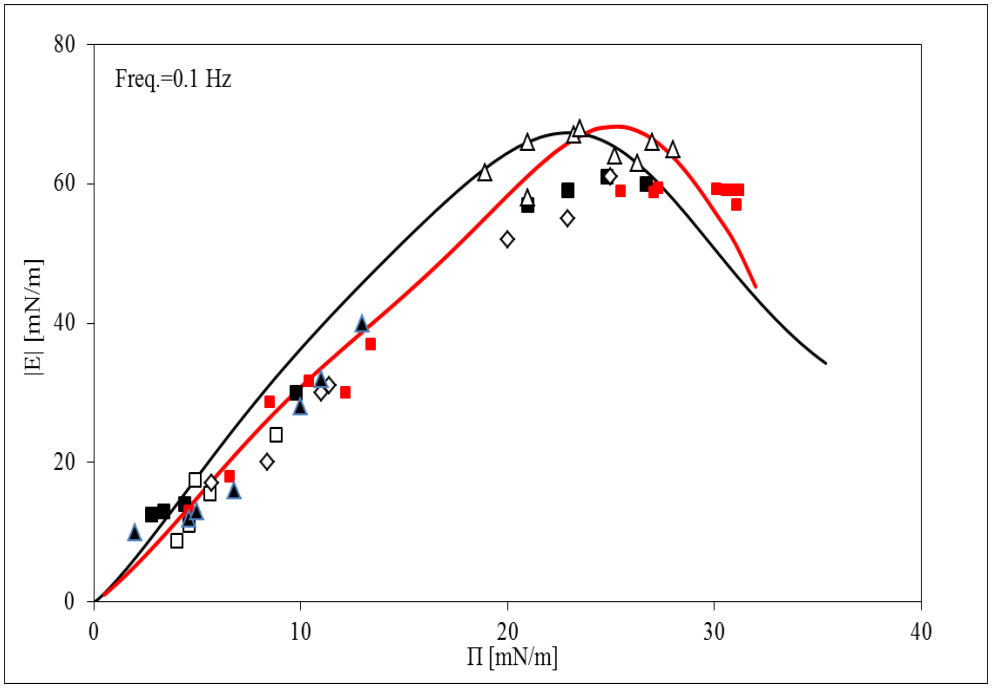

(b)

Figure 28 BLG at pH 7 at the W/TD interface (a) Viscoelasticity modulus |E| as a function of the interfacial pressure Π at different oscillation frequencies and phase angle ϕ as a function of the interfacial pressure Π for BLG; f=0.01 (□), f=0.05(◇), f=0.1 (■) and f=0.2 (▲) Hz; measured after 80,000 s; the solid and dashed curves are calculated for the frequencies of 0.01 and 0.2 Hz (b) Viscoelasticity modulus |E| as a function of the interfacial pressure Π at the frequency of 0.1 Hz, obtained from dynamic experiments at pH 7 at the W/TD interface for six different BLG concentrations; 10^{-10} and 2×10^{-8} (■), 2×10^{-10} and 5×10^{-10} (□), 10^{-9} and 2×10^{-9} (▲), 0.5×10^{-8} and 10^{-8} (◇), 0.5×10^{-7} and 10^{-7} (△) mol/l; red curves – calculated with the given theoretical model, black curves – taken from [105] for comparison; measured at 1000, 5000, 10 000, 18 000, 30 000 and 60 000 s; data are taken from [46].

5.3.1. Effect of BLG Bulk Concentration

In the section 5.1., we showed that adsorption kinetic is influenced by BLG bulk concentration and solution pH and can be described by a new theoretical model [42, 45]. Generally the adsorption of proteins at liquid/liquid interfaces is a time process and higher protein concentrations leads to faster adsorption [25, 42, 45, 74]. In addition, the conformational changes when protein molecules adsorb at the W/TD interface are represented by the adsorption activity constant in the corresponding equation of state. The rate constant obtained by a best fitting of the results using the diffusion controlled adsorption model and is smallest at pH 5, i.e. the protein molecules change their conformation at the interface to the smallest extend at pH 5 while it is biggest at pH 3 [42, 45].

The concentration dependence of measured dilational elastic modulus for selected BLG concentrations of 10 mM buffered BLG solutions at pH 7 at the W/TD interface is shown in Figure 29. The results revealed that E' values are one order of magnitude higher than those of E" for the studied concentrations. For this reason, only the elasticity term is considered here. As we can see in Figure 29 (a) the dynamic dilational elastic modulus E' increases with experimental time. It is clearly shown that the values of dilational elasticity depend on the BLG bulk concentration. These are represented using the corresponding Π data in Figure 29 (b). As reported in [32, 36,107] E' data for the presented BLG concentrations collapse onto a master curve. It is clearly showed at pH 7, but it is not really true at pH 3 (cf. Appendix 5). Figure 29 (c) presents the frequency dependence of the dilational elastic modulus E' and interfacial pressure value Π after the adsorption time of 80,000 s. The values of dilational elasticity for each concentration are almost constant for all studied frequencies. The results show almost no dependencies of the E' values on the frequency for both pH values as it is typical for protein interfacial layers [32, 70, 74] and an increase of E' values depending on Π values for a given frequency is observed. For selected BLG concentrations of 10 mM buffered BLG solutions at pH 3 at the W/TD interface the gained results are plotted in Appendix 5.

(a)

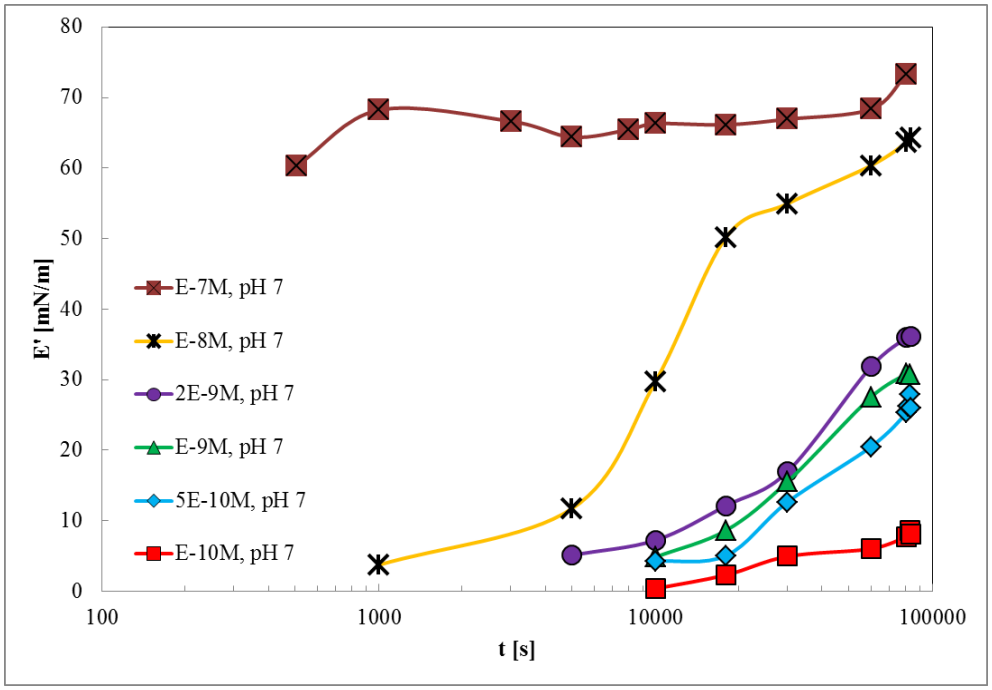
E' [mN/m]
t [s]
E-7M, pH 7
E-8M, pH 7
2E-9M, pH 7
E-9M, pH 7
5E-10M, pH 7
E-10M, pH 7

(b)

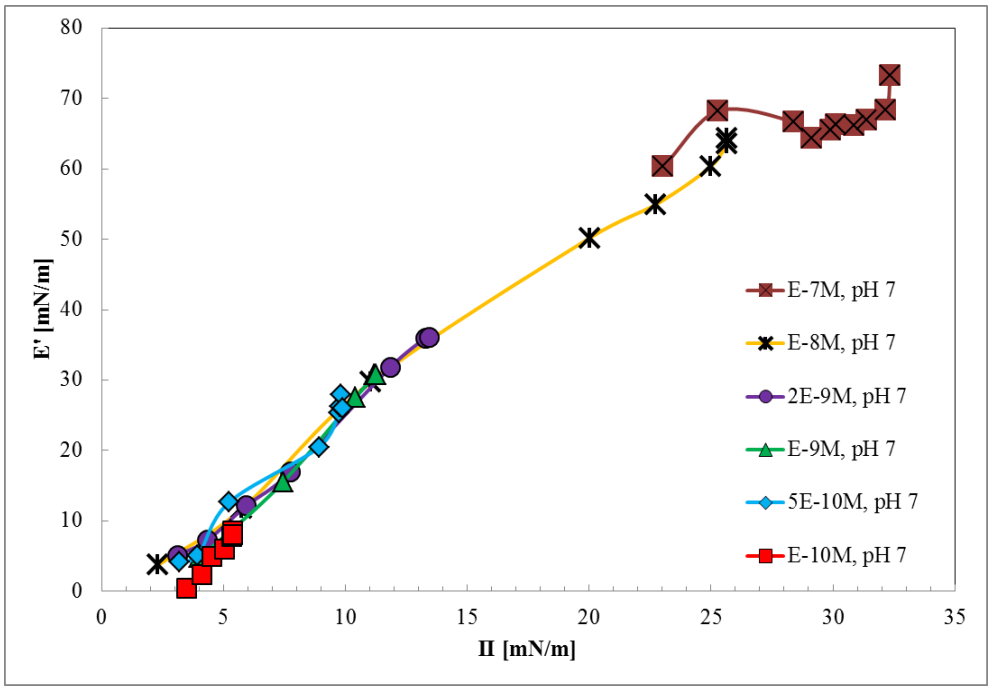
E' [mN/m]
Π [mN/m]
E-7M, pH 7
E-8M, pH 7
2E-9M, pH 7
E-9M, pH 7
5E-10M, pH 7
E-10M, pH 7

(c)

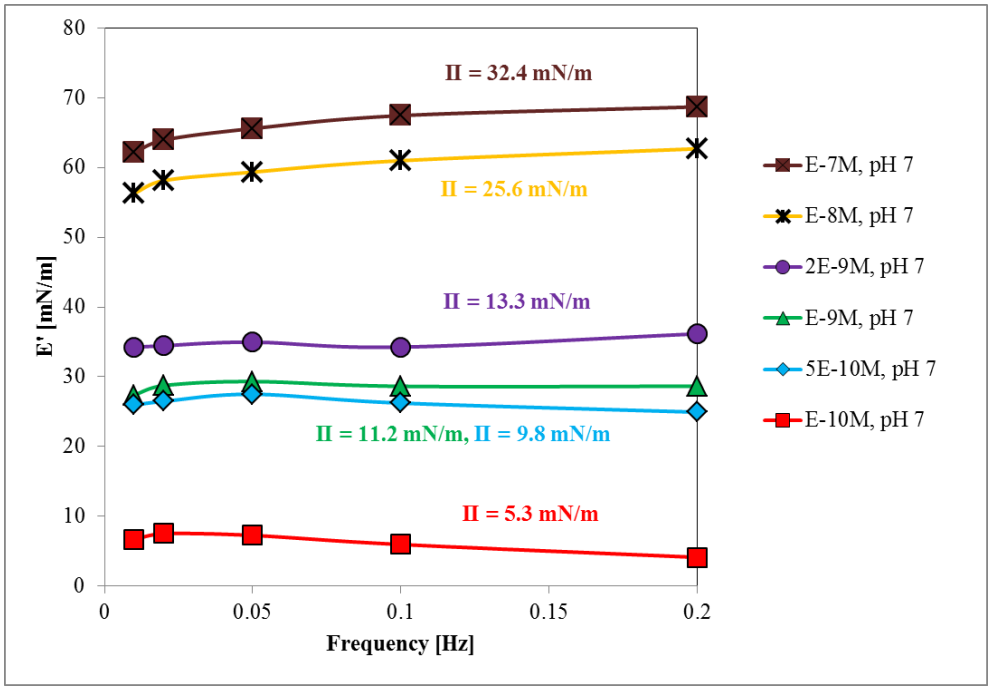

Figure 29 Interfacial properties of 10mM buffered BLG solutions for selected BLG concentrations at **pH 7** at the W/TD interface; **(a)** time evolution of the measured dynamic dilational elastic modulus E' at f = 0.1 Hz, **(b)** the measured dynamic dilational elastic modulus E' on the interfacial pressure Π at f = 0.1 Hz, **(c)** frequency dependence of the measured dynamic dilational elastic modulus E' at the adsorption time of 80,000 s, interfacial pressure for each cases are also shown in the graph; (lines are guides for the eye).

5.3.2. Effect of Solution pH

Figure 30 presents the results of the measured dynamic dilational elastic modulus E' depending on time t (a), the corresponding interfacial pressure Π at f = 0.1 Hz (b), and E' depending on frequencies f=0.01, 0.02, 0.05, 0.1 and 0.2 Hz at the adsorption time of 80,000 s at pH 7 and 3 for different concentrations of BLG. The values for the dynamic dilational elastic modulus E' increase with time and increasing interfacial pressure Π as shown in Figures 30 (a) and (b). As for the 10^{-7} mol/l BLG solution at pH 7 the maximum interfacial pressure values have already reached (cf. Figure 23 (a)), E' values of pH 7 are higher than those of pH 3 at all measured times. Figure 30 (c) shows the frequency dependence of the dilational elastic modulus E' with interfacial pressure value Π. The results show weak dependencies of E' values on the frequencies and an increase of E' values depending on Π values for given fixed frequencies. The dilational elastic modulus E' values at pH 7 are higher than those of pH 3 for all three conditions shown in Figure 30. This observation relates the elastic ability of BLG adsorbed layer, which is more active at pH 7 than pH 3. This fact is summarised in Figure 31 for all studied pH values in this work.

(a)

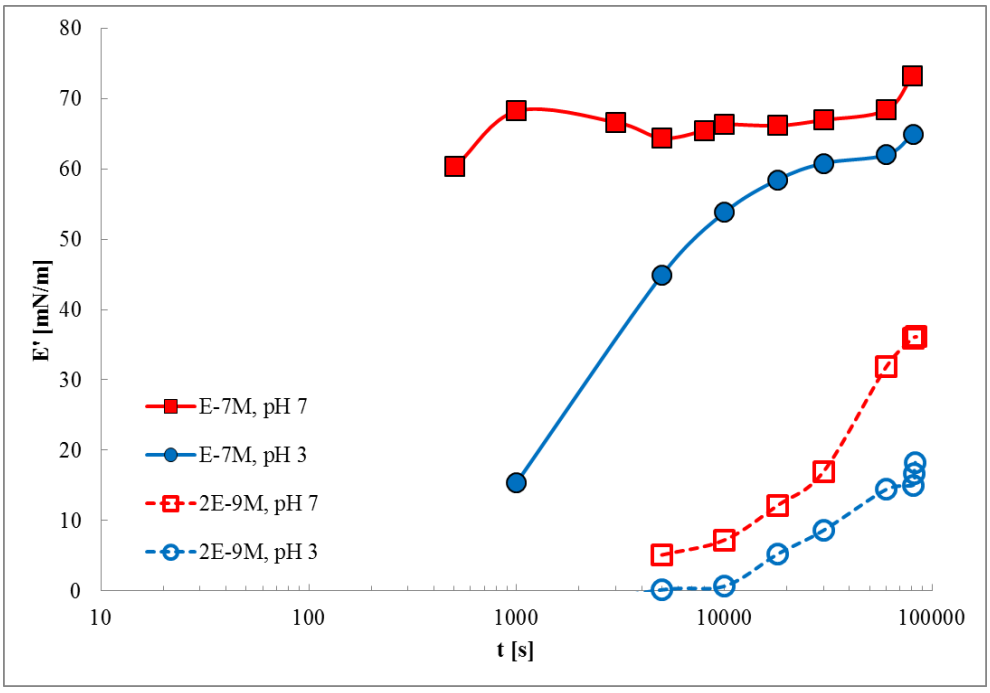

(b)

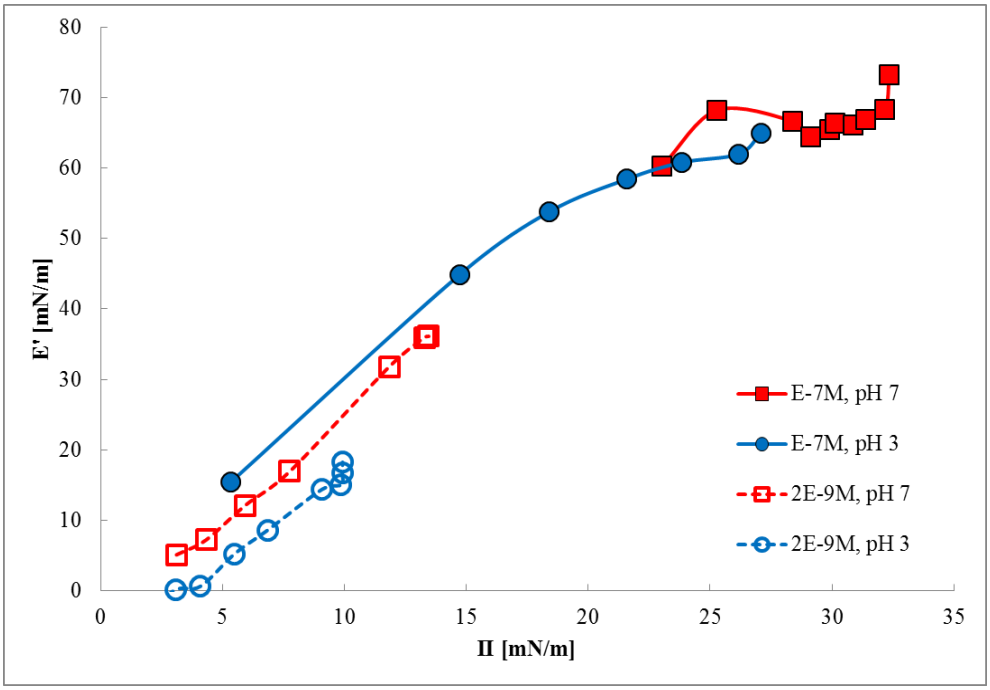

(c)

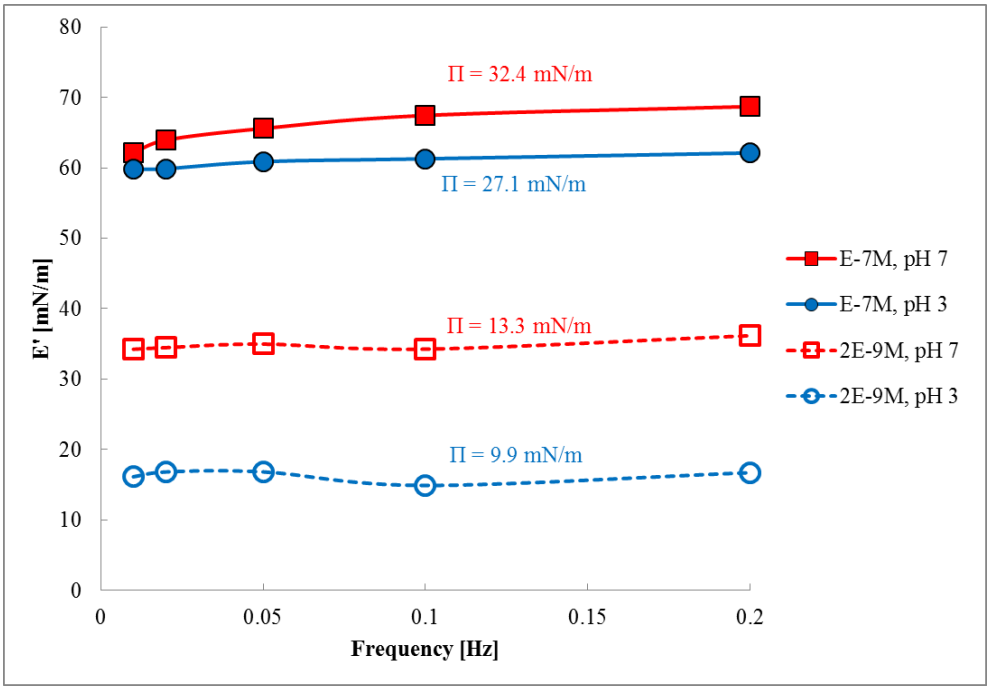

Figure 30 (a) Time evolution of the measured dynamic dilational elastic modulus E' at f = 0.1 Hz, **(b)** measured dynamic dilational elastic modulus E' on the interfacial pressure Π at f = 0.1 Hz, **(c)** frequency dependence of the dilational elastic modulus E' at the adsorption time of 80,000 s for 10 mM buffered BLG solutions of 2×10^{-9} and 10^{-7} mol/l at pH 7 and pH 3 at the W/TD interface; (lines are guides for the eye).

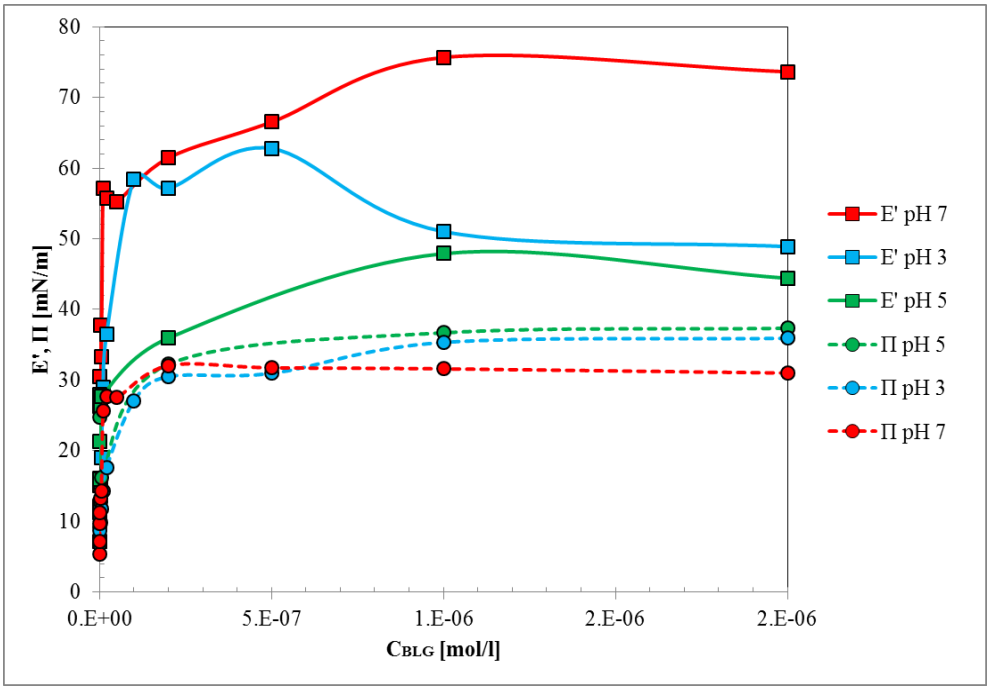

Figure 31 pH dependence of the measured dilational elastic modulus E' (squares) and interfacial pressure Π (circles) for selected BLG concentrations at pH 3, 5 and 7 at the W/TD interface at 0.1 Hz after 80,000s; (lines are guides for the eye).

5.3.3. Effect of Solution Ionic Strength

In order to investigate the role of different ionic strength, we measured the dynamic dilational viscoelasticity modulus of BLG adsorbed layers at pH 3, 5 and 7 for a constant concentration of $C_{BLG} = 10^{-6}$ mol/l at the W/TD interface for three different buffer concentrations of 1, 10 and 100 mM. Figures 32 and 33 demonstrate the corresponding data.

Increasing the buffer concentration of BLG solution from 1 to 100 mM does not evidently reduce the induction time, but all data-sets reach to similar final interfacial pressure at pH 3 and 5, whereas it is different at pH 7 (cf. Figure 21). In addition, the interfacial pressure at pH 5 for the three different buffer concentrations of 1, 10 and 100 mM are almost equal as shown in Figure 21 (b) while the influence of electrolytes on BLG adsorbed layer is very remarkable at pH 3 and 7. Similar results were also reported by Ulaganathan et al. for the W/A surface [25]. This fact can be explained by the protein net charge and the action of counter-ions. The influence of electrolytes on the BLG adsorption is negligible at any pH close to the isoelectric point (p*I,* $pI_{BLG} \approx 5.1$) and it is very noticeable at a pH value which is apart from the p*I* [24, 35]. All these findings are also valid for the visco-elasticity data. As shown in Figure 32, Appendices 6 and 7, at pH 5 the dilational elasticity E' and dilational viscosity E" data on time and interfacial pressure Π are not significantly different when the buffer concentration is changed. On the contrary, the dynamic dilational elasticity E' data are distributed from ca. 45.1 to 65.8 mN/m for pH 3 and from ca. 53.2 to 65.0 mN/m for pH 7. The results for the frequency dependencies of E´ data presented in Figure 3 3 support this observation. The E' values of pH 3 and 7 are widely spread while they are very similar for pH 5. The time evolution of the dynamic dilational viscocity E' and E" on the interfacial pressure Π at f = 0.1 Hz for BLG solutions at the W/TD interface for a fixed BLG concentration of 10^{-6} mol/l for three different buffer concentration 1, 10 and 100 mM at pH 3, pH 5 and pH 7 are plotted in Appendices 6 and 7.

(a1)

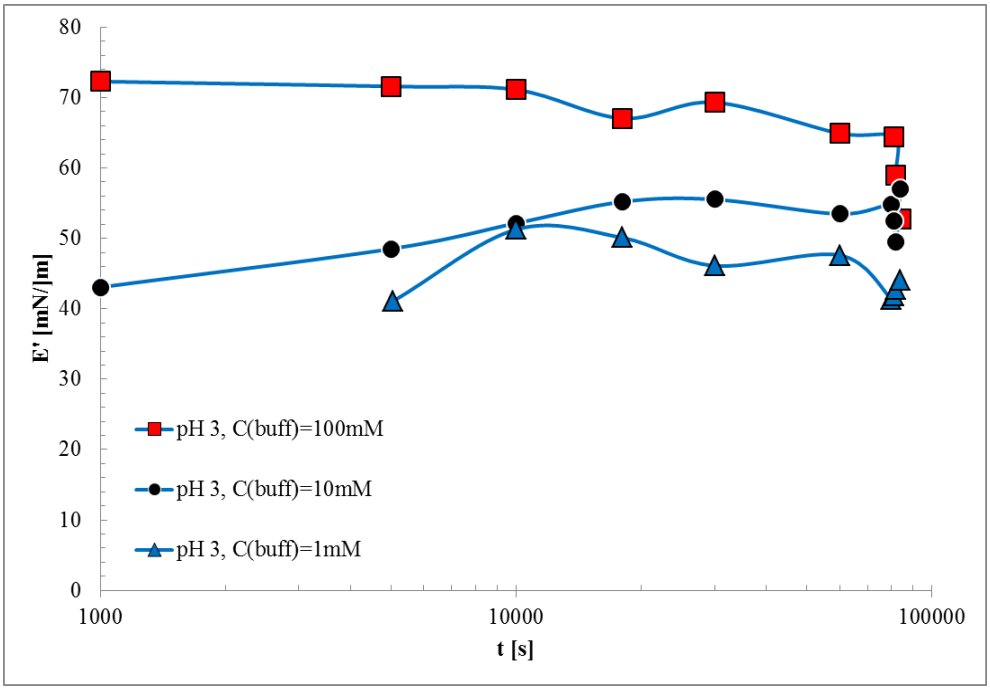
80
70
60
50
40
30
20
10
0
E' [mN/m]
1000
10000
100000
t [s]
pH 3, C(buff)=100mM
pH 3, C(buff)=10mM
pH 3, C(buff)=1mM

(a2)

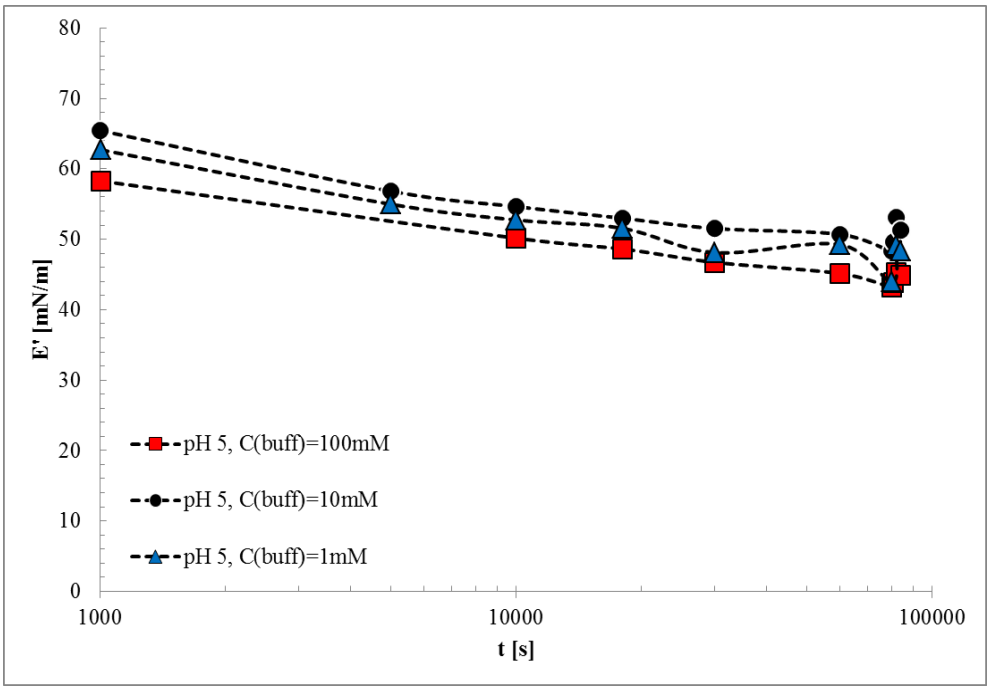
80
70
60
50
40
30
20
10
0
E' [mN/m]
1000
10000
100000
t [s]
pH 5, C(buff)=100mM
pH 5, C(buff)=10mM
pH 5, C(buff)=1mM

(a3)

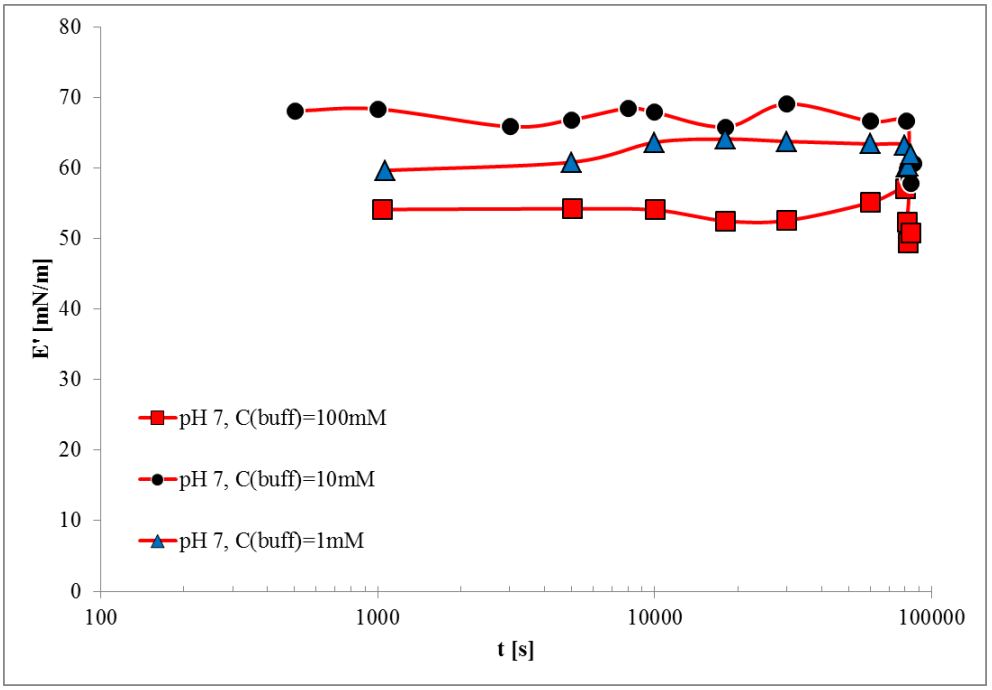
E' [mN/m]
t [s]
pH 7, C(buff)=100mM
pH 7, C(buff)=10mM
pH 7, C(buff)=1mM
0
10
20
30
40
50
60
70
80
100
1000
10000
100000

(b1)

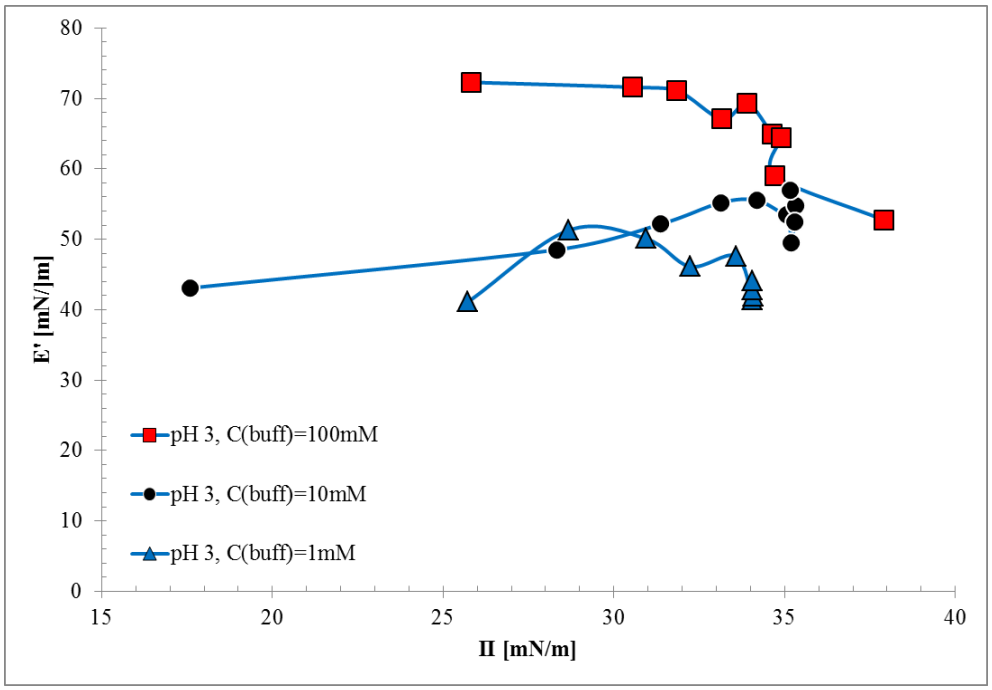
E' [mN/]m]
Π [mN/m]
pH 3, C(buff)=100mM
pH 3, C(buff)=10mM
pH 3, C(buff)=1mM
0
10
20
30
40
50
60
70
80
15
20
25
30
35
40

(b2)

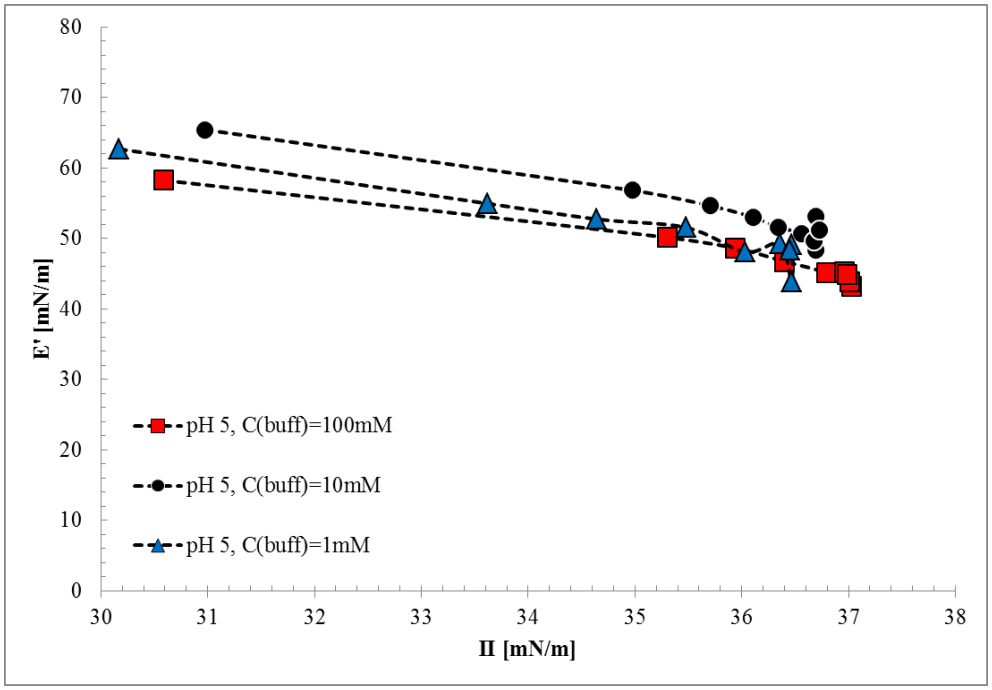

(b3)

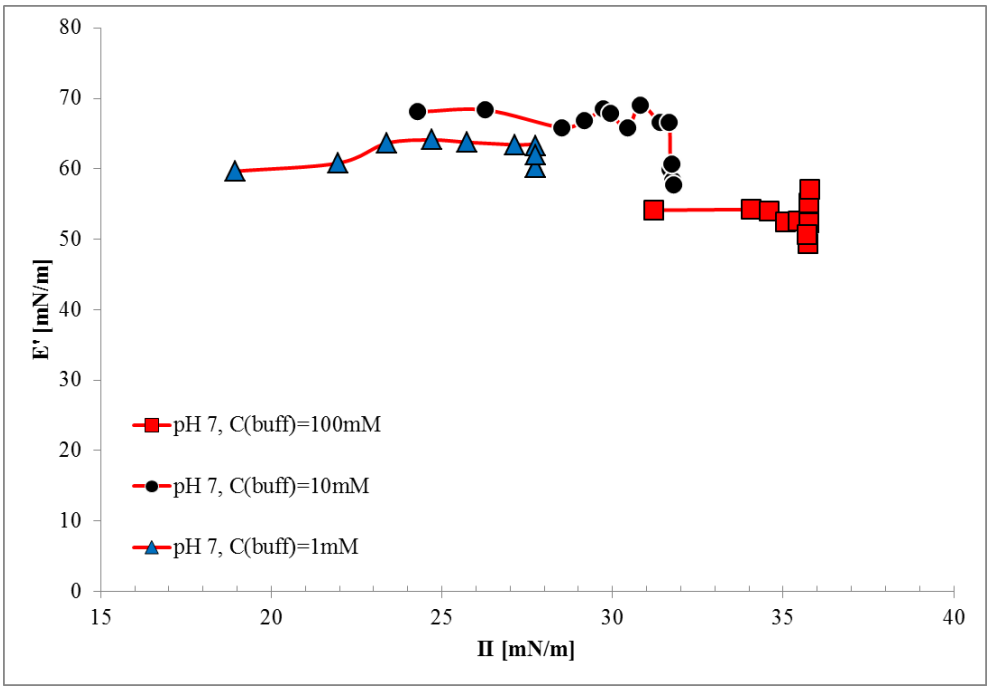

Figure 32 Interfacial properties of BLG solutions at a fixed BLG concentration of 10^{-6} mol/l for three different buffer concentration 1, 10 and 100 mM **(a)** time evolution of the dynamic dilational elasticity E' at f = 0.1 Hz **(b)** dynamic dilational elasticity E' on the interfacial pressure Π at f = 0.1 Hz at pH 3, pH 5 and pH 7; (lines are guides for the eye).

(a)

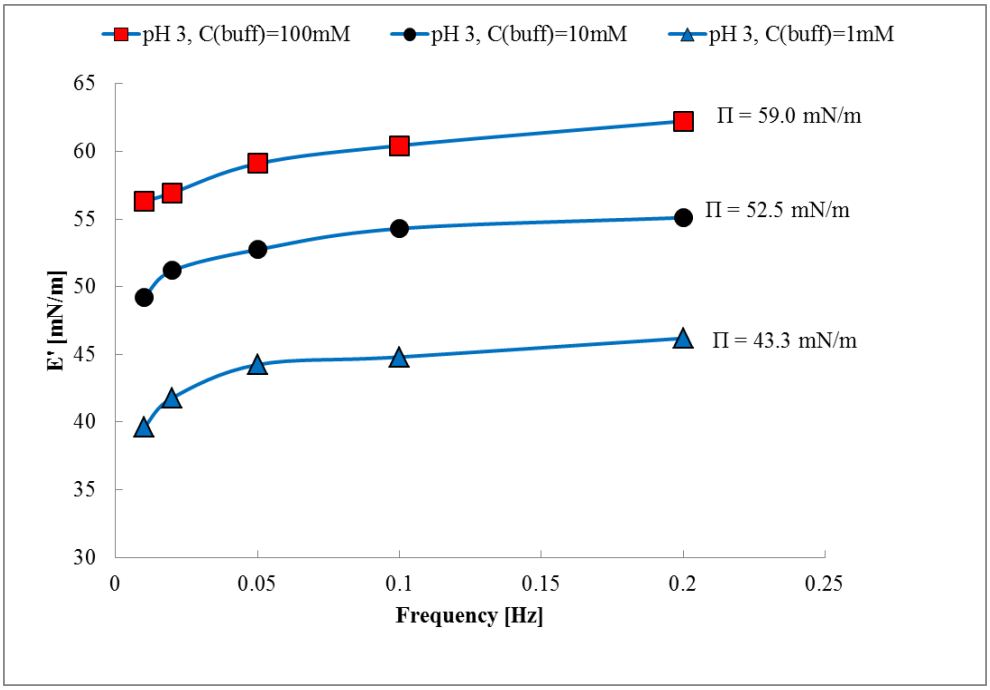
pH 3, C(buff)=100mM
pH 3, C(buff)=10mM
pH 3, C(buff)=1mM
Π = 59.0 mN/m
Π = 52.5 mN/m
Π = 43.3 mN/m
E' [mN/m]
Frequency [Hz]
65
60
55
50
45
40
35
30
0
0.05
0.1
0.15
0.2
0.25

(b)

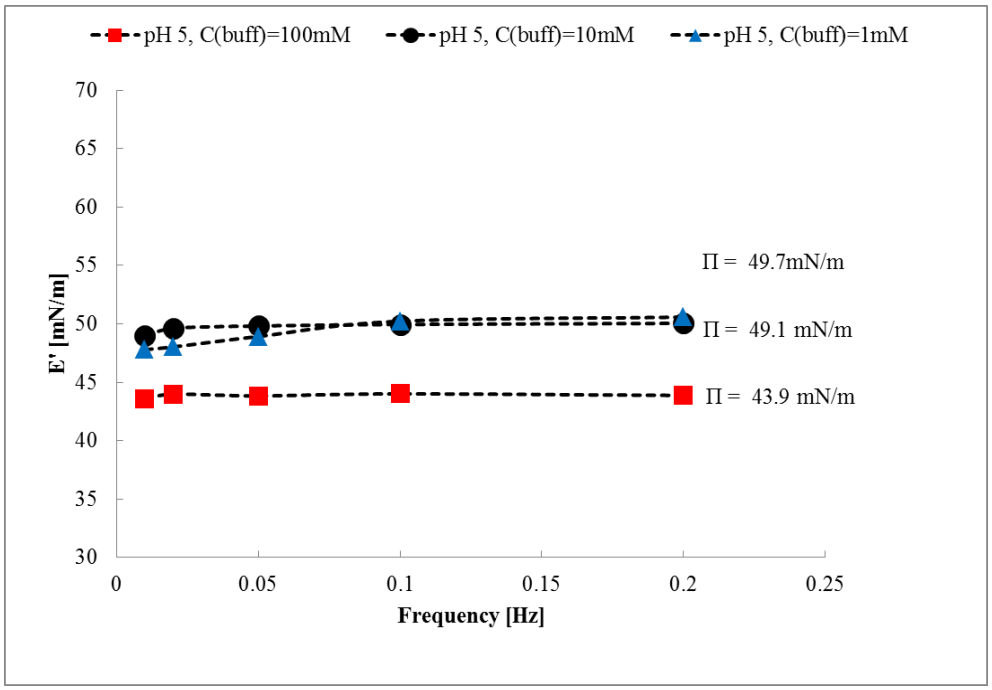
pH 5, C(buff)=100mM
pH 5, C(buff)=10mM
pH 5, C(buff)=1mM
Π = 49.7mN/m
Π = 49.1 mN/m
Π = 43.9 mN/m
E' [mN/m]
Frequency [Hz]
70
65
60
55
50
45
40
35
30
0
0.05
0.1
0.15
0.2
0.25

(c)

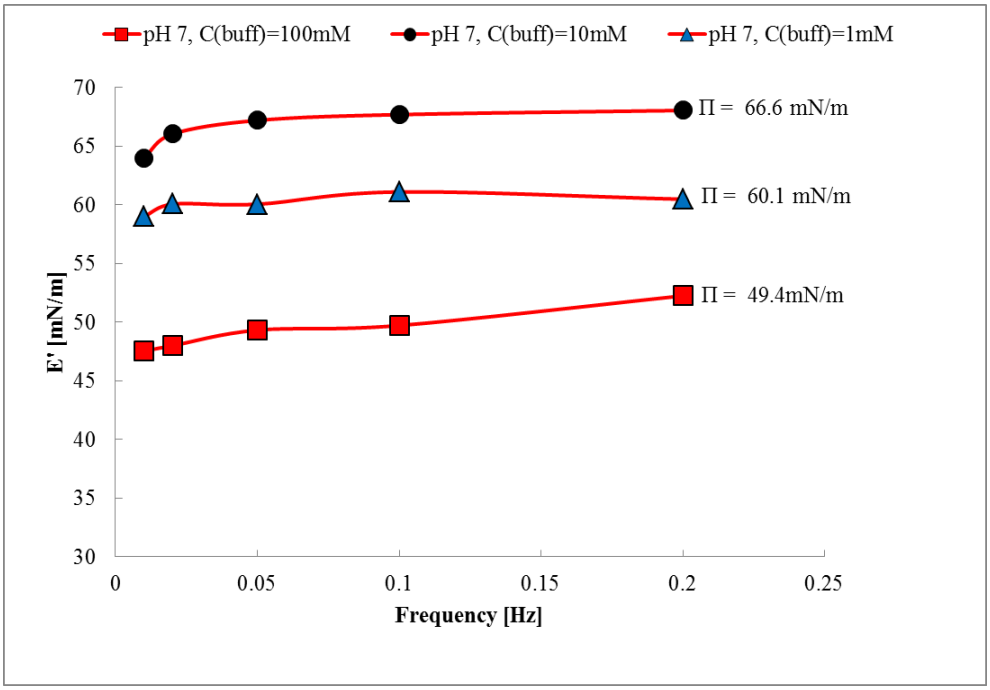

Figure 33 Frequency dependence of the dilational elastic modulus E' at the adsorption time of 80,000 s at a fixed BLG concentration of 10^{-6} mol/l for three different buffer concentrations of 1, 10 and 100mM at the W/TD interface at **(a)** pH 3, **(b)** pH 5, **(c)** pH 7; (lines are guides for the eye).

5.4. Stability of Contacting Bubbles in BLG Solutions

The coalescence of two bubbles was studied by DBMM [93, 94, 95] for different concentrations of BLG solutions and the results are compared with the adsorption characteristics of BLG at the W/A surface using the profile analysis tensiometer PAT-1 [63, 89, 92].

The measured total pressure changes in the left-hand and right-hand side cells are used to estimate the coalescence time from the recorded experimental data. The experimental process can be managed in various ways [94, 95] and one of them is shown in Figure 34. Air bubbles

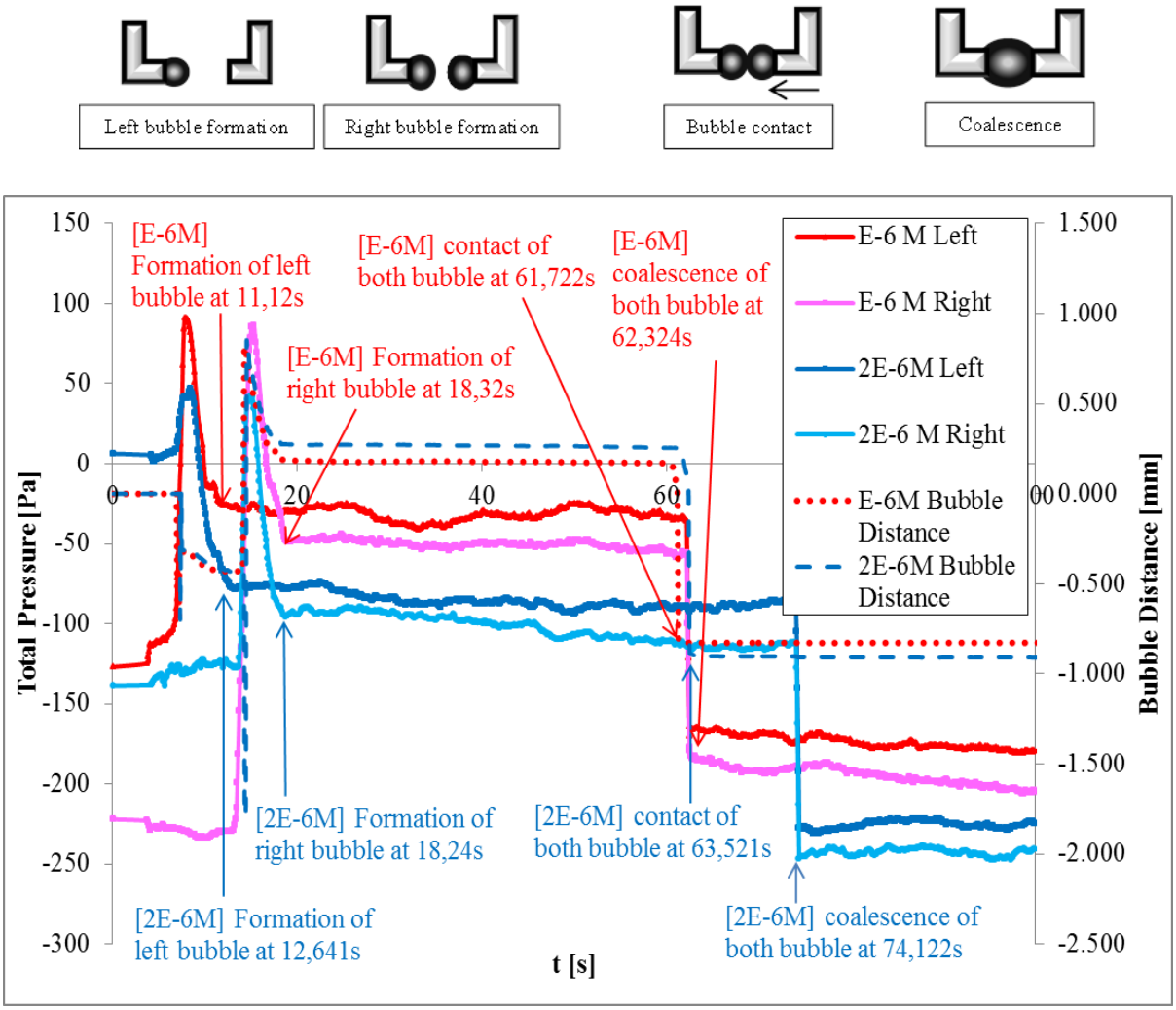

Figure 34 Examples of sudden pressure changes for the process before and after the coalescence of two 40 s pre-aged bubbles using the DBMM for C_{BLG} of 10^{-6} mol/l and 2×10^{-6} mol/l, respectively; data are taken from [94].

at the capillary tips on both sides are formed in BLG solution one after another. The bubble size is kept constant via a piezo control loop over the pre-ageing time of 40 s. Then the right bubble is moved carefully by the xyz-stage towards the left bubble and brought into contact. The moment of bubble contact can be determined by the registered geometry data. Once the bubbles are touching each other, the software starts to recognize them as one big bubble. The distance between the two objects in the record is decreasing and jumping suddenly into a certain value when they touch each other softly. This is defined as contacting point between two bubbles. However, as shown in Figure 34, this contact does not generate changes in the measured pressure data. Sudden pressure changes in both cells happen at the moment of coalescence. After the coalescence the pressures in both cells are identical. The left and right bubbles are formed at 11.12 s and 18.32 s for 10^{-6} mol/l BLG solution and 12.641 s and 18.24 s for 2×10^{-6} mol/l BLG solution, respectively. Coalescence takes place after 0.602 s and 10.601 s, for the two solutions, respectively.

The lifetime of bubbles in BLG solution can be determined according to the stabilities of these bubbles. The resistance time against coalescence between 40 s pre-aged bubbles in

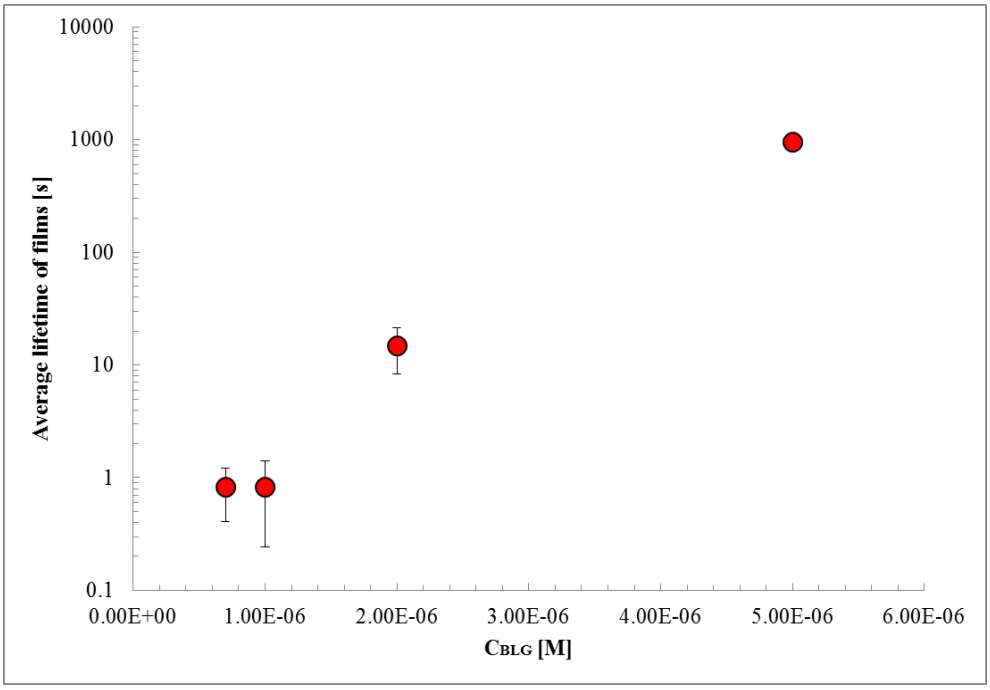

Figure 35 The lifetime of liquid films between two bubbles for different concentration of BLG solution at a fixed pre-ageing time of 40 s; data are taken from [94].

BLG solution is recorded with increasing BLG bulk concentration. It is shown in Figure 35 that the lifetime depends on the concentration of BLG solution. With increasing protein concentration the lifetime of bubbles becomes longer until no coalescence is observed at a concentration of 10^{-4} mol/l and beyond. It indicates that a certain coverage of the bubble surface by protein molecules is needed to avoid the coalescence behaviour of bubbles, hence, stabilization against coalescence can be reached by modification of the interfacial properties.

Bubble-bubble interaction is characterized by the coalescence time and it is difficult to provide detailed information of the dynamic interaction. To get the information of protein adsorption on the bubble surfaces, dynamic interfacial tension measurements have been performed. Using the Profile Analysis Tensiometer PAT-1, the dynamic interfacial tensions were measured for different concentrations of BLG solutions. In Figure 36, dynamic interfacial tension is combined with the results of DBMM which is studied for minimum ageing time to avoid coalescence between fresh air bubbles in different BLG concentrations. The obtained interfacial tensions indicate that the faster decrease of interfacial tension at the first hundred seconds is observed for the higher BLG bulk concentrations. The minimum ageing time at which coalescence between two air bubbles in BLG solution occur is marked in Figure 36 together with the standard deviation. Using this time, we can estimate surface tension of BLG at the bubble surfaces. Although there are some slight differences depending on the concentration, surface tension is in the range between 62.6 mN/m and 66.7 mN/m, except for 5×10^{-5} mol/l and 10^{-4} mol/l. The reason why we exclude these two concentrations is the interfacial tension decreases very quickly and cannot be determined with sufficient accuracy using the PAT-1 instrument.

The combined information on dynamic interfacial tension measurements and minimum ageing time to avoid coalescence demonstrate that the interfacial tensions of the bubble surfaces have to be decreased by about 7 mN/m to prevent an instantaneous coalescence when the two bubbles contact each other. Figure 36 shows that the W/A surface is faster covered at the higher protein concentration while it needs more time at low concentration to have the required number of adsorbed protein molecules. Using the same procedure as described in [99] the amount of protein covering the bubble surface can be estimated and is about 2 mg/m². With increasing time and concentration, the surface layer becomes more and more packed. In [99] it was discussed that from a certain surface pressure on, the formation of a secondary adsorption layer starts, i.e. in adsorption equilibrium this happens at about

2×10^{-6} mol/l. The total adsorption, according to the published data, increases up to about 5 mg/mm² [94].

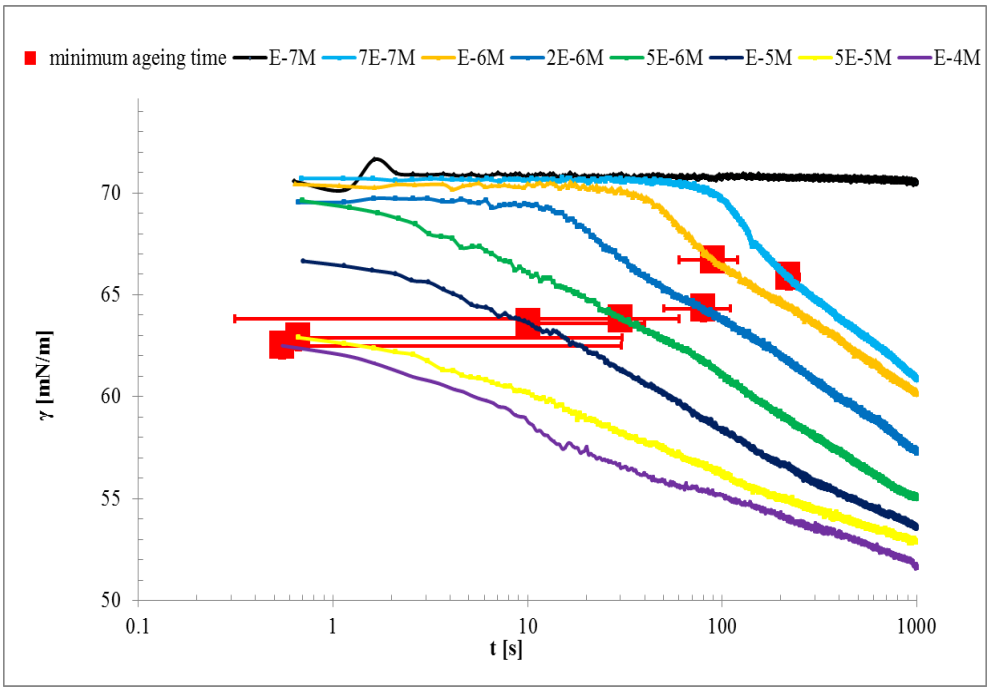

Figure 36 The combination of the results of dynamic interfacial tension measurements (curves) using PAT-1 and the minimum ageing time to avoid coalescence using DBMM (symbols with standard deviation) for BLG solution at different BLG concentration at pH 6; data are taken from [94].

Due to the complex experimental handling, experiments with two droplets contacting each other, i.e. model experiments to mimic the situation in emulsions, are yet pending. It can be expected, however, that the developed methodology for the DBMM will work in the same successful way. These experiments will be performed in future studies.

6. SUMMARY AND CONCLUSIONS

The interfacial tension isotherms of BLG adsorption at the solution/tetradecane (W/TD) interface at the solution pH of 3, 5 and 7 can be well described by a thermodynamic model. All model parameters obtained by fitting the experimental data to the theory are more or less identical for the three pH values, except the surface activity parameter b, which increases with the pH.

A new diffusion controlled model to describe the protein adsorption kinetics is proposed. The classical model with time-independent adsorption activity coefficient, referred to as the TIC model [41], fails to adequately describe our experimental results. In contrast, the new model with a time-dependent (or surface-coverage dependent) adsorption activity coefficient, named as the TDC model [42, 45], is successfully applied to the dynamic interfacial tension data measured by drop profile analysis tensiometry. Figure 37 represents an example for the quality of data interpretation.

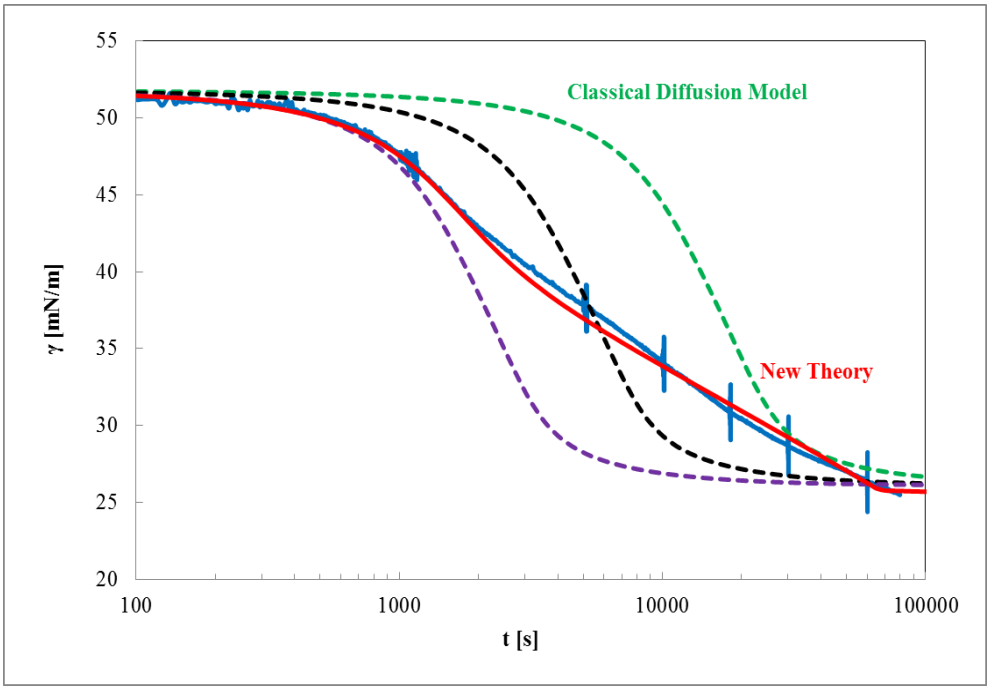

Figure 37 Dynamic interfacial tension γ(t) for a BLG solution with a concentration of 10^{-7} mol/l at pH 3 at the W/TD interface; blue curve – experimental data, dashed curves – calculations using the TIC model for different diffusion coefficients, red curve – calculations using the TDC model and a fixed diffusion coefficient.

The results make clear that the measured dynamic interfacial tensions cannot be properly described by a pure diffusion controlled (TIC) model. In contrast, the proposed combined model of diffusional transport and an additional time process can describe the experimental data properly. The model assumes that the conformational changes of adsorbed protein molecules can be reflected by changes in the adsorption activity coefficient.

When protein molecules come into the interface, they are subjected to conformational changes. Protein molecules start to adsorb at the interface in a folded conformation. At low bulk concentrations they have enough free space at the interface to unfold. An unfolded protein molecule occupies a larger interfacial area. Moreover, at water/oil interfaces the hydrophobic parts of the protein molecules have the tendency to penetrate into the oil phase which is supported by the conformational change. The consequence of this changed conformation is taken into account in terms of a change in the adsorption constant parameter in the corresponding equation of state. The rate (kinetic) constant k obtained by a best fitting of the experimental results using the proposed mixed adsorption model depends on the BLG bulk concentration and on the solution pH. The kinetic constant k for BLG solutions is the smallest at pH 5 (negligible net charge and compact molecular structure), which physically means that the protein molecules change their conformation at the interface to the smallest extent at these conditions. In contrast, it is the biggest at pH 3 (highest net charge and increased affinity to the aqueous subphase) which means the conformational changes of the proteins are the largest.

The adsorption behaviour generally shows increasing interfacial pressure and elasticity with increasing the protein concentration. A comparison of the model calculations of the adsorption behaviour of BLG at the W/TD interface [42, 45] with those at the water/air (W/A) surface [25, 32] is presented in Figure 38 (a). The interfacial pressure of BLG adsorbed layers at the W/TD interface starts to increase at concentrations many orders of magnitude lower than that for the W/A surface. In addition, the isotherms at the W/A surface are much steeper than the corresponding ones at the W/TD interface. While the adsorption isotherms at the W/A surface reach the critical point of secondary layer formation [74] at rather low protein concentrations, the critical points are reached at much higher protein bulk concentrations at the W/TD interface. In addition, the interfacial pressure values Π^* at these critical concentrations are much larger at the W/TD interface than at the W/A surface by almost a factor of three. Hence, one could conclude that the adsorbed amounts at the W/TD interface

should be much larger than at the W/A surface. However, the corresponding Γ-values shown in Figure 38 (c) are only slightly higher than those calculated for BLG at the W/A surface. Therefore, we must conclude that it is not the total adsorbed amount that leads to the high interfacial pressure values observed at the W/TD interface, but the interfacial structure resulting from a strong interaction between the hydrophobic parts of the adsorbed protein molecules and the TD.

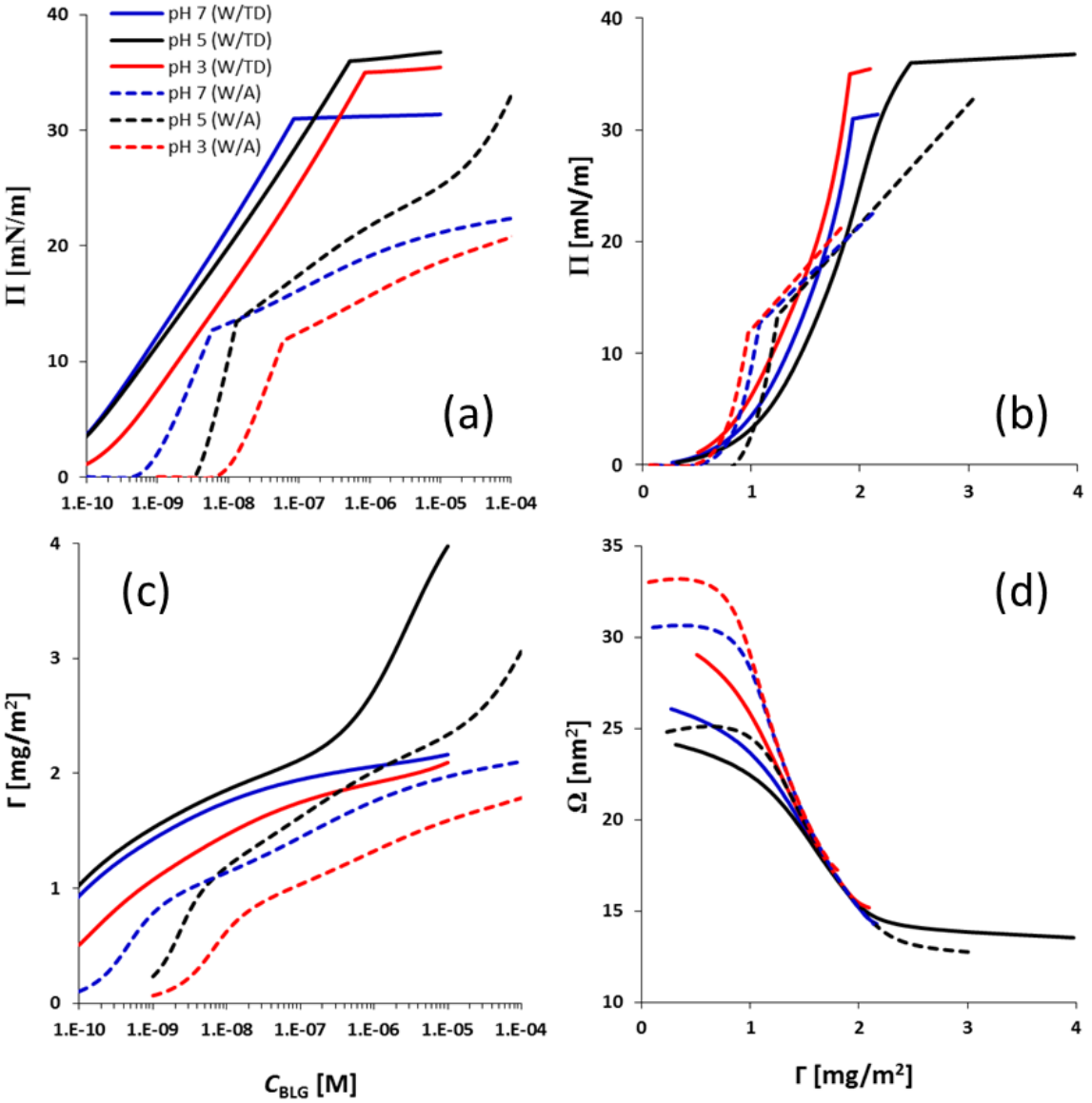

Figure 38 Comparison of BLG adsorbed layers at the W/A and W/TD interfaces, respectively; **(a)** Experimental interfacial pressure Π–C_{BLG} isotherms, **(b)** calculated dependence of Π on the adsorbed amount Γ of BLG, **(c)** calculated dependences of the adsorbed amount of BLG on C_{BLG}, **(d)** calculated dependences of the molecular area Ω on the adsorbed amount of BLG at three selected pH values of 3, 5 and 7 at the W/TD (solid lines) and the W/A (dashed lines) interfaces; pH 7 - blue lines, pH 5 - black lines, pH 3 - red lines.

ACKNOWLEDGEMENTS

I would like to express my sincerely gratitude to my supervisor Prof. Dr. Gerald Brezesinski for providing me with the opportunity to submit my thesis at the University of Potsdam.

Throughout my doctoral studies I have always been able to rely on the advice and support of my group leader, Dr. habil. Reinhard Miller. Thank you for giving me such opportunity to carry out this interesting project as a PhD student. I cannot thank enough for your dedication, guidance, consideration, support and supervision through my PhD. Your expert guidance and quick thinking have helped me to guide my steps in these past four years and I will always be grateful to you for guiding my development in academia. Also thank you for encouraging me to reach beyond my limit and giving me such opportunities to organize great international conferences, European Student Colloids Conference 2013, Food Colloids 2014 and Bubble and Drops Interfaces 2015. Through these conferences, I have met good people and friends from all over the world.

I would like to express my heartfelt gratitude and acknowledgement to my third supervisor, Doktor Allwissend, Dr. Jürgen Krägel. I have remembered the day when I met you first. Since then, you became my great assistor and adviser.

I have learnt a lot from all of you, not only as supervisors, but also as wonderful mentors. Many thanks to you for making all achievements become possible.

I would also like to say big thanks to Sabine Siegmund. You probably don't know how much I like you and rely on you. You were a good colleague and at the same time you are my best friend during my stay at MPIKG. I cannot imagine the lab without you. Inside and outside of the lab, you are the best. Danke schön für alles.

I kindly say many thanks to Prof. Valentin B. Fainerman for your help in the theoretical analysis of my experimental data.

I acknowledge my excellent senior colleagues Dr. Rainer Wüstneck, Prof. Dieter Vollhardt, Dr. Nina M. Kovalchuk, Dr. Volodja I. Kovalchuk, Dr. Eugene V. Aksenenko, Prof. James K. Ferri, Prof. Boris Noskov, Prof. A. Wilhelm Neumann and Prof. Giuseppe Loglio for their scientific advice and efforts.

Throughout my time at the Max Planck Institute of Colloids and Interfaces, I have been privileged to work with many excellent people. It was just a routine, but precious time for me drinking coffee or tea with you in our coffee corner. I want to thank all my group members and co-workers, Dr. Georgi G. Gochev, Dr. Abhijit Dan, Dr. Nenad Mucic, Dr. Antonio Perazzo, Dr. Dominik Kosior, Irina Berndt, Samee Faraji, Dr. Luisma Pérez-Mosqueda, Dr. Liguo Shen, Ildyko Kovach, Inga Retzlaff, Dr. Aliyar Javadi, Dr. Mohsen Karbaschi, Narges Moradi, Dr. Chenyu Jin, Dr. Julia Schneider and Dr. Martin Haase, who helped me to overcome research difficulties and supported me. Especially thanks go to Vamseekrishna Ulaganathan who was sitting next to me and being my punching bag for over 4 years. Thank you for your great patience.

I would also like to say special thanks to Dr. Sara Llamas and Dr. Xiaowei Hu. Both of you stayed in Golm only for 2 months and 1 year, respectively, but I had happy time because you were here. You were supporting and standing by me when I find myself in times of trouble. As the proverb says, you showed me that a friend in need is a friend indeed. ¡Gracias!. Xiexie 謝謝.

Last but not least, I would like to thank my daddy and mommy for their sacrifices and support. Also I am very thankful to my brothers and sisters, Seunghwan, Eunju, Yousun, Hyukchul and Seunghui, and my lovely nephews, Jaehun, Dohun and Hyunjune for their encouragement, without all your constant love and belief in me I couldn't complete this work. 고마워요. 사랑합니다.

Appendix 1 Dynamic interfacial tensions γ(t) for various concentrations of BLG solution at the W/TD interface at pH 3; blue curves – experimental data, black curves – calculated using the TIC model, red curves – calculated using the TDC model which implies additional dependence of surface activity coefficient on time.

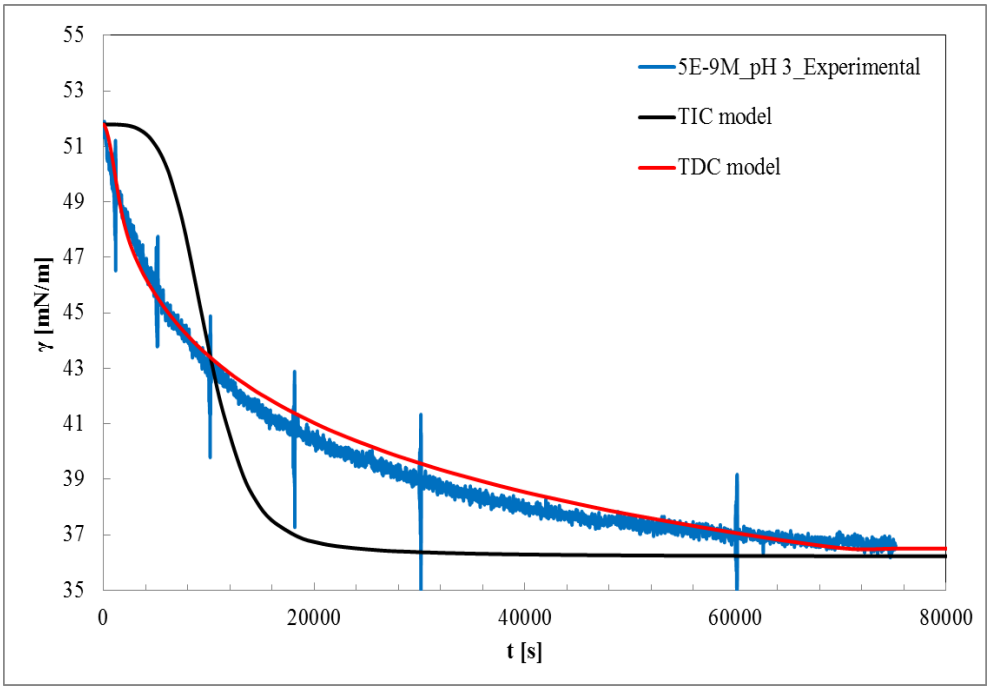

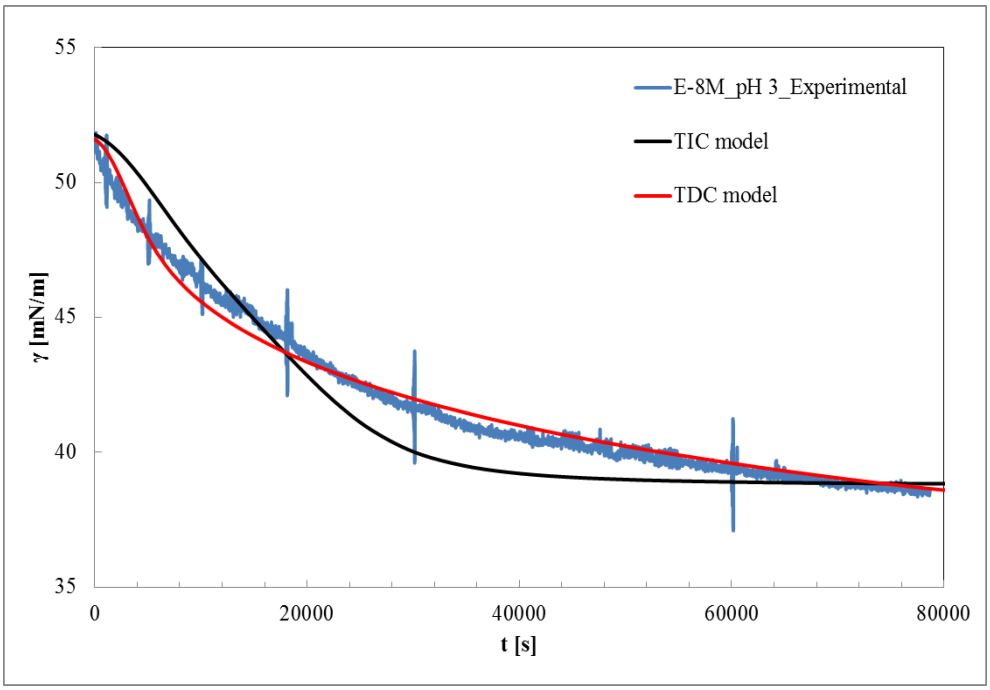

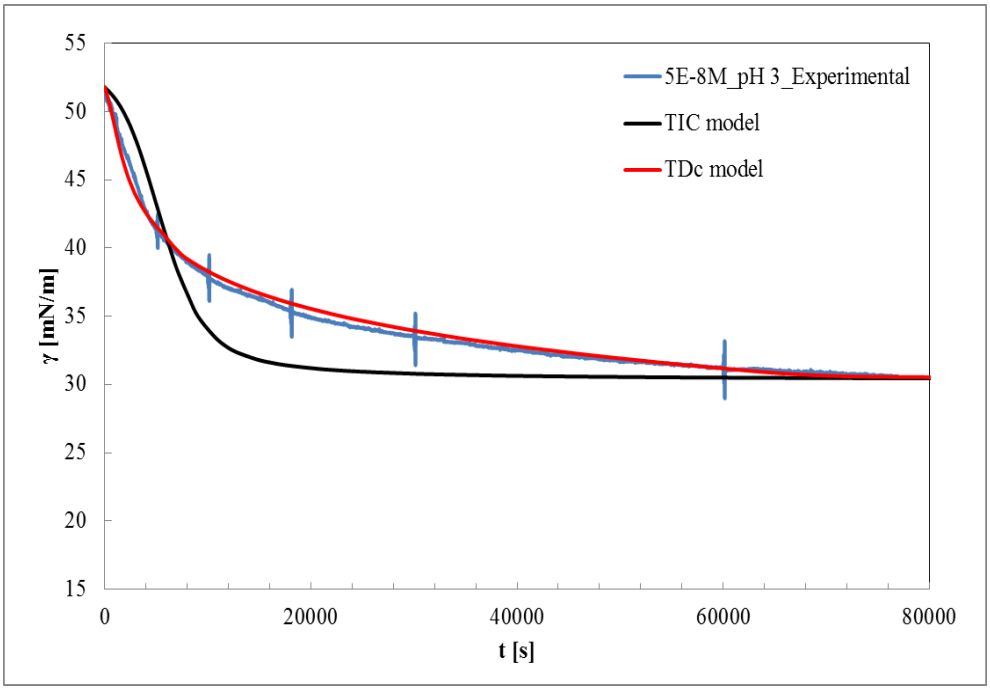
5E-8M_pH 3_Experimental
TIC model
TDc model
γ [mN/m]
t [s]
55
50
45
40
35
30
25
20
15
0
20000
40000
60000
80000

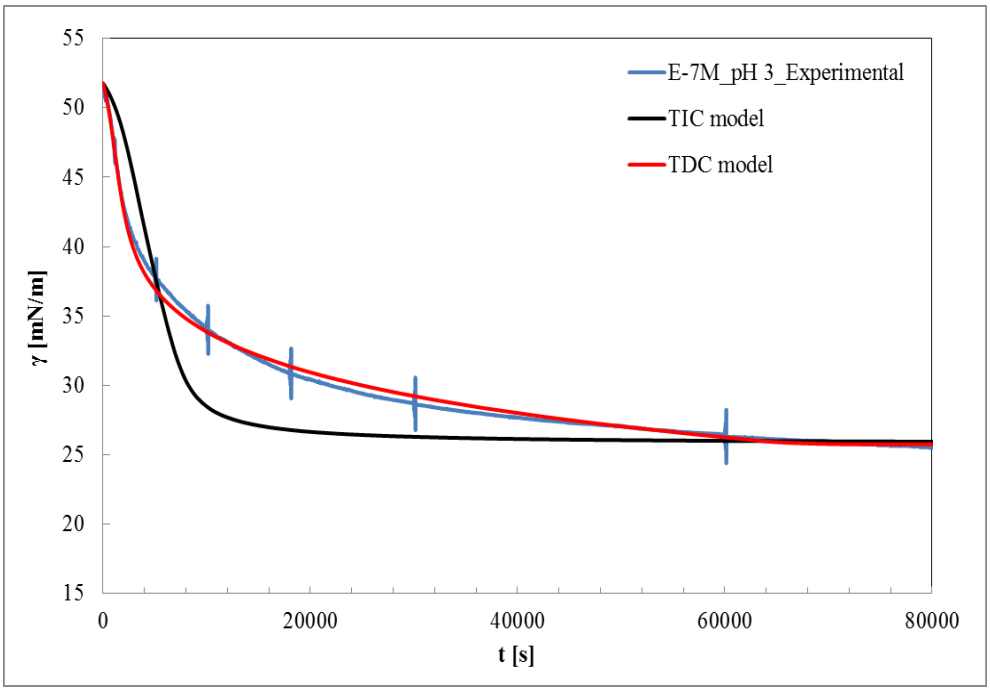
E-7M_pH 3_Experimental
TIC model
TDC model
γ [mN/m]
t [s]
55
50
45
40
35
30
25
20
15
0
20000
40000
60000
80000

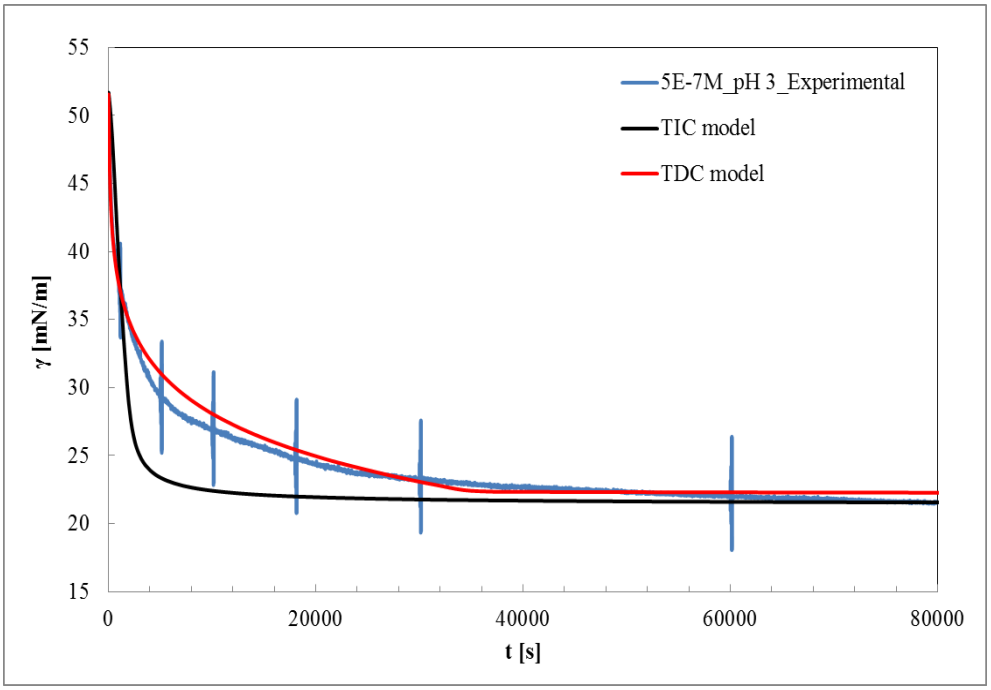
5E-7M_pH 3_Experimental
TIC model
TDC model
γ [mN/m]
t [s]
55
50
45
40
35
30
25
20
15
0
20000
40000
60000
80000

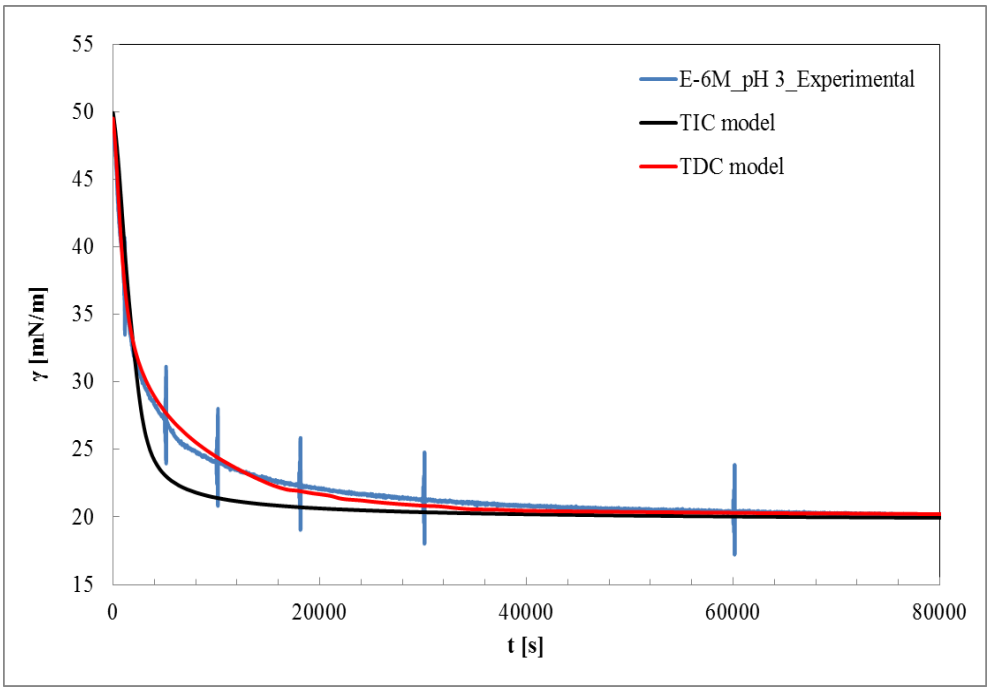
E-6M_pH 3_Experimental
TIC model
TDC model
γ [mN/m]
t [s]
55
50
45
40
35
30
25
20
15
0
20000
40000
60000
80000

Appendix 2 Dynamic interfacial tensions γ(t) for various concentrations of BLG solution at the W/TD interface at pH 5; blue curves – experimental data, black curves – calculated using the TIC model, red curves – calculated using the TDC model which implies additional dependence of surface activity coefficient on time.

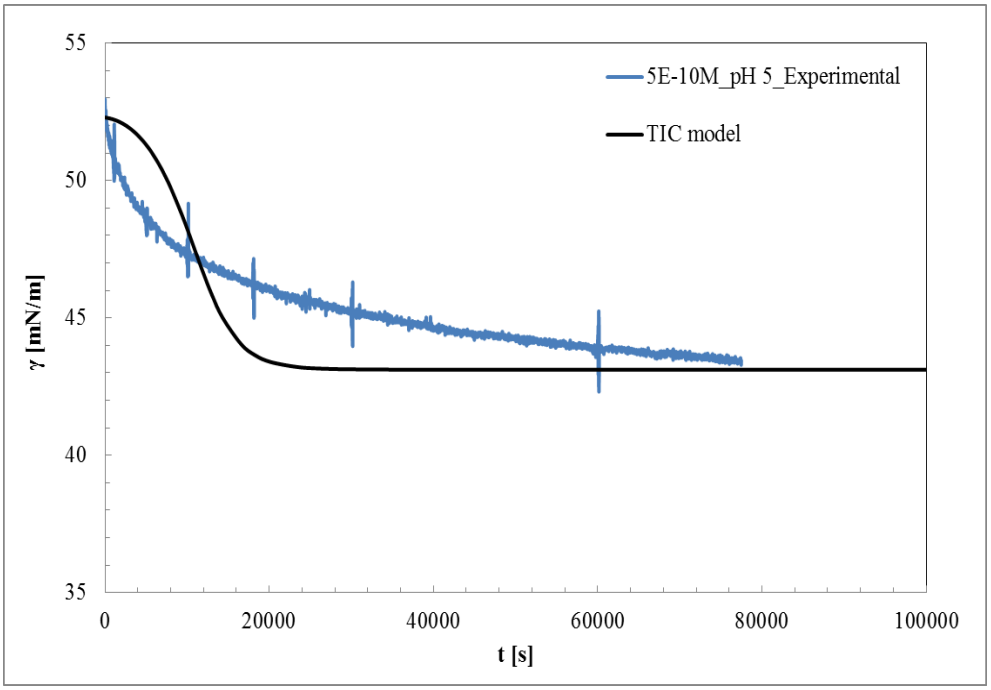

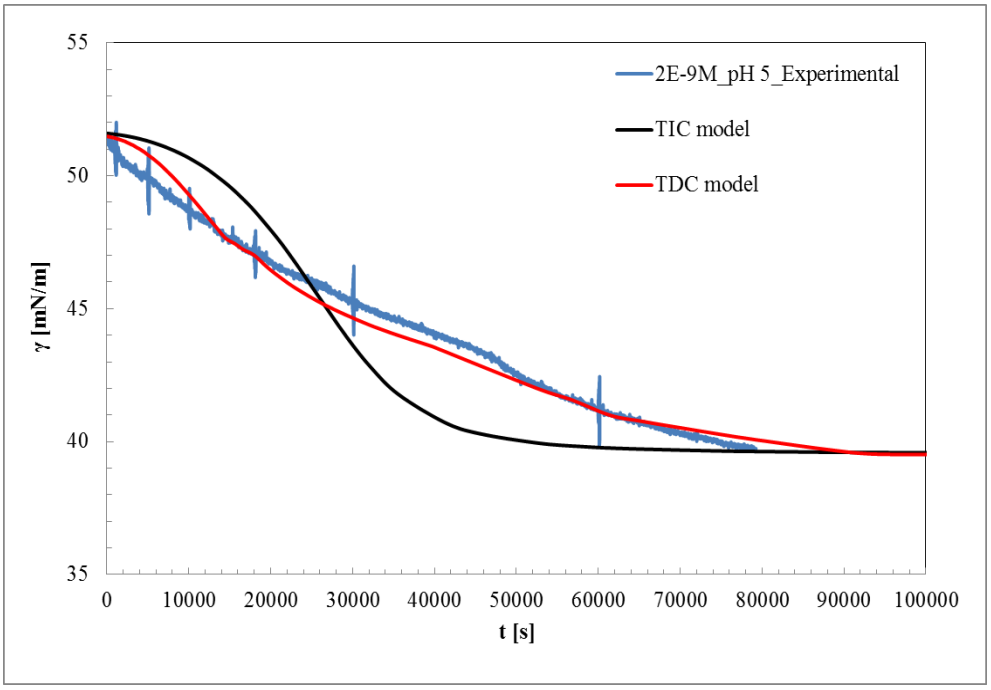

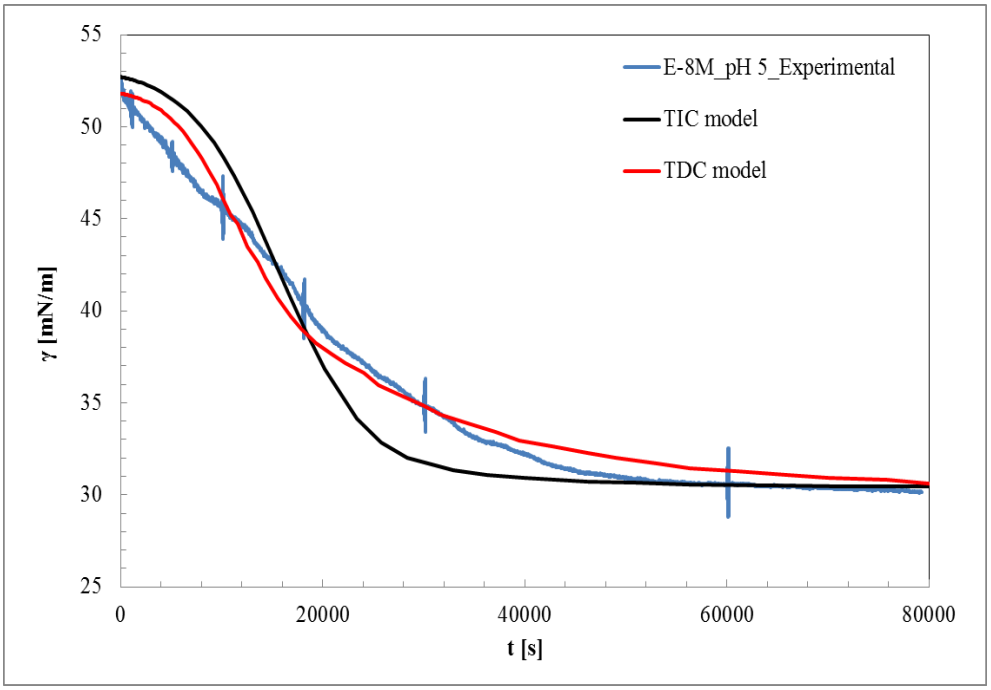
E-8M_pH 5_Experimental
TIC model
TDC model
γ [mN/m]
t [s]
55
50
45
40
35
30
25
0
20000
40000
60000
80000

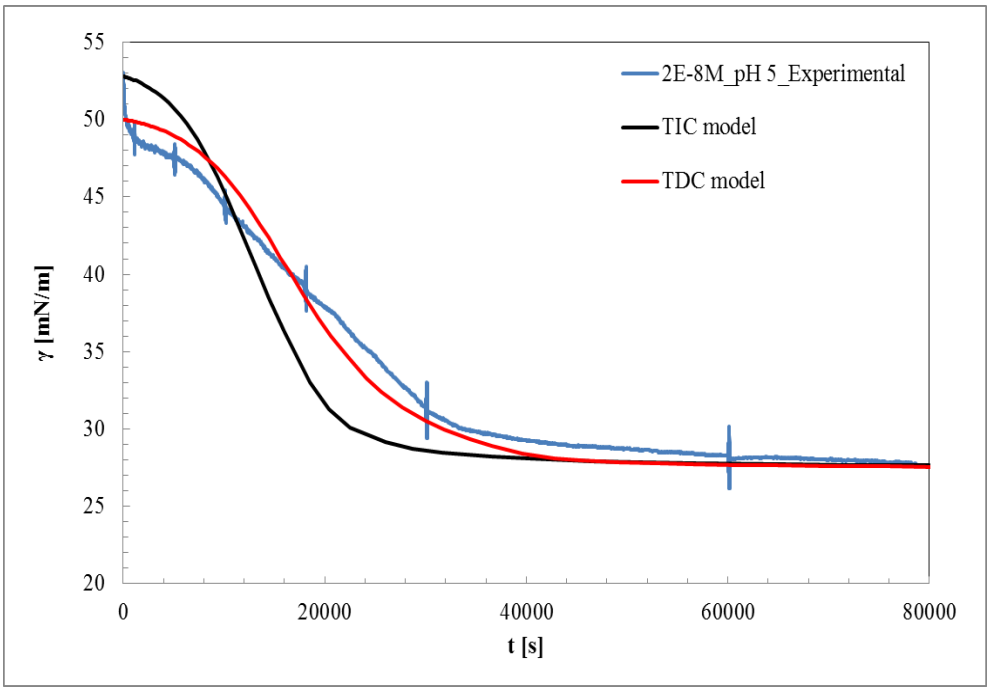
2E-8M_pH 5_Experimental
TIC model
TDC model
γ [mN/m]
t [s]
55
50
45
40
35
30
25
20
0
20000
40000
60000
80000

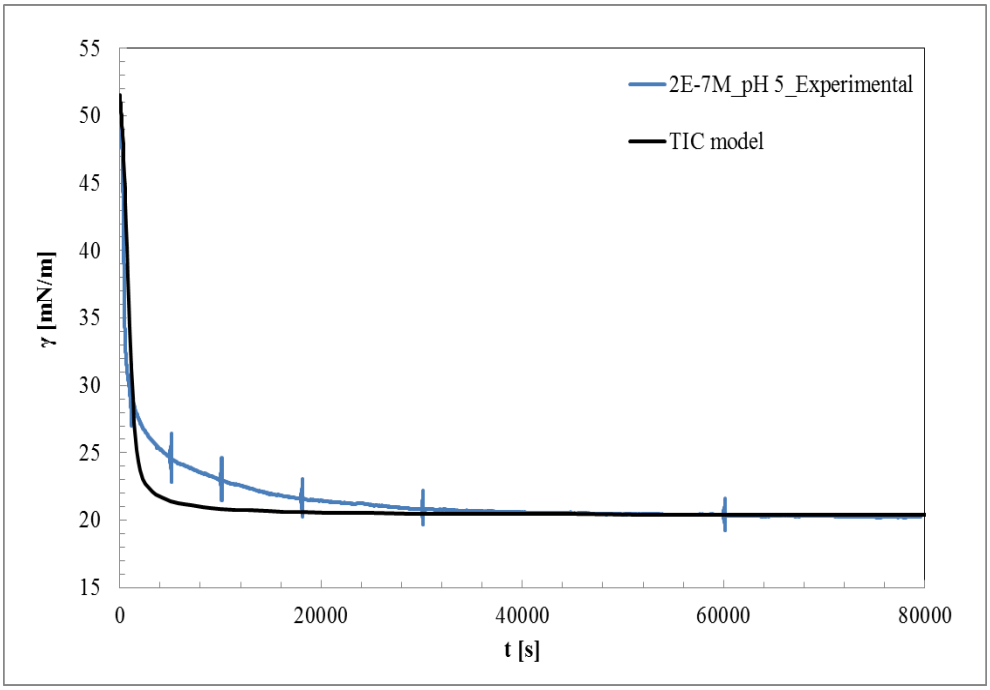
55
50
45
40
35
30
25
20
15
γ [mN/m]
0
20000
40000
60000
80000
t [s]
2E-7M_pH 5_Experimental
TIC model

Appendix 3 Dynamic interfacial tensions γ(t) for various concentrations of BLG solution at the W/TD interface at pH 7; blue curves – experimental data, black curves – calculated using the TIC model, red curves – calculated using the TDC model which implies additional dependence of surface activity coefficient on time.

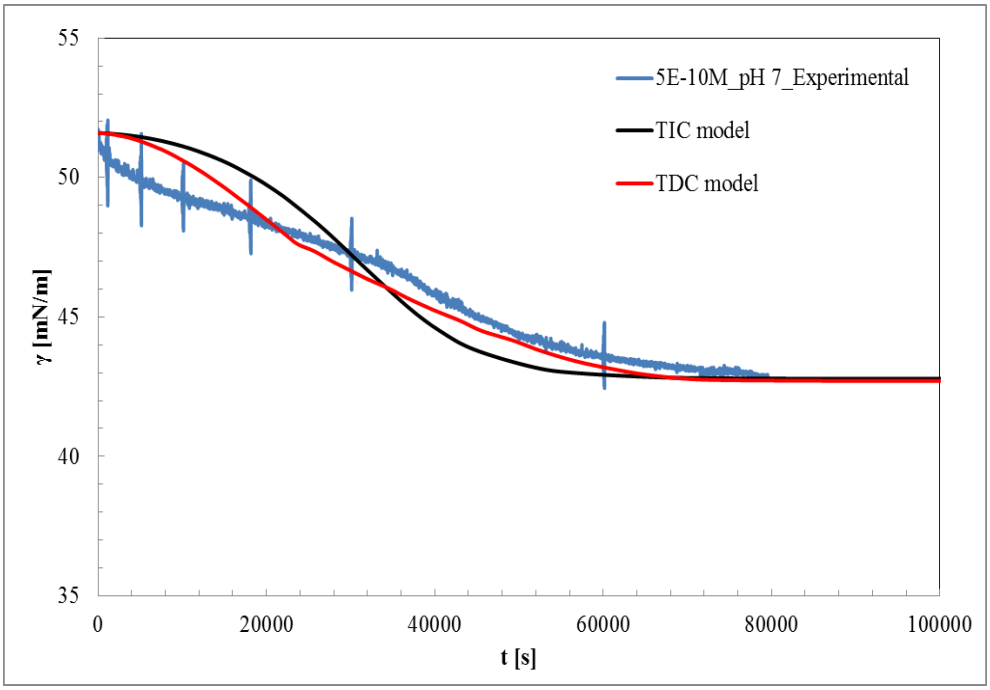

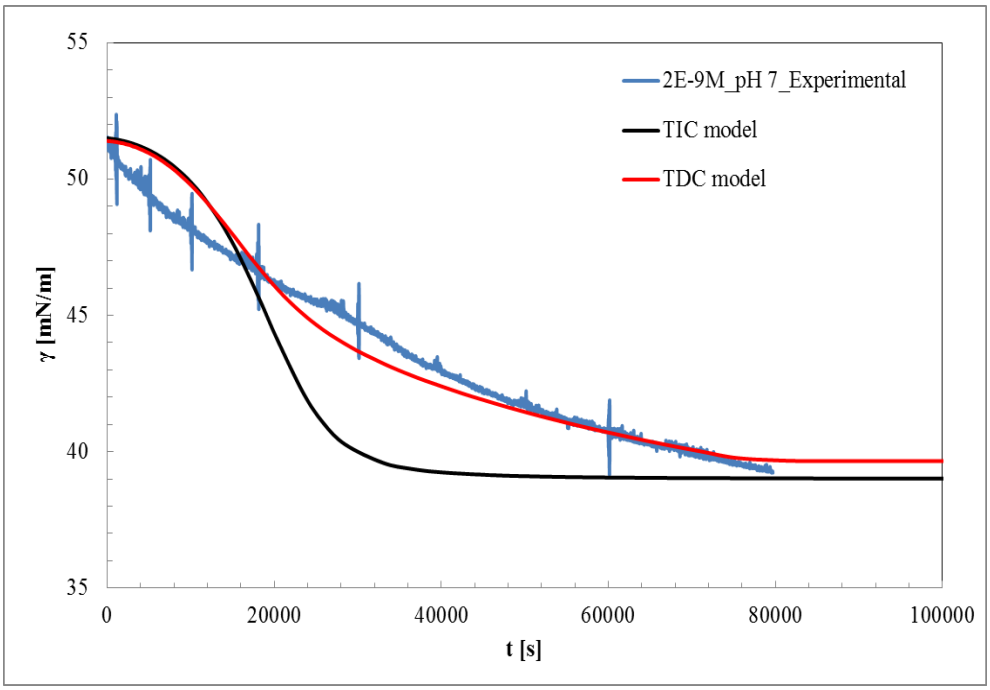

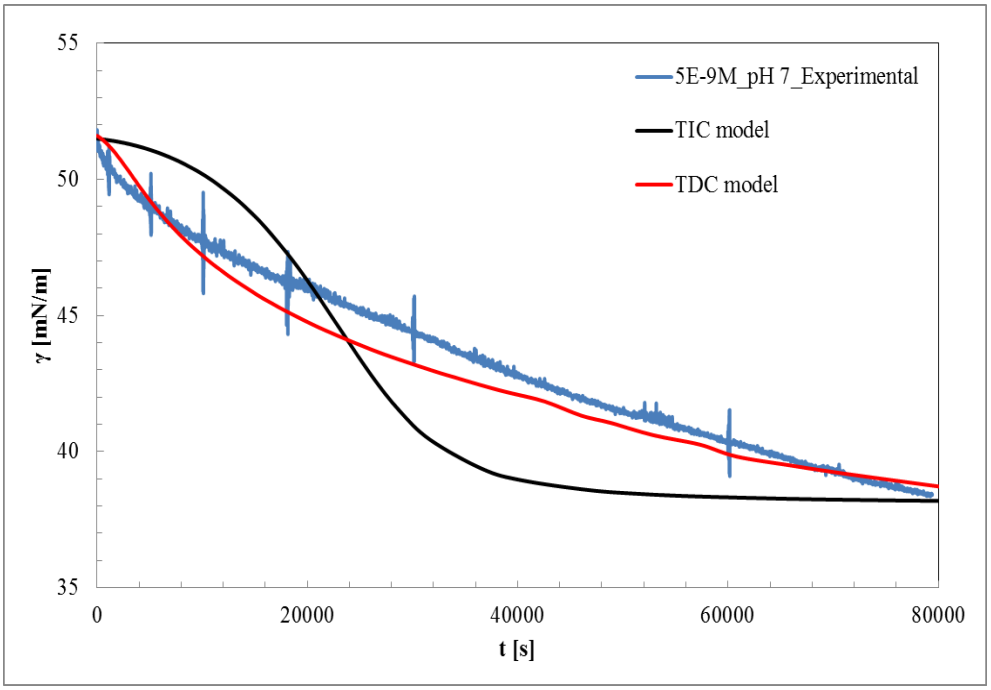
55
50
45
40
35
γ [mN/m]
0
20000
40000
60000
80000
t [s]
5E-9M_pH 7_Experimental
TIC model
TDC model

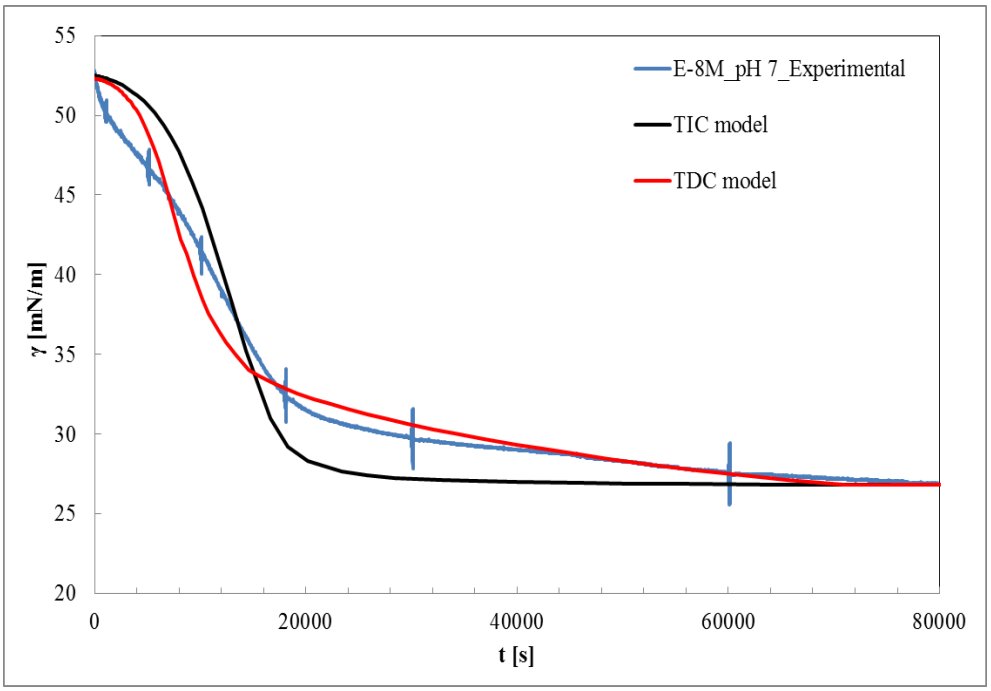
55
50
45
40
35
30
25
20
γ [mN/m]
0
20000
40000
60000
80000
t [s]
E-8M_pH 7_Experimental
TIC model
TDC model

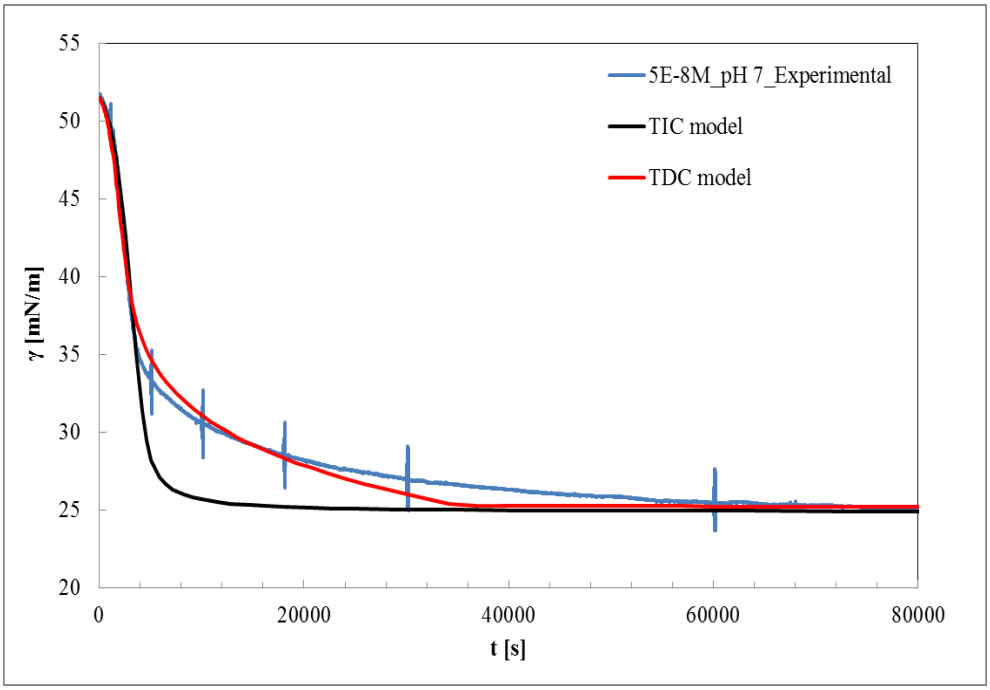
5E-8M_pH 7_Experimental
TIC model
TDC model
γ [mN/m]
t [s]
55
50
45
40
35
30
25
20
0
20000
40000
60000
80000

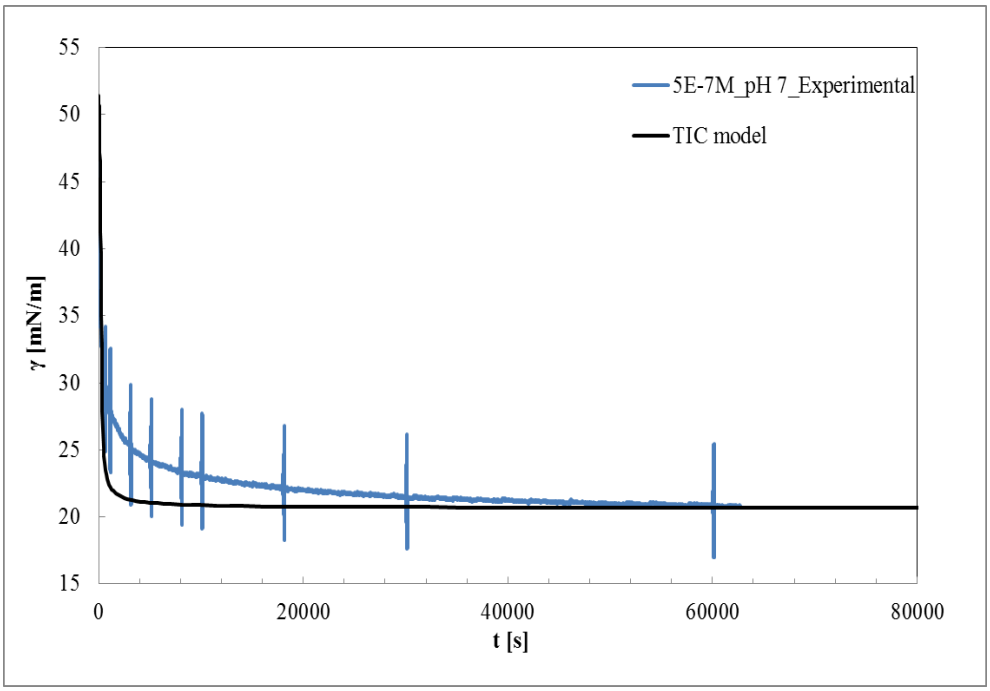
5E-7M_pH 7_Experimental
TIC model
γ [mN/m]
t [s]
55
50
45
40
35
30
25
20
15
0
20000
40000
60000
80000

Appendix 4 Evolution of the interfacial pressure Π(t) for different BLG concentrations at three pH value of pH 3, 5 and 7 at the W/TD interface; 5×10^{-9} mol/l (the concentration between a and b of Figure 18) and 10^{-7} mol/l (the concentration between b and c of Figure 18); (lines are guides for the eye).

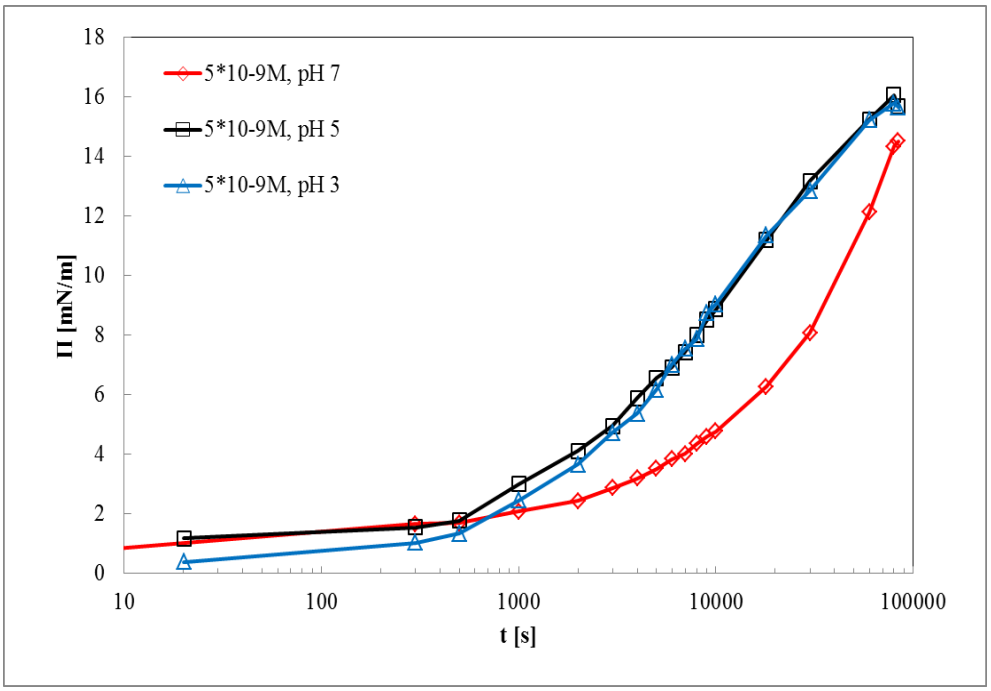

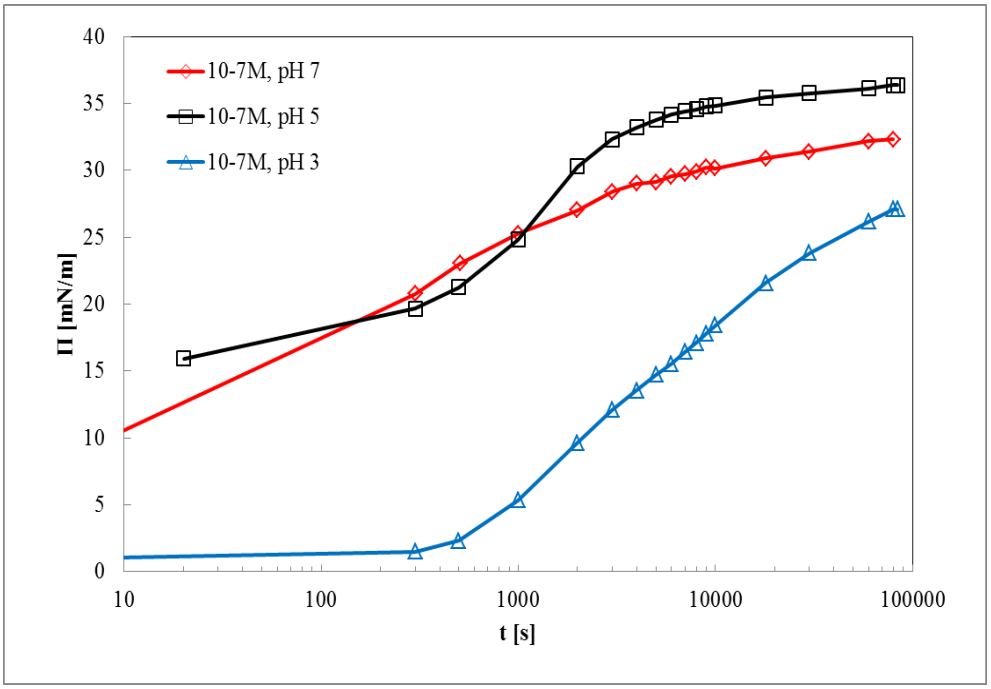

Appendix 5 Interfacial properties of 10mM buffered BLG solutions for selected BLG concentrations at pH 3 at the W/TD interface; **(a)** time evolution of the measured dynamic dilational elastic modulus E' at f = 0.1 Hz, **(b)** the measured dynamic dilational elastic modulus E' on the interfacial pressure Π at f = 0.1 Hz, **(c)** frequency dependence of the measured dynamic dilational elastic modulus E' at the adsorption time of 80,000 s, the interfacial pressure for each cases are also shown in the graph; (lines are guides for the eye).

(a)

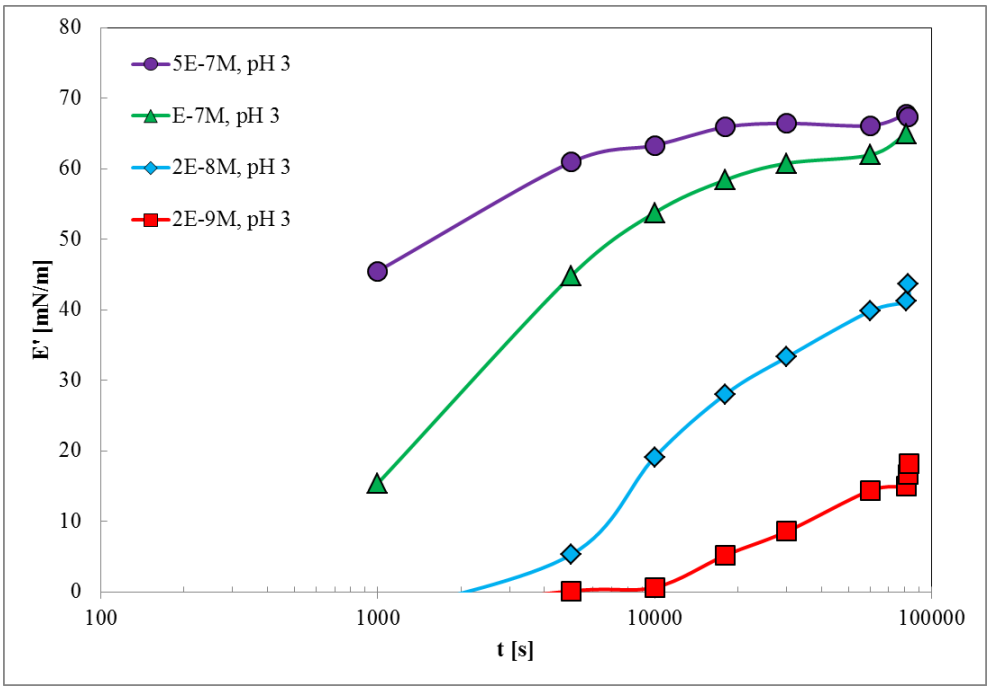

(b)

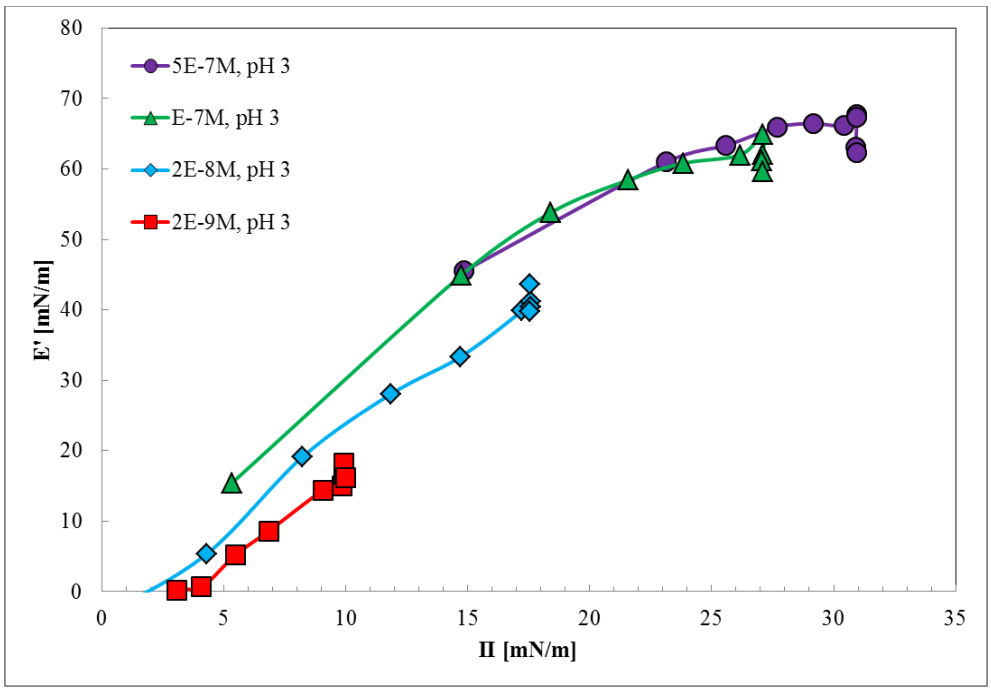

(c)

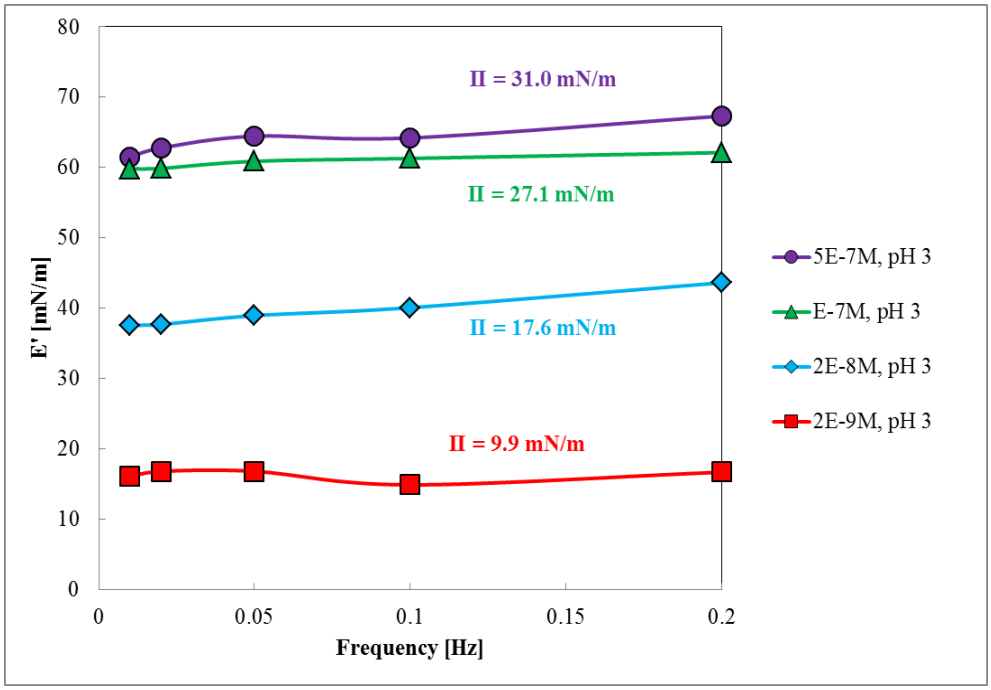
80
70
60
50
40
30
20
10
0
E' [mN/m]
0
0.05
0.1
0.15
0.2
Frequency [Hz]
Π = 31.0 mN/m
Π = 27.1 mN/m
Π = 17.6 mN/m
Π = 9.9 mN/m
5E-7M, pH 3
E-7M, pH 3
2E-8M, pH 3
2E-9M, pH 3

Appendix 6 Time evolution of the dynamic dilational viscocity E" at f = 0.1 Hz for BLG solutions at a fixed BLG concentration of 10^{-6} mol/l for three different buffer concentration 1, 10 and 100 mM at pH 3, 5 and 7; (lines are guides for the eye).

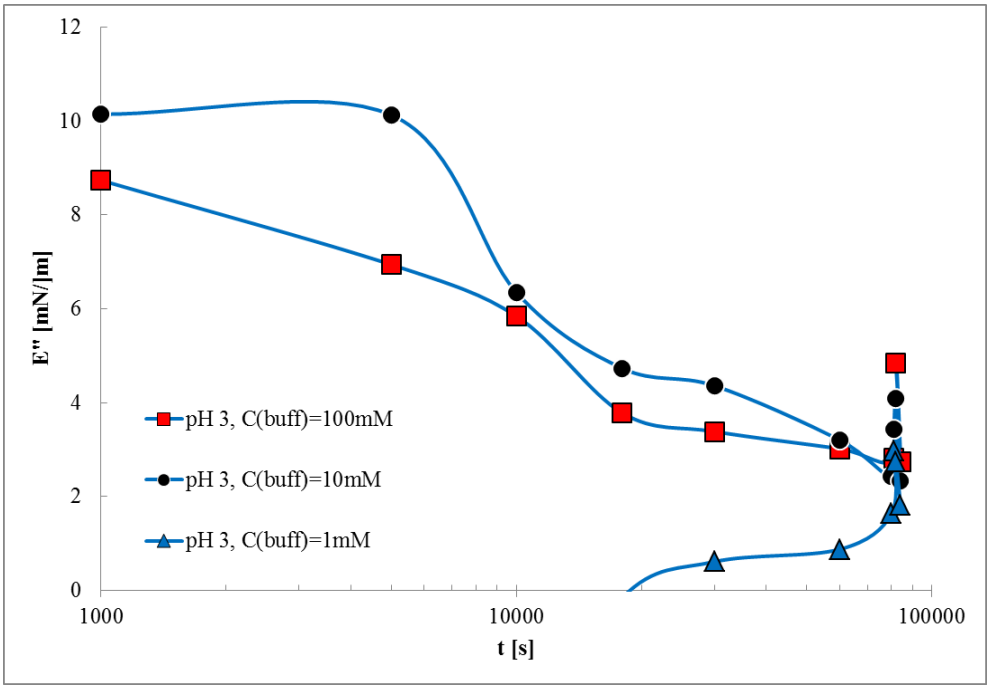

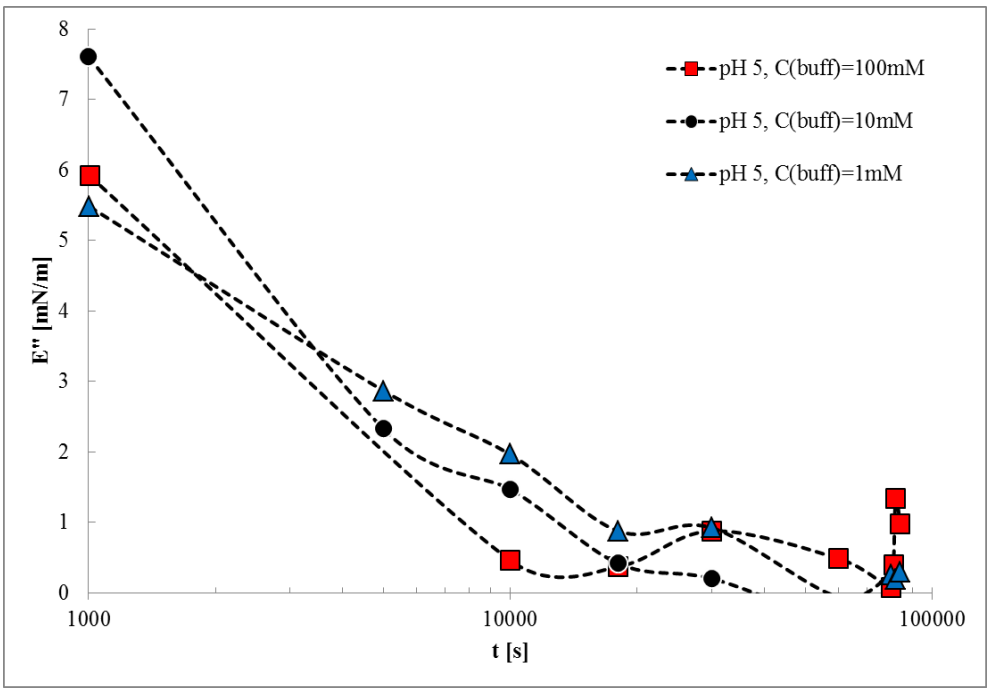

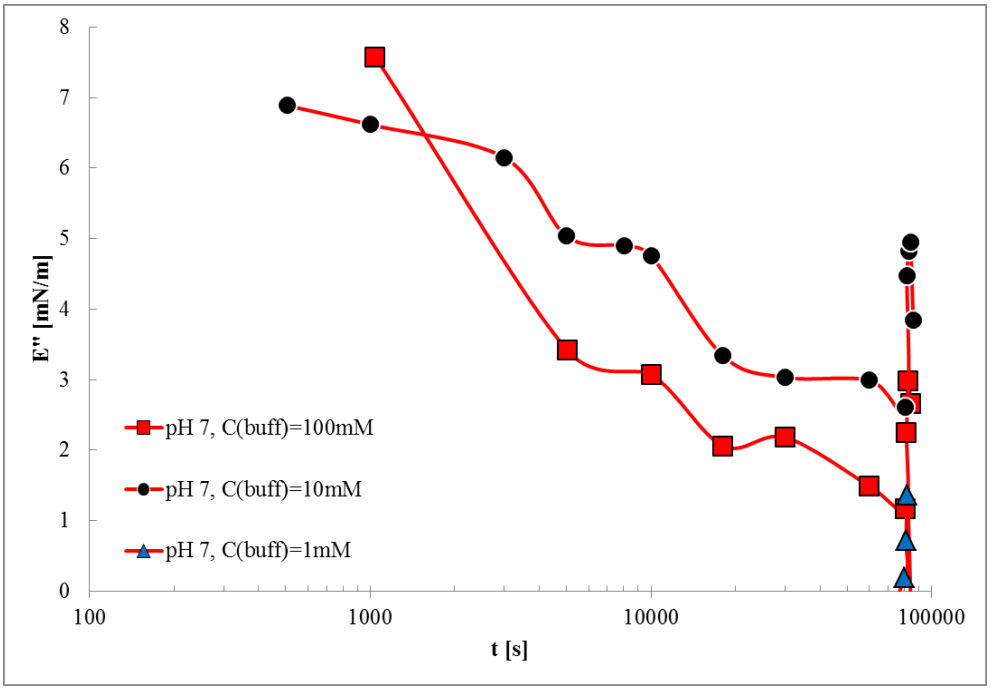
8
7
6
5
4
3
2
1
0
E" [mN/m]
100
1000
10000
100000
t [s]
pH 7, C(buff)=100mM
pH 7, C(buff)=10mM
pH 7, C(buff)=1mM

Appendix 7 Dynamic dilational viscocity E" on the interfacial pressure Π at f = 0.1 Hz for BLG solutions at a fixed BLG concentration of 10^{-6} mol/l for three different buffer concentration 1, 10 and 100 mM at pH 3, 5 and 7; (lines are guides for the eye).

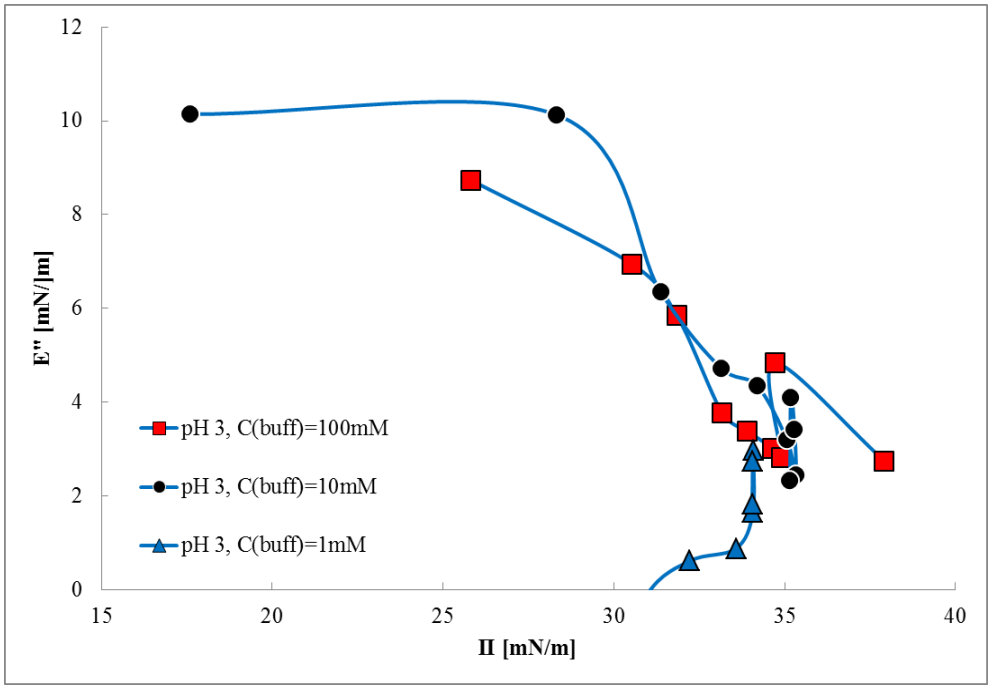

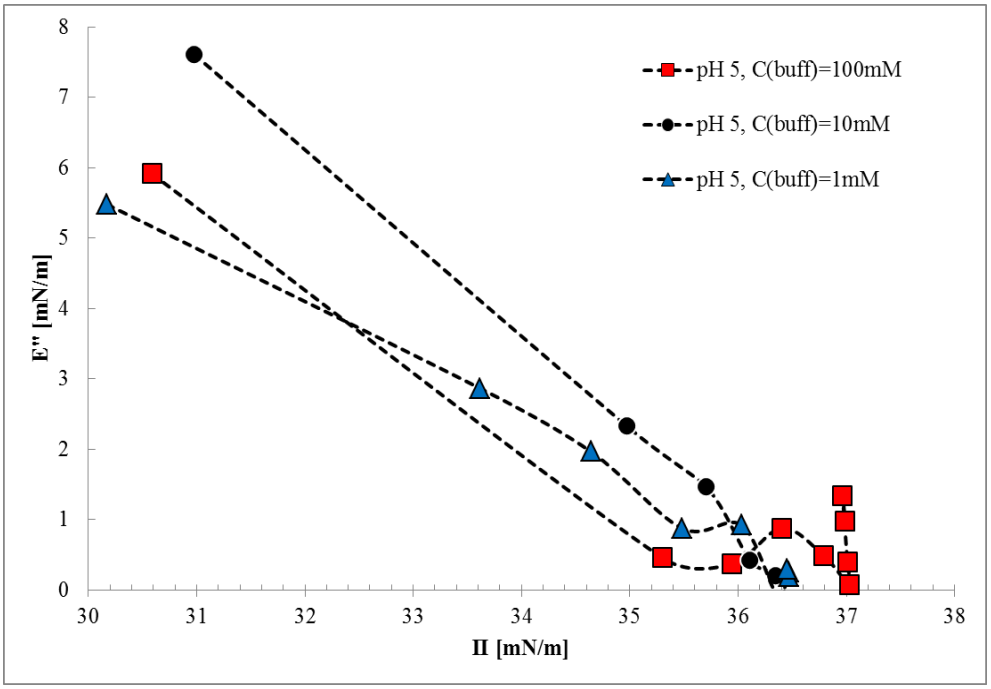

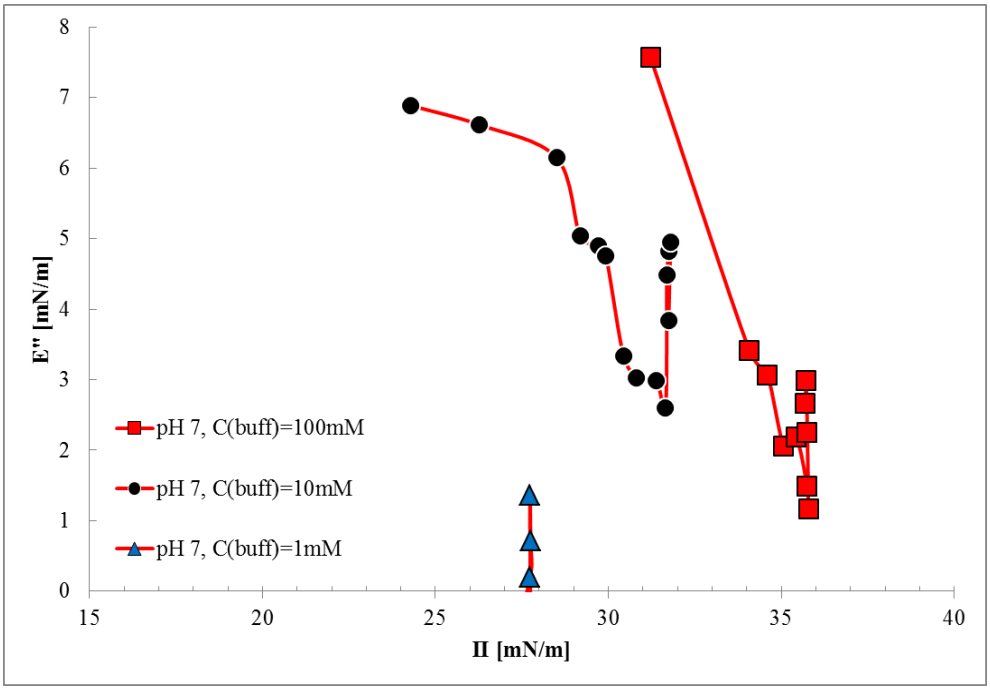
E" [mN/m]
Π [mN/m]
pH 7, C(buff)=100mM
pH 7, C(buff)=10mM
pH 7, C(buff)=1mM
0
1
2
3
4
5
6
7
8
15
20
25
30
35
40

REFERENCES

1 Bos, M. A., & van Vliet, T. (2001). Interfacial rheological properties of adsorbed protein layers and surfactants: a review. *Advances in Colloid and Interface Science, 91*(3), 437-471.

2 *Proteins at liquid interfaces* (Vol. 7). (1998). (D. Möbius, & R. Miller, Trans.) Elsevier.

3 Damodaran, S. (2004). Adsorbed layers formed from mixtures of proteins. *Current opinion in colloid & interface science, 9*(5), 328-339.

4 Dickinson, E. (1999). Adsorbed protein layers at fluid interfaces: interactions, structure and surface rheology. *Colloids and Surfaces B: Biointerfaces, 15*(2), 161-176.

5 *Food colloids: fundamentals of formulation* (Vol. 258). (2001). (E. Dickinson, & R. Miller, Trans.) Royal society of chemistry.

6 Engelhardt, K., Peukert, W., & Braunschweig, B. (2014). Vibrational sum-frequency generation at protein modified air–water interfaces: Effects of molecular structure and surface charging. *Current Opinion in Colloid & Interface Science, 19*(3), 207-215.

7 Noskov, B. A. (2014). Protein conformational transitions at the liquid–gas interface as studied by dilational surface rheology. *Advances in colloid and interface science, 206*, 222-238.

8 Ruso, J. M., & Piñeiro, Á . (Eds.). (2013). *Proteins in solution and at interfaces: methods and applications in biotechnology and materials science* (Vol. 8). John Wiley & Sons.

9 Sagis, L. M., & Fischer, P. (2014). Nonlinear rheology of complex fluid–fluid interfaces. *Current Opinion in Colloid & Interface Science, 19*(6), 520-529.

10 Yampolskaya, G., & Platikanov, D. (2006). Proteins at fluid interfaces: adsorption layers and thin liquid films. *Advances in colloid and interface science, 128*, 159-183.

11 Bos, M. A., Dunnewind, B., & van Vliet, T. (2003). Foams and surface rheological properties of β-casein, gliadin and glycinin. *Colloids and Surfaces B: Biointerfaces, 31*(1), 95-105.

12 Dan, A., Wüstneck, R., Krägel, J., Aksenenko, E. V., Fainerman, V. B., & Miller, R. (2014). Interfacial adsorption and rheological behavior of β-casein at the water/hexane interface at different pH. *Food Hydrocolloids, 34*, 193-201.

13 Dan, A., Gochev, G., Krägel, J., Aksenenko, E. V., Fainerman, V. B., & Miller, R. (2013). Interfacial rheology of mixed layers of food proteins and surfactants. *Current Opinion in Colloid & Interface Science, 18*(4), 302-310.

14 Dan, A., Wüstneck, R., Krägel, J., Aksenenko, E. V., Fainerman, V. B., & Miller, R. (2013). Adsorption and dilational rheology of mixed β-casein/DoTAB layers formed by sequential and simultaneous adsorption at the water/hexane interface. *Langmuir, 29*(7), 2233-2241.

15 Dickinson, E. (1998). Proteins at interfaces and in emulsions stability, rheology and interactions. *Journal of the Chemical Society, Faraday Transactions, 94*(12), 1657-1669.

16 Mackie, A. R., Gunning, A. P., Ridout, M. J., Wilde, P. J., & Morris, V. J. (2001). Orogenic displacement in mixed β-lactoglobulin/β-casein films at the air/water interface. *Langmuir, 17*(21), 6593-6598.

17 Mackie, A. R., Gunning, A. P., Wilde, P. J., & Morris, V. J. (2000). Competitive displacement of β-lactoglobulin from the air/water interface by sodium dodecyl sulfate. *Langmuir, 16*(21), 8176-8181.

18 Maldonado-Valderrama, J., Fainerman, V. B., Gálvez-Ruiz, M. J., Martń -Rodriguez, A., Cabrerizo-Vílchez M. & Miller R. (2005). Dilatational rheology of β-casein adsorbed layers at liquid-fluid interfaces. *The Journal of Physical Chemistry B, 109*(37), 17608-17616.

19 Mellema, M., Clark, D. C., Husband, F. A., & Mackie, A. R. (1998). Properties of β-casein at the air/water interface as supported by surface rheological measurements. *Langmuir, 14*(7), 1753-1758.

20 Murray, B. S. (2007). Stabilization of bubbles and foams. *Current Opinion in Colloid & Interface Science, 12*(4), 232-241.

21 Maldonado-Valderrama, J., & Patino, J. M. (2010). Interfacial rheology of protein–surfactant mixtures. *Current Opinion in Colloid & Interface Science, 15*(4), 271-282.

22 Maldonado-Valderrama, J., Miller, R., Fainerman, V. B., Wilde, P. J., & Morris, V. J. (2010). Effect of gastric conditions on β-lactoglobulin interfacial networks: Influence of the oil phase on protein structure. *Langmuir, 26*(20), 15901-15908.

23 MacRitchie, F., & Alexander, A. E. (1963). Kinetics of adsorption of proteins at interfaces. Part III. The role of electrical barriers in adsorption. *Journal of Colloid Science, 18*(5), 464-469.

24 Song, K. B., & Damodaran, S. (1991). Influence of electrostatic forces on the adsorption of succinylated. beta.-lactoglobulin at the air-water interface. *Langmuir, 7*(11), 2737-2742.

25 Ulaganathan, V., Retzlaff, I., Won, J. Y., Gochev, G., Gehin-Delval, C., Leser, M., Noskov, B. A., & Miller, R. (2016). β-Lactoglobulin Adsorption Layers at the Water/Air Surface: 1. Adsorption Kinetics and Surface Pressure Isotherm: Effect of pH and Ionic Strength. *Colloids and Surfaces A: Physicochemical and Engineering Aspects,* http://dx.doi.org/doi:10.1016/j.colsurfa.2016.03.008.

26 Joos, P., & Serrien, G. (1991). The principle of Braun—Le Châtelier at surfaces. *Journal of colloid and interface science, 145*(1), 291-294.

27 Miller, R., Aksenenko, E. V., Fainerman, V. B., & Pison, U. (2001). Kinetics of adsorption of globular proteins at liquid/fluid interfaces. *Colloids and Surfaces A: Physicochemical and Engineering Aspects, 183*, 381-390.

28 Hambling, S. G., McAlpine, A. S., Sawyer L., & Fox, P. F. (1992). β-Lactoglobulin. In *Advanced dairy chemistry-1: Proteins* (Vol. Ed. 2, pp. 141-190). London: Elsevier Applied Science.

29 Kontopidis G., Holt, C., & Sawyer, L. (2004). Invited review: β-lactoglobulin: binding properties, structure, and function. *Journal of dairy science, 87*(4), 785-796.

30 Sawyer L. & Kontopidis G. (2000). The core lipocalin bovine β-lactoglobulin. *Biochimica et Biophysica Acta (BBA)-Protein Structure and Molecular Enzymology, 1482*(1), 136-148.

31 Jost, R. (1993). Functional characteristics of dairy proteins. *Trends in Food Science & Technology, 4*(9), 283-288.

32 Ulaganathan, V., Retzlaff, I., Won, J. Y., Gochev, G., Gehin-Delval, C., Leser, M., Noskov, B. A., & Miller, R. (2016). β-Lactoglobulin Adsorption Layers at the Water/Air Surface: 2. Dilational Rheology: Effect of pH and Ionic Strength. *Colloids and Surfaces A: Physicochemical and Engineering Aspects.* http://dx.doi.org/10.1016/j.colsurfa.2016.08.064

33 Atkinson, P. J., Dickinson, E., Horne, D. S., Leermakers, F. A., & Richardson, R. M. (1996). Theoretical and experimental investigations of adsorbed protein structure at a fluid interface. *Berichte der Bunsengesellschaft für physikalische Chemie, 100*(6), 994-998.

34 Beierlein, F. R., Clark, T., Braunschweig, B., Engelhardt, K., Glas, L., & Peukert, W. (2015). Carboxylate Ion Pairing with Alkali-Metal Ions for β-Lactoglobulin and Its Role on Aggregation and Interfacial Adsorption. *The Journal of Physical Chemistry B, 119*(17), 5505-5517.

35 Davis, J. P., Foegeding, E. A., & Hansen, F. K. (2004). Electrostatic effects on the yield stress of whey protein isolate foams. *Colloids and Surfaces B: Biointerfaces, 34*(1), 13-23.

36 Delahaije, R. J., Gruppen, H., Giuseppin, M. L., & Wierenga, P. A. (2014). Quantitative description of the parameters affecting the adsorption behaviour of globular proteins. *Colloids and Surfaces B: Biointerfaces*, 199-206.

37 Engelhardt, K., Lexis, M., Gochev, G., Konnerth, C., Miller, R., Willenbacher, N., Peukert, W., & Braunschweig, B. (2013). pH effects on the molecular structure of β-lactoglobulin modified air–water interfaces and its impact on foam rheology. *Langmuir, 29*(37), 11646-11655.

38 Noskov, B. A., Mikhailovskaya, A. A., Lin, S. Y., Loglio, G., & Miller, R. (2010). Bovine serum albumin unfolding at the air/water interface as studied by dilational surface rheology. *Langmuir, 26*(22), 17225-17231.

39 Pezennec, S., Gauthier, F., Alonso, C., Graner, F., Croguennec, T., Brule, G., & Renault, A. (2000). The protein net electric charge determines the surface rheological properties of ovalbumin adsorbed at the air–water interface. *Food Hydrocolloids, 14*(5), 463-472.

40 Roberts, S. A., Kellaway, I. W., Taylor, K. M., Warburton, B., & Peters, K. (2005). Combined surface pressure-interfacial shear rheology study of the effect of pH on the adsorption of proteins at the air-water interface. *Langmuir, 21*(16), 7342-7348.

41 Wüstneck, R., Fainerman, V. B., Aksenenko, E. V., Kotsmar, C., Pradines, V., Krägel, J., & Miller, R. (2012). Surface dilatational behavior of β-casein at the solution/air interface at different pH values. *Colloids and Surfaces A: Physicochemical and Engineering Aspects, 404*, 17-24

42 Won, J. Y., Gochev, G., Ulaganathan, V., Krägel, J., Aksenenko, E. V., Fainerman, V. B., & Miller, R. (2016). Mixed Adsorption Mechanism for the Kinetics of BLG Interfacial Layer Formation at the Solution/Tetradecane Interface. *Colloids and*

Surfaces A: Physicochemical and Engineering Aspects. http://dx.doi.org/10.1016/j.colsurfa.2016.08.024

43 Gochev, G., Aksenenko, E., Fainerman, V., & Miller, R. (2016). β-Lactoglobulin Adsorption Layers at the Water/Air Surface: 3. Theoretical Modeling: Effect of pH. *submitted to Langmuir.*

44 Miller, R., Aksenenko, E.V., Zinkovych, Igor I., Fainerman, V.B. (2015). Adsorption of proteins at the aqueous solution/alkane interface: co-adsorption of protein and alkane, *Adv. Colloid Interface Sci., 222*, 509-516.

45 Won, J. Y., Gochev, G., Ulaganathan, V., Krägel, J., Aksenenko, E. V., Fainerman, V. B., & Miller, R. (2016). Effect of Solution pH on the Adsorption of BLG at the Solution/Tetradecane Interface. *Colloids and Surfaces A: Physicochemical and Engineering Aspects,* http://dx.doi.org/doi:10.1016/j.colsurfa.2016.05.042.

46 Won, J.Y., Gochev, G.G., Ulaganathan, V., Krägel, J., Aksenenko, E.V., Fainerman, V.B., Miller, R. (2016) Dilational viscoelasticity of BLG Adsorption Layers at the Solution/Tetradecane Interface - Effect of pH and Ionic Strength, *Colloids and Surfaces A: Physicochemical and Engineering Aspects. http://dx.doi.org/10.1016/j.colsurfa.2016.08.054*

47 Ruckenstein, E. (1996). Microemulsions, macroemulsions, and the Bancroft rule. *Langmuir, 12*(26), 6351-6353.

48 Fainerman, V. B., Miller, R., & Kovalchuk, V. I. (2003). Influence of the two-dimensional compressibility on the surface pressure isotherm and dilational elasticity of dodecyldimethylphosphine oxide. *The Journal of Physical Chemistry B, 107*(25), 6119-6121.

49 Exerowa, D., Gotchev, G., Kolarov, T., Kristov, K., Levecke, B., & Tadros, T. (2009). Comparison of oil-in-water emulsion films produced using ABA or AB n copolymers. *Colloids and Surfaces A: Physicochemical and Engineering Aspects, 335*(1), 50-54.

50 Exerowa, D., Gotchev, G., Kolarov, T., Kristov, K., Levecke, B., & Tadros, T. (2009). Oil-in-water emulsion films stabilized by polymeric surfactants based on inulin with different degree of hydrophobic modification. *Colloids and Surfaces A: Physicochemical and Engineering Aspects, 334*(1), 87-91.

51 Gotchev, G., Kolarov, T., Levecke, B., Tadros, T., Khristov, K., & Exerowa, D. (2007). Interaction forces in thin liquid films stabilized by hydrophobically modified inulin

polymeric surfactant. 3. Influence of electrolyte type on emulsion films. *Langmuir, 23*(11), 6091-6094.

52 Basheva, E. S., Gurkov, T. D., Christov, N. C., & Campbell, B. (2006). Interactions in oil/water/oil films stabilized by β-lactoglobulin; role of the surface charge. *Colloids and Surfaces A: Physicochemical and Engineering Aspects, 282*, 99-108.

53 Dimitrova, T. D., Leal-Calderon, F., Gurkov, T. D., & Campbell, B. (2001). Disjoining pressure vs thickness isotherms of thin emulsion films stabilized by proteins. *Langmuir, 17*(26), 8069-8077.

54 Koczo, K., Nikolov, A. D., Wasan, D. T., Borwankar, R. P., & Gonsalves, A. (1996). Layering of sodium caseinate submicelles in thin liquid films—A new stability mechanism for food dispersions. *Journal of colloid and interface science, 178*(2), 694-702.

55 Murray, B. S., & Dickinson, E. (1996). Interfacial rheology and the dynamic properties of 410 adsorbed films of food proteins and surfactants. *Food Science Technology International, 2*(3), 131-145.

56 Narsimhan, G. (1992). Maximum disjoining pressure in protein stabilized concentrated oil-in-water emulsions. *Colloids and surfaces, 62*(1), 41-55.

57 Velev, O. D., Campbell, B. E., & & Borwankar, R. P. (1998). Effect of calcium ions and environmental conditions on the properties of β-casein stabilized films and emulsions. *langmuir, 14*(15), 4122-4130.

58 Dukhin, S. S., Kretzschmar, G., & Miller, R. (1995). *Dynamics of adsorption at liquid interfaces: theory, experiment, application* (Vol. 1). (D. Moebius, & R. Miller, Eds.) Elsevier.

59 Miller, R., Joos, P., & Fainerman, V. B. (1994). Dynamic surface and interfacial tensions of surfactant and polymer solutions. *Advances in Colloid and Interface Science, 49*, 249-302.

60 Henry, W. (1803). Experiments on the Quantity of Gases Absorbed by Water, at Different Temperatures, and under Different Pressures. *Philosophical Transactions of the Royal Society of London, 93*, 29-42.

61 Langmuir, I. (1917). The constitution and fundamental properties of solids and liquids. II. Liquids. *Journal of the American Chemical Society, 39*(9), 1848-1906.

62 von Szyszkowski, B. (1908). Experimentelle Studien über kapillare Eigenschaften der wässrigen Lösungen von Fettsäuren. *Z. phys. Chem, 64*, 385-414.

63 Pradines, V., Fainerman, V., Aksenenko, E., Krägel, J., Mucic, N., & Miller, R. (2010). Adsorption of alkyl trimethylammonium bromides at the water/air and water/hexane interfaces. *Colloids and Surfaces A: Physicochem. Eng. Aspects, 371*, 22-28.

64 Fainerman, V. B., Kovalchuk, V. I., Aksenenko, E. V., Michel, M., Leser, M. E., & Miller, R. (2004). Models of two-dimensional solution assuming the internal compressibility of adsorbed molecules: a comparative analysis. *Journal of Physical Chemistry B, 108*(36), 13700-13705.

65 Singer, S. J. (1948). Note on an equation of state for linear macromolecules in monolayers. *The Journal of Chemical Physics, 16(9)*, 872-876.

66 Graham, D. E., & Phillips, M. C. (1979). Proteins at liquid interfaces: I. Kinetics of adsorption and surface denaturation. *Journal of Colloid and Interface Science, 70(3)*, 403-414.

67 Graham, D. E., & Phillips, M. C. (1979). Proteins at liquid interfaces: II. Adsorption isotherms. *Journal of Colloid and Interface Science, 70(3)*, 415-426.

68 Graham, D. E., & Phillips, M. C. (1979). Proteins at liquid interfaces: III. Molecular structures of adsorbed films. *Journal of Colloid and Interface Science, 70(3)*, 427-439.

69 Fainerman, V., Lucassen-Reynders, E., & Miller, R. (2003). Description of the adsorption behaviour of proteins at water/fluid interfaces in the framework of a two-dimensional solution model. *Advances in colloid and interface science, 106*(1), 237-259.

70 Kotsmar, C., Pradines, V., Alahverdjieva, V., Aksenenko, E., Fainerman, V., Kovalchuk, V., Krägel, J., Leser, M. E., Noskov, B. A., & Miller, R. (2009). Thermodynamics, adsorption kinetics and rheology of mixed protein–surfactant interfacial layers. *Advances in colloid and interface science, 150*(1), 41-54.

71 Miller, R., Fainerman, V. B., Aksenenko, E. V., Leser, M. E., & Michel, M. (2004). Dynamic surface tension and adsorption kinetics of β-Casein at the solution/air interface. *Langmuir, 20*(3), 771-777.

72 Miller, R., Fainerman, V. B., Makievski, A. V., Krägel, J., Grigoriev, D. O., Kazakov, V. N., & Sinyachenko, O. V. (2000). Dynamics of protein and mixed protein/surfactant adsorption layers at the water/fluid interface. *Advances in Colloid and Interface Science, 86*(1), 39-82.

73 Fainerman, V. B., & Miller, R. (1999). Equation of state for concentrated protein surface layers at the water/air interface. *Langmuir, 15*(5), 1812-1816.

74 Gochev, G., Retzlaff, I., Aksenenko, E. V., Fainerman, V. B., & Miller, R. (2013). Adsorption isotherm and equation of state for β-Lactoglobulin layers at the air/water surface. *Colloids and Surfaces A: Physicochemical and Engineering Aspects, 422*, 33-38.

75 Ward, A. F., & Tordai, L. (1946). Time-dependence of boundary tensions of solutions I. The role of diffusion in time-effects. *The Journal of Chemical Physics, 14*(7), 453-461.

76 Liu, J., Wang, C., & Messow, U. (2004). Adsorption kinetics at air/solution interface studied by maximum bubble pressure method. *Colloid and Polymer Science, 283*(2), 139-144.

77 Sengupta, T., & Damodaran, S. (1998). Role of dispersion interactions in the adsorption of proteins at oil-water and air-water interfaces. *Langmuir, 14(22)*, 6457-6469.

78 Tempel, M. V., Lucassen, J., & Lucassen-Reynders, E. H. (1965). Application of surface thermodynamics to Gibbs elasticity. *The Journal of Physical Chemistry, 69*(6), 1798-1804.

79 Lucassen, J., & Van Den Tempel, M. (1972). Dynamic measurements of dilational properties of a liquid interface. *Chemical Engineering Science, 27*(6), 1283-1291.

80 Lucassen, J., & Van den Tempel, M. (1972). Longitudinal waves on visco-elastic surfaces. *Journal of Colloid and Interface Science, 41*(3), 491-498.

81 Benjamins, J., & Lucassen-Reynders, E. H. (2009). Interfacial rheology of adsorbed protein layers. In R. Miller, & L. Liggieri (Eds.), *Interfacial Rheology, Progress in Colloid and Interface Science Series* (Vol. 1, p. 253). Leiden: Brill.

82 Toro-Sierra, J., Tolkach, A., & Kulozik, U. (2013). Fractionation of alpha-Lactalbumin and beta-Lactoglobulin from Whey Protein Isolate Using Selective Thermal Aggregation, an Optimized Membrane Separation Procedure and Resolubilization Techniques at Pilot Plant Scale. *Food and Bioprocess Technology, 6*, 1032-1043.

83 Clark, D., Husband, F., Wilde, P., Cornec, M., Miller, R., Krägel, J. & Wüstneck , R. (1995). Evidence of extraneous surfactant adsorption altering adsorbed layer properties of β-lactoglobulin. *Journal of the Chemical Society, Faraday Transactions, 91*(13), 1991-1996.

84 Saad, S. M., Policova, Z., Acosta, E. J., & Neumann, A. W. (2010). Range of validity of drop shape techniques for surface tension measurement. *Langmuir, 26*(17), 14004-14013.

85 Cheng, P., Li, D., Boruvka, L., Rotenberg, Y., & Neumann, A. W. (1990). Automation of axisymmetric drop shape analysis for measurements of interfacial tensions and contact angles. *Colloids and Surfaces, 43*(2), 151-167.

86 del Rio, O. I., & Neumann, A. W. (1997). Axisymmetric Drop Shape Analysis: Computational Methods for the Measurement of Interfacial Properties from the Shape and Dimensions of Pendant and Sessile Drops. *Journal of Colloid and Interface Science, 196*(2), 136-147.

87 Rotenberg, Y., Boruvka, L., & Neumann, A. W. (1983). Determination of surface tension and contact angle from the shapes of axisymmetric fluid interfaces. *Journal of Colloid and Interface Science, 93*(1), 169-183.

88 Chen, P., Kwok, D.Y., Prokop, R.M., del Rio; O.I., Susnar; S.S., & Neumann, A.W. (1998). Axisymmetric Drop Shape Analysis (ADSA) and its Applications, in "Drops and bubbles in interfacial research", "Studies in Interface Science", Vol. 6, Pages 61–138.

89 Loglio, G., Pandolfini, P., Miller, R., Makievski, A., Ravera, F., Ferrari, M., & Liggieri, L. (2001). Drop and bubble shape analysis as tool for dilational rheology studies of interfacial layers. In D. Möbius, & R. Miller (Eds.), *Novel Methods to Study Interfacial Layers, Studies in Interface Science* (Vol. 11, pp. 439-484). Amsterdam: Elsevier.

90 Maze, C., & Burnet, G. (1969). A non-linear regression method for calculating surface tension and contact angle from the shape of a sessile drop. *Surface Science, 13*, 451-470.

91 Bashforth, F., & Adams, J. C. (1883). *An Attempt to Test the Theory of Capillary Action.* Cambridge Univ.

92 Mucic, N., Moradi, N., Javadi, A., Aksenenko, E., Fainerman, V., & Miller, R. (2014). Mixed adsorption layers at the aqueous CnTAB solution/hexane vapour interface. *Colloids and Surfaces A: Physicochemical and Engineering Aspects, 442*, 50-55.

93 Loglio, G., Pandolfini, P., Ravera, F., Pugh, R., Makievski, A. V., Javadi, A., & Miller, R. (2011). Experimental observation of drop-drop coalescence in liquid-liquid systems:

instrument design and features. In R. Miller, & L. Liggieri (Eds.), *Bubble and drop interfaces* (Vol. 2, pp. 385-400). Leiden: Brill.

94 Won, J. Y., Krägel, J., Gochev, G., Ulaganathan, V., Javadi, A., Makievski, A. V., & Miller, R. (2014). Bubble–bubble interaction in aqueous β-Lactoglobulin solutions. *Food Hydrocolloids, 34*, 15-21.

95 Won, J. Y., Krägel, J., Makievski, A. V., Javadi, A., Gochev, G., Loglio, G., Pandolfini, P., Leser, M. E., Gehin-Delval, C., & Miller, R. (2014). Drop and bubble micro manipulator (DBMM)—A unique tool for mimicking processes in foams and emulsions. *Colloids and Surfaces A: Physicochemical and Engineering Aspects, 441*, 807-814.

96 Javadi, A., Krägel, J., Makievski, A. V., Kovalchuk, V. I., Kovalchuk, N. M., Mucic, N., Loglio, G., Pandolfini, P., Karbaschi, M., & Miller, R. (2012). Fast dynamic interfacial tension measurements and dilational rheology of interfacial layers by using the capillary pressure technique. *Colloids and Surfaces A: Physicochemical and Engineering Aspects, 407*, 159-168.

97 Javadi, A., Mucic, N., Karbaschi, M., Won, J. Y., Dan, A., Ulaganathan, V., Gochev, G., Makievski, A. V., Kovalchuk, V. I., Kovalchuk, N. M., Krägel, J., & Miller, R. (2013). Characterization methods for liquid interfacial layers. *The European Physical Journal Special Topics, 222*(1), 7-29.

98 Makievski, A. V., Wüstneck, R., Grigoriev, D. O., Krägel, J., & Trukhin, D. V. (1998). Protein adsorption isotherms studied by axisymmetric drop shape analysis. *Colloids and Surfaces A: Physicochemical and Engineering Aspects, 143*(2), 461-466.

99 Pradines, V., Krägel, J., Fainerman, V. B., & Miller, R. (2008). Interfacial properties of mixed β-lactoglobulin−SDS layers at the water/air and water/oil interface. *The Journal of Physical Chemistry B, 113*(3), 745-751.

100 Wüstneck, R., Krägel, J., Miller, R., Fainerman, V. B., Wilde, P. J., Sarker, D. K., & Clark, D. C. (1996). Dynamic surface tension and adsorption properties of β-casein and β-lactoglobulin. *Food Hydrocolloids, 10*(4), 395-405.

101 Basch, J. J., & Timasheff, S. N. (1967). Hydrogen ion equilibria of the genetic variants of bovine β-lactoglobulin. *Archives of Biochemistry and Biophysics, 118*(1), 37-47.

102 Nozaki, Y., Bunville, L. G., & Tanford C. (1959). Hydrogen Ion Titration Curves of β-Lactoglobulin 1. Journal of the American Chemical Society, 81(21), 5523-5529.

103 Benjamins, J. (2000). Static and dynamic properties of proteins adsorbed at liquid interfaces. *Wageningen Universiteit.*

104 Krägel, J., O'Neill, M., Makievski, A. V., Michel, M., Leser, M. E., & Miller, R. (2003). Dynamics of mixed protein–surfactant layers adsorbed at the water/air and water/oil interface. *Colloids and Surfaces B: Biointerfaces, 31(1)*, 107-114.

105 Lucassen-Reynders, E. H., Benjamins, J., & Fainerman, V. B. (2010). Dilational rheology of protein films adsorbed at fluid interfaces. *Current Opinion in Colloid & Interface Science, 15*(4), 264-270.

106 Benjamins, J., De Feijter, J. A., Evans, M. T., Graham, D. E., & Phillips, M. C. (1975). Dynamic and static properties of proteins adsorbed at the air/water interface. *Faraday discussions of the Chemical Society, 59*, 218-229.

107 Benjamins, J., Lyklema, J., & Lucassen-Reynders, E. H. (2006). Compression/expansion rheology of oil/water interfaces with adsorbed proteins. Comparison with the air/water surface. *Langmuir, 22*(14), 6181-6188.